Positron Interactions in Metals

David B. Rees.

B.Sc. (London)

A thesis submitted for
the degree of
Master of Philosophy
in the University of London.

Bedford College,
London.
1974.

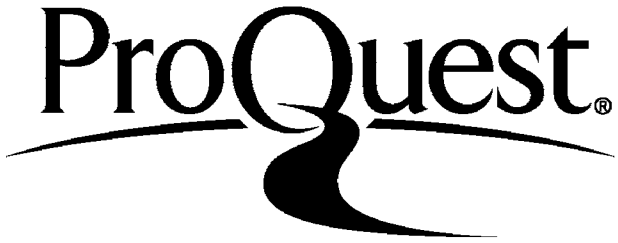

ABSTRACT

The thesis introduces positrons, their creation and annihilation, and describes how they can be used to demonstrate channelling. The design and construction of the electronic system used to investigate channelling is described and the system is also used in an experiment to find the stopping power of positrons in aluminium. Details are then given of various methods previously used to obtain the monovacancy formation energies in metals together with a new method based on the phenomenon of Doppler Broadening of the positron annihilation radiation frequency. The relative merits of the different methods are discussed and values for the monovacancy formation energy in Copper, Aluminium and Zinc obtained from experimental data are presented and compared with previous values. A brief description is then given of an extension of the Doppler Broadening technique into the field of neutron irradiation damage together with some tentative conclusions.

CONTENTS

CHAPTER 1

POSITRONS AND POSITRON ANNIHILATION

1.1 INTRODUCTION

Positrons were first predicted by Dirac. If all the negative energy states for electrons are filled then the 'sea' of occupied states is not detectable because all transitions are forbidden by Pauli's Principle. An electron could make a transition to a vacant positive energy state if it obtained at least $2m_0c^2$ energy when it would be observable as would the 'hole' or positron left in the negative energy states (Fig. 1.1). The hole would behave as an electron except that it would appear to move in the opposite direction to an electron in an electromagnetic field, i.e. the hole has opposite charge to an electron. The hole would also be unstable in the presence of positive energy electrons which could easily fall into the hole thereby liberating $2m_0c^2$ energy. Conservation of momentum requires that the energy be liberated by emission of at least two quanta in opposite directions having minimum energy m_0c^2.

In 1932 positrons were discovered by the observation of tracks in a cloud chamber exposed to cosmic radiation at Pasadena, California (Anderson, 1933). The curvature of the tracks showed that two particles had been created simultaneously and that they had equal masses but opposite charges. One of the particles was identified as an electron.

The energy of the two γ rays produced by a positron electron annihilation (Fig. 1.2) was first measured to be 510.96 KeV (Klemperer, 1934). It was later shown that one in every 370 annihilations occurs with the emission of 3 quanta (Ore and Powell, 1949). Measurement of triple coincidences (Rich, 1951) led to the theory that the ratio of 3γ : 2γ annihilations would decrease if the positron and electron formed a quasi-stable positronium atom before annihilating. Singlet positronium would decay promptly (10^{-10} sec) emitting 2 quanta whilst the triplet state would have a longer lifetime (10^{-7} sec) before annihilating and emitting 3 quanta.

1.2 POSITRON THEORY

A quanta of energy E creates 2 oppositely charged particles of mass m_+ and m_-. At the instant of creation the particles are ejected with energies E_+ and E_-. To create a mass m requires energy equal to mc^2 so if the quanta is completely used up then

$$E = (m_+ + m_-)c^2 + E_+ + E_-$$

Measurement of all the other quantities allows m_+ to be calculated and from experiments

$$m_+ = (1.02 \pm 0.10)m_- \qquad \text{and}$$

$$(m_+ + m_-)c^2 = 1.02 \text{ MeV}$$

The positron is identical to the electron except that it has the opposite charge.

Fig 1.1 Electron Energy States.

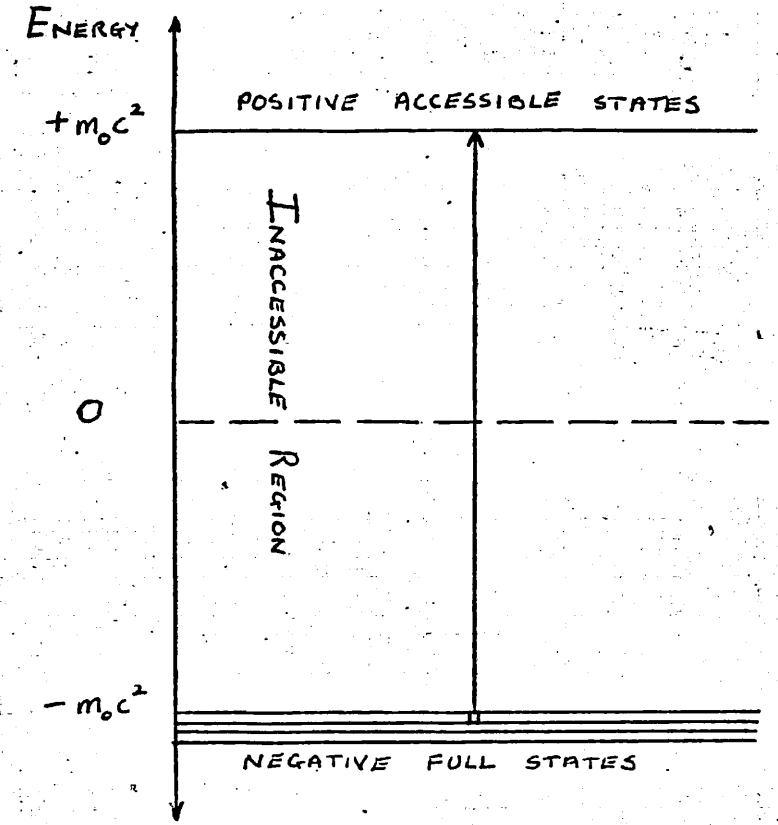

Fig 1.2 Space Time (World) Map of Positron Annihilation.

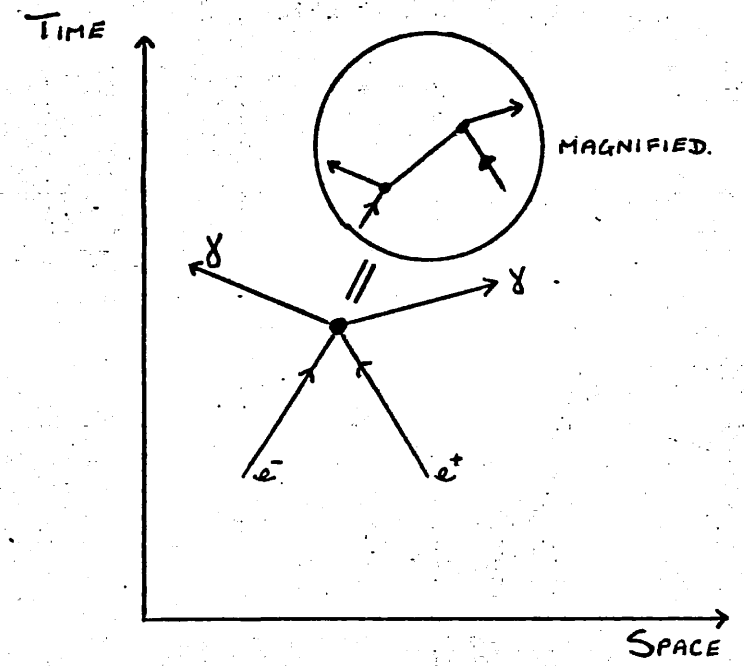

Fig 1.1 Electron Energy States.

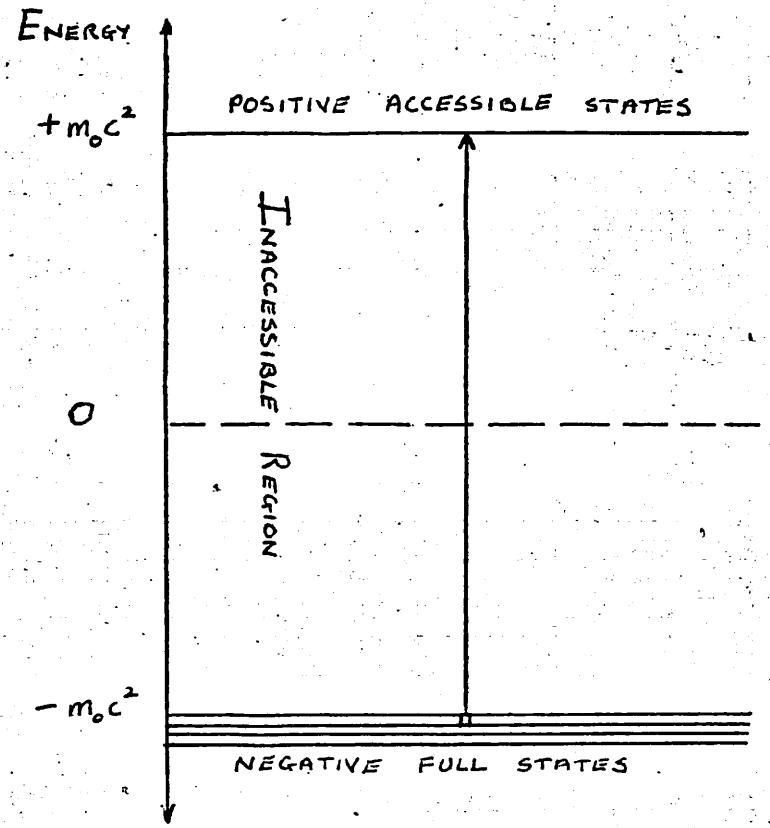

Fig 1.2 Space Time (World) Map of Positron Annihilation.

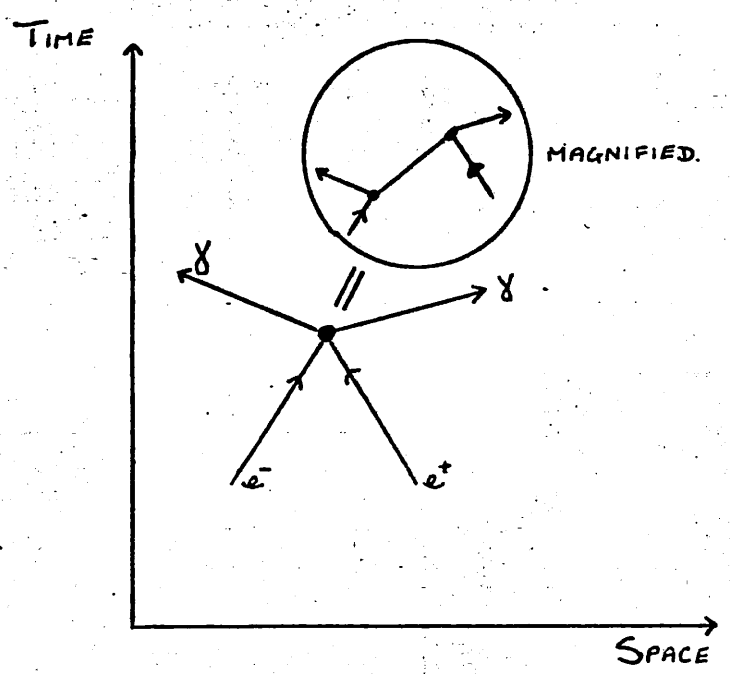

Pair creation is forbidden in free space by conservation of energy and momentum and usually occurs in the field of an atomic nucleus which recoils with the excess momentum imparted by the photon. Loss of kinetic energy to the nucleus is small because of the relative masses. Small differences in the energies of the positron and the electron are due to potential energy differences in the field of the positive nucleus.

In the Compton effect photons transfer only a proportion of their energy to the target electron and pass on as degraded radiation. Pair production requires the total absorption of the photon by the electron which is lifted out of the negative energy state to a positive energy state leaving a positron behind. Since $(m_+ + m_-)c^2$ $\approx$ 1.02 MeV this is the minimum threshold energy for pair production and the cross section increases with increasing photon energy above 1.02 MeV (Fig. 1.3) and with the atomic number of the element concerned. In lead the photon absorption is appreciable above 5MeV when it accounts for the greater part of the total attenuation of the photons.

The positron is entirely stable in vacuo but annihilates with an approaching electron, the exact reverse of pair production. The two quanta released at annihilation must take away the threshold energy, i.e. mass of the electron and positron, and the energies of the annihilating pair E_- and E_+

$$2h\nu = 1.02 \text{ MeV} + E_- + E_+$$

FIG 1.3 ATTENUATION OF ELECTROMAGNETIC RADIATION IN LEAD.

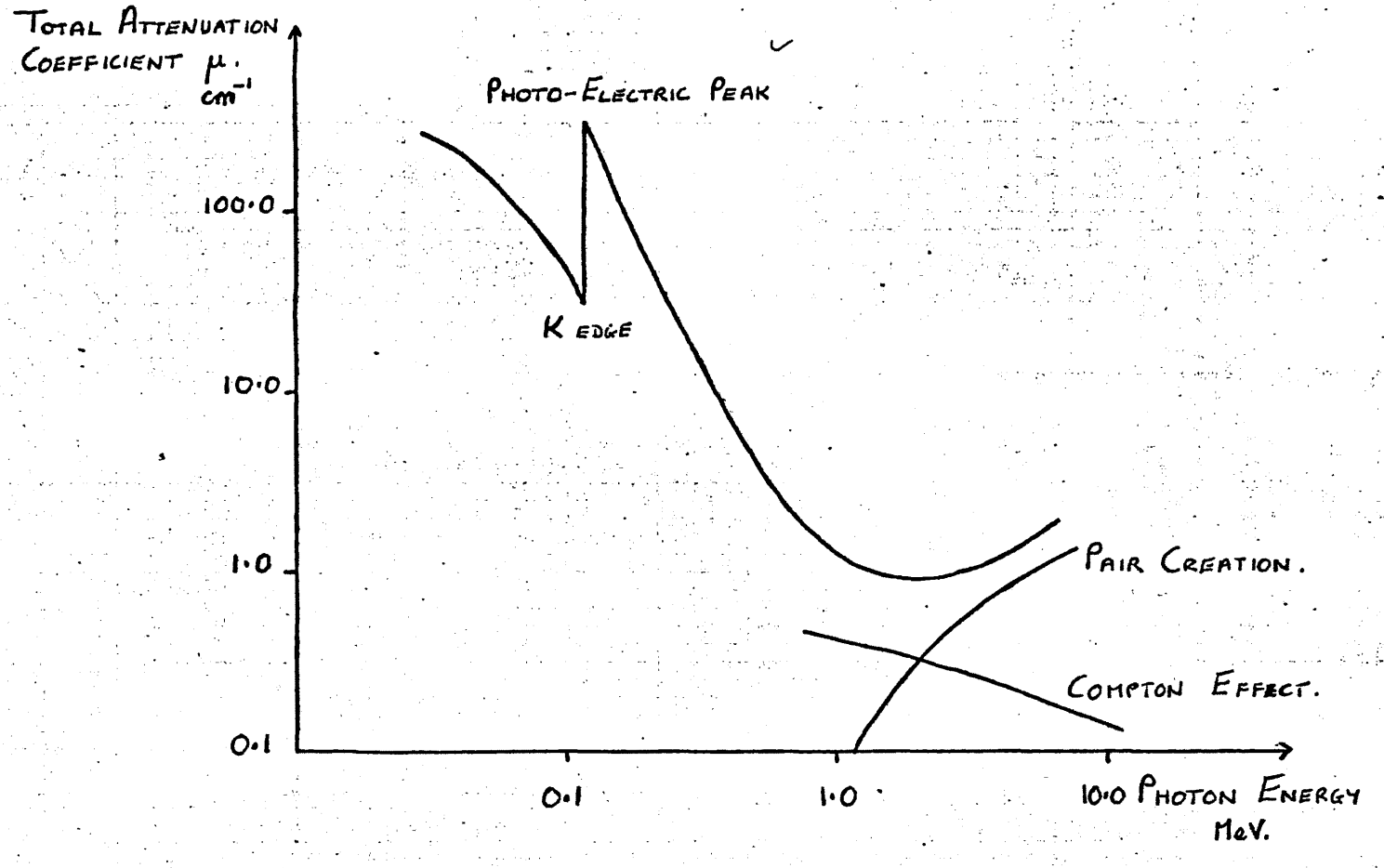

Usually slow positrons and slow electrons annihilate so that E_+ and E_- are negligible. Conservation of momentum and energy shows that the two quanta must be emitted with the same energy, 510KeV, in exactly opposite directions. Two photon annihilation occurs if the spins of the positron and electron are antiparallel. If they are parallel conservation of spin parity implies that at least three quanta must be emitted. The rate of annihilation of slow positrons in matter is given by

$$\tau^{-1} = \lambda = C_s \Psi_s^2 + C_t \Psi_t^2 \qquad \text{where}$$

Ψ_s^2 = density of electrons with antiparallel spin direction at the average positron position, i.e. forms singlet state and annihilates with two quanta emitted.

Ψ_t^2 = the same for parallel spin direction, i.e. forms triplet state and annihilates with three quanta emitted.

C_s and C_t are fundamental interaction rates in the singlet and triplet states respectively.

$$C_s = 4\pi c \left(\frac{e^2}{mc^2}\right)^2 \approx 3 \times 10^{-14} \text{ cm}^3 \text{ sec}^{-1}$$

$$C_t = 4\pi c \left(\frac{e^2}{mc^2}\right)^2 \frac{4\alpha}{9\pi}(\pi^2 - 9) \approx \frac{1}{1115} C_s$$

$$\approx 2.7 \times 10^{-17} \text{ cm}^3 \text{ sec}^{-1}$$

If the effects of coulomb forces are neglected then $\psi_s^2 = \frac{n_e}{4}$ and $\psi_t^2 = \frac{3n_e}{4}$ where n_e is the number of electrons per cc. of matter, i.e. the electron density. If coulomb forces are taken into account but the positrons are still assumed to move freely through the medium then n_e becomes the effective number of electrons per cc. of matter.

1.3 ANNIHILATION LIFETIMES

Neither the positron nor the electron are at rest when they annihilate but usually have energies of about 13eV. The annihilation quanta are therefore not emitted at exactly 180° to each other but have an angular spread about the 180° line. (De Beneditti et al., 1950). The positrons reach these low energies, i.e. are thermalised, by inelastic collisons with the outer atomic electrons of the annihilation medium.

Coincidence resolution curves for the annihilation quanta indicated that the positron lifetime in metals was surprisingly consistent (Bell and Graham, 1953). Amorphous solids gave two lifetimes whose relative intensity was not temperature dependent although the actual lifetimes did vary with temperature. If triplet positronium was formed in amorphous solids as well as the singlet form found in metals then the triplet positronium could decay directly or via the singlet state giving rise to two lifetimes.

Alternatively, positrons rapidly slowed down to

energies where the probability of positronium formation was large could exist in two excited states. In metals the upper excited state 2S would be rapidly de-excited to the lower 1S state by collisions with conduction band electrons so that only one lifetime would be observed. In non-metals with few free electrons the excited state would be relatively stable producing a second lifetime (Dixon and Trainor, 1955). The relative intensities of the two lifetimes would be determined by gross parameters, e.g. the binding energy difference between the 2S and 1S states, so they would be insensitive to environment. Both states are weakly bound so the lifetime would be temperature dependent.

A third theory (Berko and Hereford, 1956) suggested that the longer lifetime in amorphous substances was due to the conversion rate from triplet to singlet states. Thus, annihilation from the triplet state would result in 3 quanta being emitted so that there would be a relation between the 3 quanta annihilation rate and the competing process of conversion shown by the intensity of the long lifetime component. A bound state in metals was also discounted and it was suggested that a proper theory of the electron density in metals would explain the similarity between lifetimes in metals. If positrons reached very low energies before annihilating then the shape of the angular distribution about 180° would be dictated by the annihilating electrons. The expected shape could be obtained from the area under a slice through the Fermi sphere at a height proportional to the component of

electron momentum corresponding to the relative angle. The distribution should be an inverted parabola capable of giving information about the electron distribution with respect to momentum.

The parabola should have a sharp cut off which became smeared out at higher temperatures with increasing electron and positron motion. Assuming a Boltzmann distribution of positron energy the effective positron temperature could be obtained and was found to be linear with specimen temperature except at very low temperatures (Kim et al., 1967). Therefore, positrons are probably thermalized except below about 160°K when the thermalization time becomes longer than the annihilation time.

An angular correlation curve technique was used to find the mechanism which produced three lifetimes in some materials like Teflon (McGervey and Walters, 1970). Each lifetime should produce a different curve and so the lifetimes were measured by a coincidence method but with the detectors at different angles to obtain an angular correlation effect. Tao and Green had suggested that τ_1, the shortest lifetime, was due to free annihilation, τ_2 was due to positronium pick off, i.e. the positron annihilating with an electron other than its partner in the positronium atom and τ_3 was due to positronium decay. An alternative suggested by Brandt and Spirn was that τ_1 was due to positronium decay in crystalline regions, τ_2 was due to free annihilation and τ_3 was due to positronium decay. McGervey and Walters' results showed that τ_2 was probably due to free annihilation or

to annihilation whilst the positron was in a bound state with the teflon molecule.

However, it was also shown that the pick off rate from positronium was important in the decay of positronium although not necessarily the cause of τ_2 (Brandt and Fahs, 1970). Work on alhaline earth fluorides, metal oxides and ionic crystals indicated that the longer lifetimes were due to annihilation from complexes formed either with electrons or with some part of the atomic structure. Patro and Sen (1971) suggested that in condensed matter the shortest lifetime was due to parapositronium decay, τ_2 was due to free annihilation and τ_3 was due to the pick off decay of orthopositronium (which would also explain Berho and Hereford's results).

The angular correlation curve for a deformed metal was found to be narrower than that for an annealed sample. A similar effect on the curve and a change in lifetime could be produced by heating a sample to create vacancies (Connors and West, 1969). Positrons may tend to annihilate in low electron density regions around dislocations or vacancies. In order to verify this a special electronic system which measured the angular correlation line width directly was used (MacKenzie et al., 1970). The middle parabolic part of the curve should be due to annihilation with free electrons whilst the higher momentum tails should be due to annihilation with core electrons. Positrons trapped at a vacancy or dislocation would be subject to a spurious electron distribution of free electrons so that the curve would become narrower and the lifetimes would change. The line width was shown to be

related to the number of trapped positrons which is itself proportional to the number of vacancies or dislocations.

The effect on the line width of deforming samples of previously annealed metals, thereby producing lattice defects, showed that there was a large difference in the electron distribution seen by positrons annihilating at a lattice defect (Takagi et al., 1971). Positrons become thermalised on entering a metal within 10^{-12} sec. by losing energy in inelastic collisions with electrons and the lattice. The positron annihilates after 10^{-10} sec. at a rate, λ, which depends on the total electron density at the positron:

$$\lambda = \lambda_{\text{valence}} + \lambda_{\text{core}}$$

λ_{valence} = rate due to valence electrons whose momentum distribution P_v has the form of an inverted parabola

λ_{core} = rate due to core electrons whose momentum distribution P_c has a gaussian form.

Increases in mean lifetimes on heating or deforming the metal are due to annihilation in lower electron densities found at vacancies and dislocations and depend on the defect concentration (Connors et al., 1971). A statistical curve, taking rates of annihilation, escape rates from vacancies, and the activation energy for vacancy formation into account, of the increase in the mean lifetime with temperature showed good correlation with experiment. Over a normal temperature spread, increasing the temperature

decreases the likelihood of annihilation with core electrons. However, low concentrations of impurities or electrostatically different components in an alloy will obscure the effect.

In a metal with a uniform 'gas' of valence electrons the positron electron pair can be considered to be repeatedly scattered via a suitably screened interaction before annihilation. So the response of the electronic system is to screen the direct positron electron interaction and to produce an enhanced electron density around the positron. The annihilation rate can thus be expressed in terms of the rate for a non-interacting system of the same density multiplied by an enhancement factor which is almost independent of the electron momentum. If a contribution to the total rate from the core electrons is included this can be another enhancement factor since the tightly bound core electrons are excited to unoccupied states above the fermi level and undergo repeated scattering with the positron before annihilation in the same way as the valence electrons (West, 1971). These enhancement factors are small compared to the screening effect of the valence electrons and can be neglected. The displaced charge density around the positron, i.e. the shielding is made up from contributions from each electron band, each one giving an area, A, proportional to its partial annihilation rate, under the correlation curve. The valence electrons will give a parabolic curve and the core electrons a much broader curve.

If the total annihilation rate $\mu = \mu_v + \mu_c$

then:

$$\frac{\mu_v}{\mu_c} = \frac{A_v}{A_c}$$

μ_v is found to be smaller than expected so the screening between the positron and the valence electrons is enhanced probably because the core electrons affect the so called 'free' electron gas density of valence electrons.

At defects in the lattice the core electron screening would be much less but any effect this has on the annihilation rate would be masked by both the drop in core annihilation rate and by the effect of a lower valence electron density.

CHAPTER 2

DESIGNS AND CONSTRUCTION OF THE ELECTRONICS AND INSTRUMENTATION

2.1 THE GAMMA-RAY COINCIDENCE SYSTEM

The system used to detect the annihilation radiation from the positron electron interaction was a standard triple coincidence system based on the design by Bell and Petch. The gamma-ray detectors used were scintillation counters which produced two types of pulse. One pulse was fast and was used to detect the coincidence of the incoming gamma-rays and the other pulse was slow but linear and was used to detect the gamma-ray energy. If a gamma-ray of 511KeV hits each of the scintillation counters within 20nSecs. the system should register them as being due to a positron annihilating. A block diagram of the system is given in Fig. 2.1.

The fast line pulses are led to a time pickoff device which produces a very fast rise time pulse. This pulse is not linear but occurs after a very short delay from the time when the anode pulse is input. These pulses are suitable for the fast coincidence unit which tests whether pulses in the two arms come within say 20nSecs. of each other.

The slow line pulses are fed via pre-amplifier and amplifier to a pulse height analyser. These pulses are linear with respect to gamma-ray energy and the analyser tests to see if the incoming gamma-ray had 511 KeV energy. If both gamma rays had the correct energy and occurred

FIG. 2.1 TRIPLE COINCIDENCE SYSTEM (BELL AND PETCH)

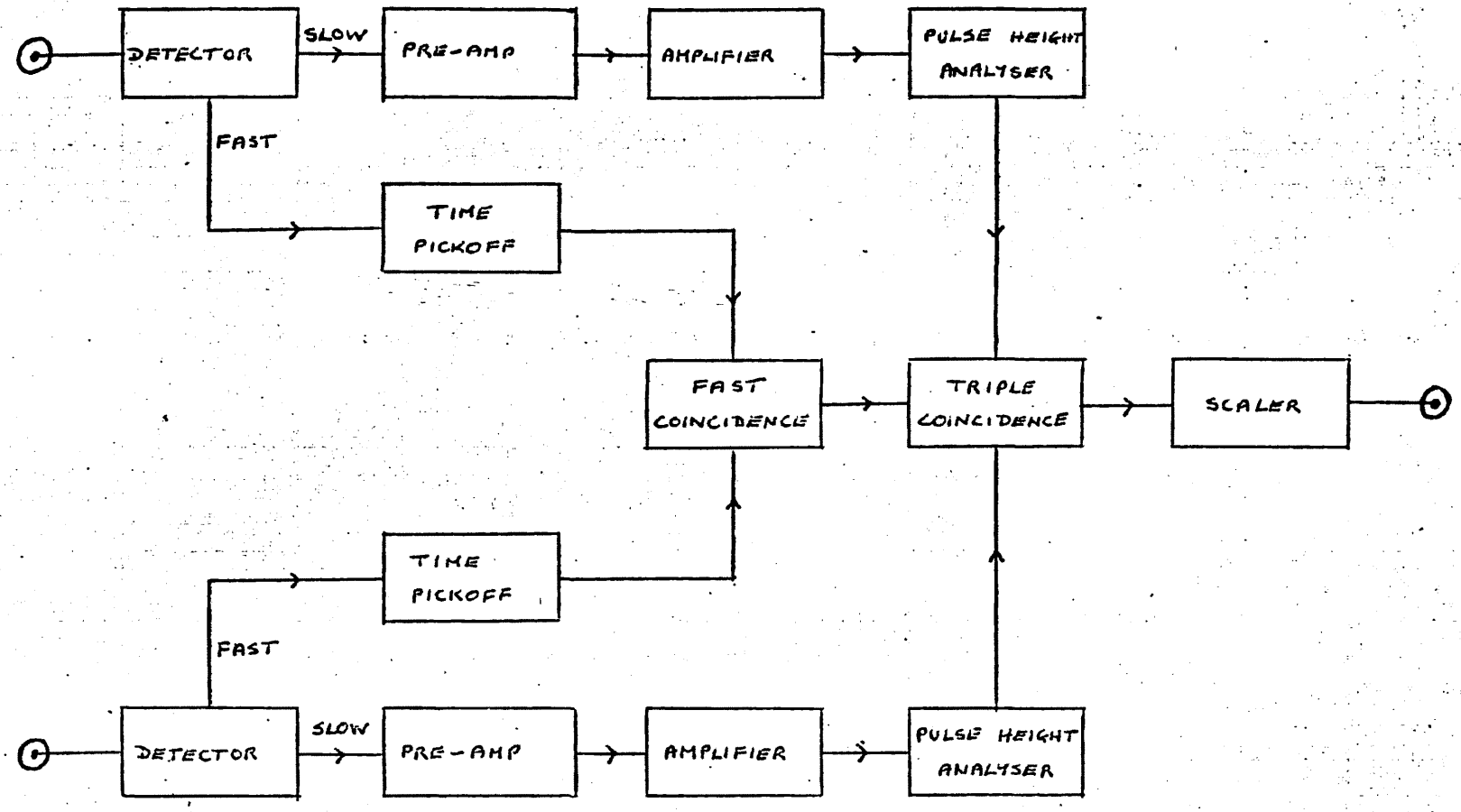

within 20nSecs. then three pulses will arrive at the triple coincidence unit at the same time. If this occurs the triple coincidence unit outputs an information pulse which is counted by a scaler. The number counted by the scaler within a set period of time is the number of positron annihilations detected by the system in that time.

The pre-amplifiers used were Harwell '2000 Series' type 1660A modified so that the H.T. for the photo-multiplier tubes did not go through the unit. Input was from the eighth dynode and output was to the amplifier.

The amplifiers used were Harwell '2000 Series' low level amplifier type 2070A. The differentiation time of the amplifier was modified to 15μ Secs. the same as the rise time of the input pulses. The amplifier originally had a differentiation time of 150μ Secs. which would result in a very long output pulse which would cause pulse pile up. The output was to the pulse height analyser.

2.2 SCINTILLATION COUNTERS

These counters consisted of 2 inch diameter, 2 inch thick NaI(Tl) crystals mounted on E.M.I. type 9813 KB fast photo-multiplier tubes. The dynode chain (Fig. 2.2) was based on one recommended by E.M.I. for use with this tube. The anode load resistor was chosen as 100 ohms to match the cable to prevent ringing and to produce current pulses rather than a voltage signal. The E.H.T. applied was 1.8KV when:

FIG 2.2 DYNODE CHAIN FOR PHOTOMULTIPLIER TUBES TYPE 9813KB.

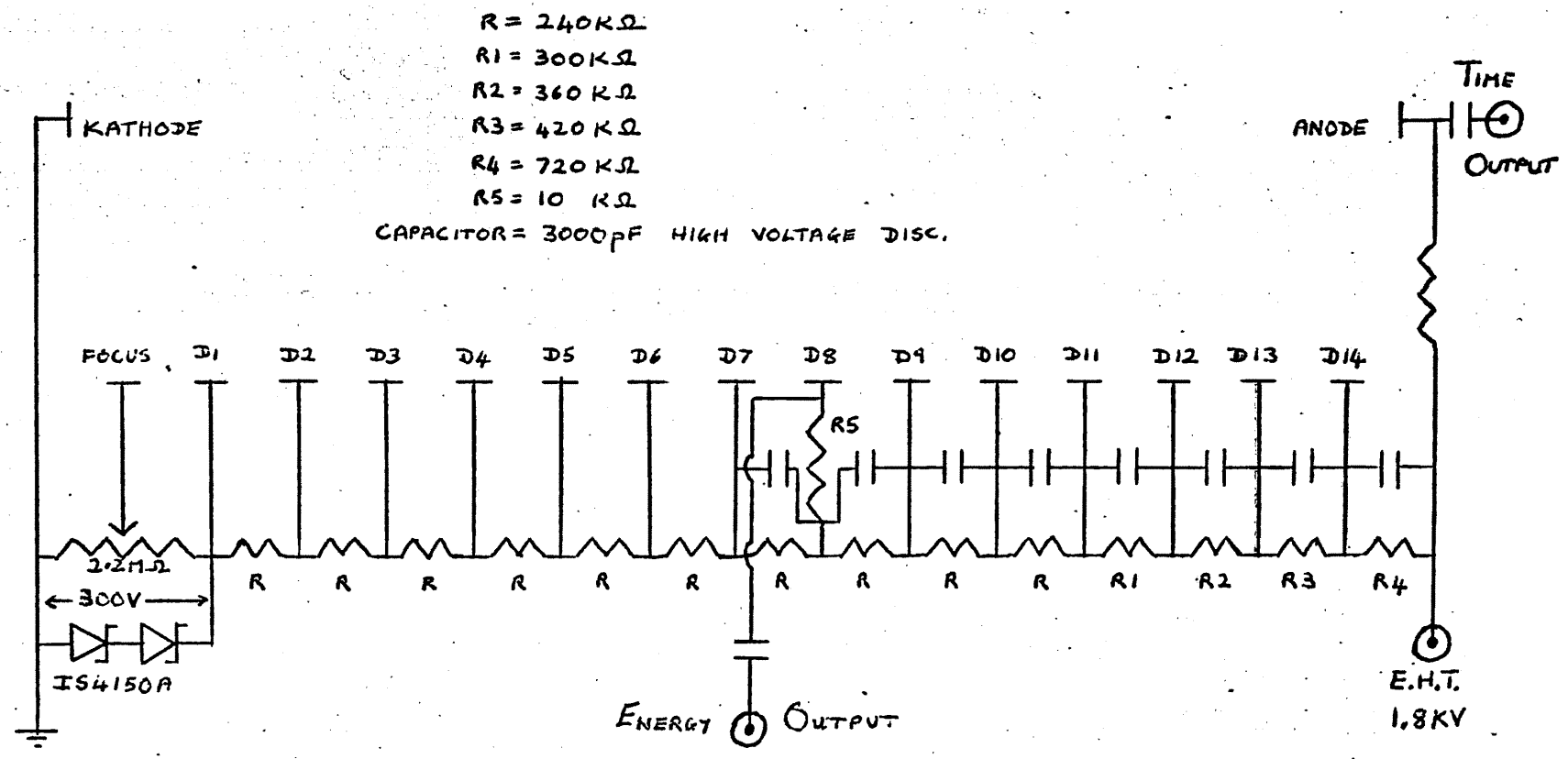

a) typical anode pulse	rise time	= 70nSecs.
	amplitude	= .01 Volts
	duration	= .2μ Sec.
b) typical dynode pulse	rise time	= 10μ Secs.
	amplitude	= 2.0 Volts
	duration	= 200μ Sec.

The anode pulses were very noisy because of the low load resistor but this was taken into account by the time pick-off unit. The dynode pulse was taken from the eighth dynode and this was decoupled to the seventh and all higher number dynodes in order to prevent the H.T. on any of the dynodes being affected. In order to produce a fast anode pulse the potential difference between dynodes increased rapidly near the anode. Calibration graphs were obtained for $^{137}C_s$ and $^{60}C_o$ to find the efficiencies of the counters which were 8.5% and 9.0%.

2.3 TIME PICKOFF UNIT

The fast ocincidence resolution time should be as short as possible, say 20nSecs. Sodium Iodide (Tl) crystals have a scintillation time of about 250nSecs. (Fig. 2.3) and the photo-multiplier tube requires a finite time to produce an anode pulse which is not consistent because of drift, and the anode pulse was typically .2μ Sec. long (Fig. 2.4). In order to produce a short fast pulse suitable for the coincidence work a tunnel diode is used and this will switch extremely fast very soon after the start of the anode pulse. This is used to trigger an

avalanche transistor which is non-linear but which produces large fast pulses suitable for input to the coincidence circuits.

The tunnel diode must trigger at an extremely low input voltage which must be variable so that it can discriminate against noise. The output from the avalanche transistor must occur after a set time from the input of the anode pulse and it must be of variable short length and have an amplitude of at least 2 Volts.

Operation

The anode pulse from the photo-multiplier tube is input to the cathode end of the tunnel diode which is biased to operate in a monostable mode. The correct bias is obtained from the resistor chain composed of the load resistor (5.6 ohm) and the variable bias resistor (1 Kohm) such that the operating point is just within the first stable region at A (Fig. 2.5). If the input current pulse is greater than $I_p - I_A$ the diode is forced into the negative conductance region and the voltage across the diode increases momentarily so that it reaches the third stable region at B. The voltage pulse, whose amplitude and width are governed by the 4.7μ H inductance, the diode's junction capacitance and other capacitances in the circuit, is taken to the base of the avalanche transistor. When the anode current pulse ends there is insufficient current to maintain the diode at B and the voltage drops to V_v when it jumps to V_D which is below V_A so the diode climbs back to its operating point A.

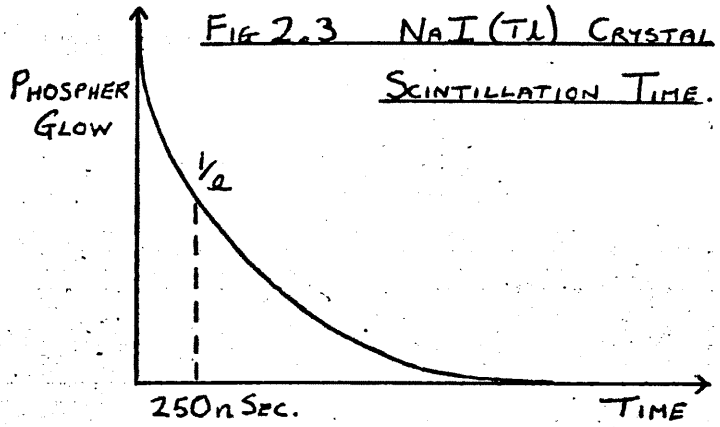

FIG 2.3 NaI(Tl) CRYSTAL SCINTILLATION TIME.

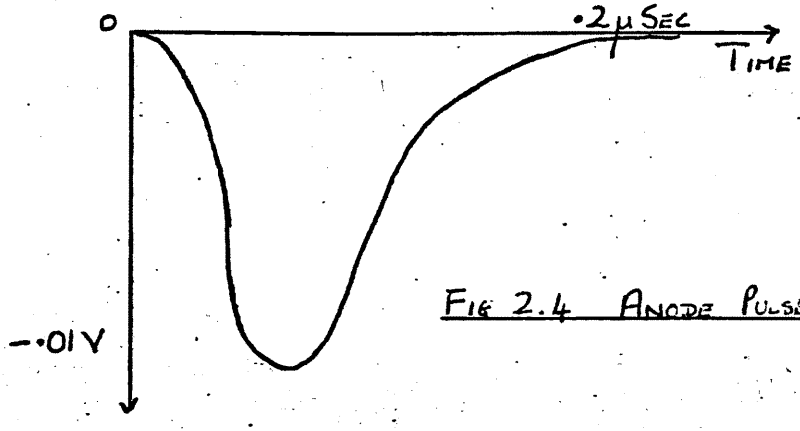

FIG 2.4 ANODE PULSE.

FIG 2.5 TUNNEL DIODE CHARACTERISTIC.

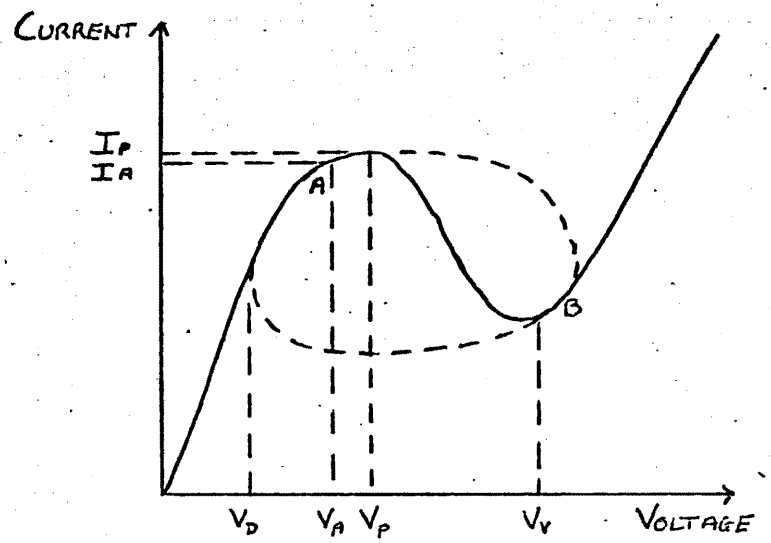

FIG 2.6 AVALANCHE TRANSISTOR CHARACTERISTIC.

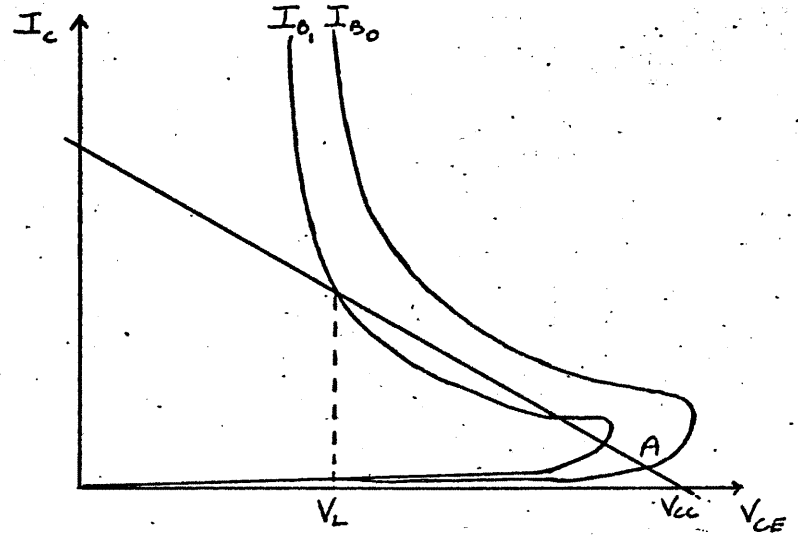

The avalanche transistor is biased to a just stable point on its characteristic curves at C by the current I_{BO} controlled by the base bias resistors (Fig. 2.6). The pulse from the tunnel diode increases the base current to I_{BI} which means that the transistor is no longer in a stable region and it breaks down until the voltage across it is equal to the latching voltage V_L. Thus a large current pulse is applied to the delay line, due to this voltage step, which is reflected at the open end with inversion. When the inverted reflection reaches the collector the current i_c is brought to zero and the transistor goes off. Thus V_{CE} must return to its previous stable point corresponding to C, ending the output pulse which is taken from the emitter. The pulse length is proportional to the length of the delay cable. Fig. 2.7 shows the circuit diagram and Fig. 2.8 shows the printed circuit layout. To prevent r.f. interference the power lines were decoupled and the unit was placed in a mu-metal box.

2.4 PULSE HEIGHT ANALYSER

The height of the photo-multiplier dynode pulse is a linear function of the energy released in the scintillator by the impinging particle. When positrons annihilate they release two 511 KeV gamma-rays and these must be isolated from the background radiation which also affects the scintillation counters. This is done by discriminating against all pulses except those whose height is equivalent to 511 KeV. The spectrum of pulses obtained from the

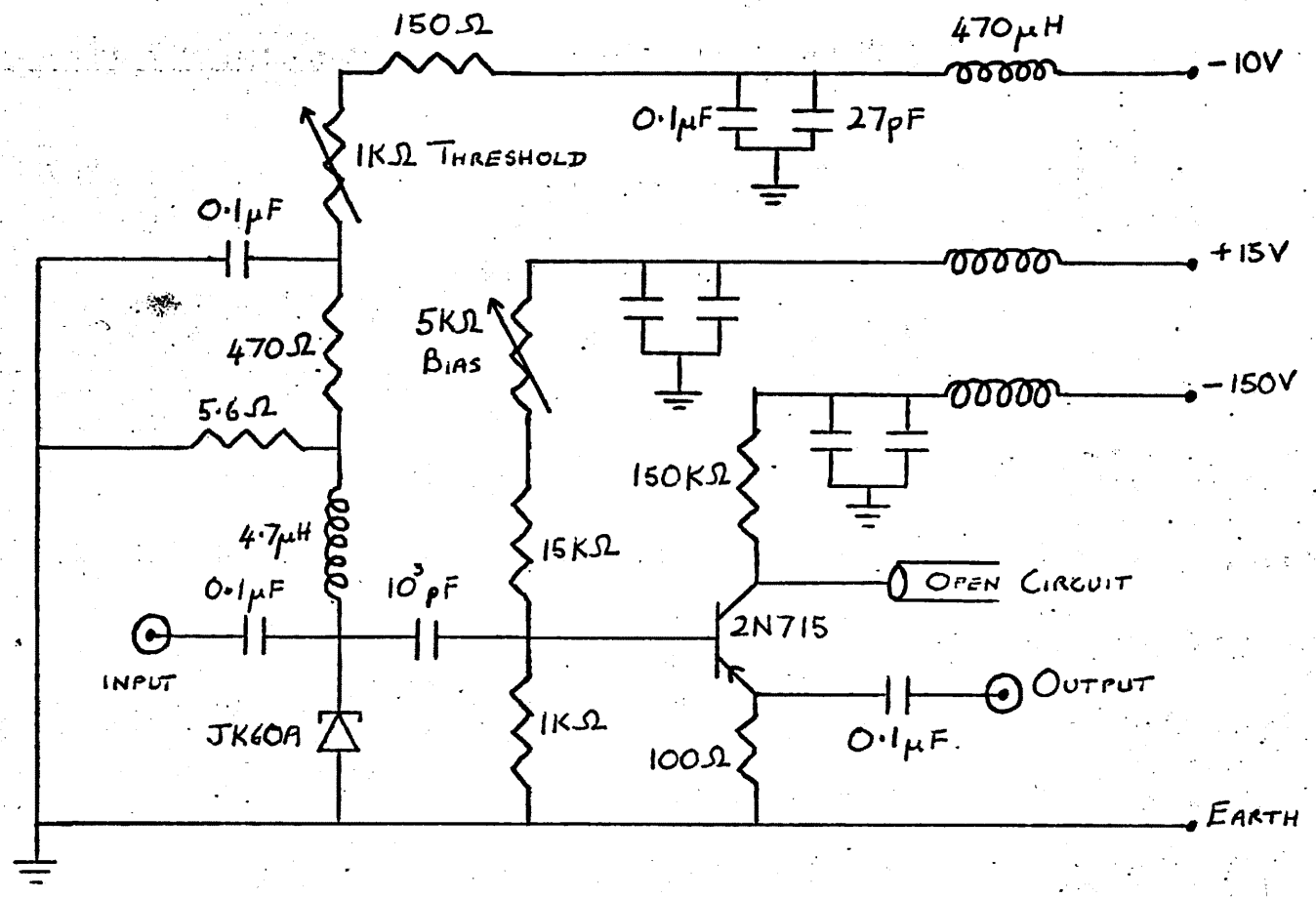

FIG 2.7 TIME PICKOFF UNIT CIRCUIT DIAGRAM

FIG 2.8 TIME PICKOFF UNIT PRINTED CIRCUIT.

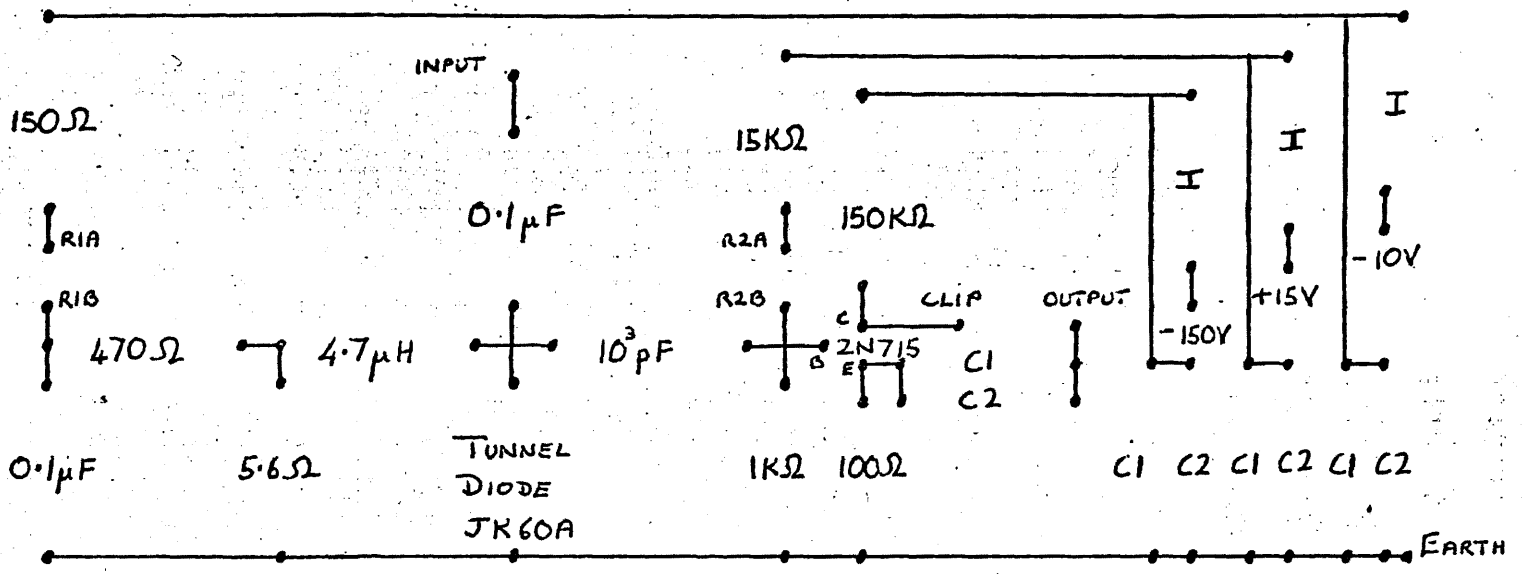

R1A AND R1B TO THRESHOLD POTENTIOMETER 1KΩ.
R2A AND R2B TO BIAS POTENTIOMETER 5KΩ.
C1 = 27pF
C2 = 0·1μF
I = 470μH

amplifiers has a range of 0 to 4.5 Volts with the 511 KeV line at about 3.5 Volts. The pulse height analyser must determine whether the maximum amplitude of an input pulse lies between two set limits normally either side of about 3.5 Volts for this experiment. If the pulse has the correct height the analyser must output a standard information pulse after a fixed interval from the start of the input pulse. To make the analyser generally useful the upper and lower limits must be variable between 0 and 1 Volt and 0 and 5 Volts respectively. The gap between upper and lower limits must remain constant if the lower limit is changed. The input must accept pulses between 0 and 5 Volts and output information pulses of about 3.5 Volts and 500nSecs duration.

Operation

Fig. 2.9 shows a block diagram of one analyser. Since the system has two slow lines the unit built contained two pulse height analysers which were completely independent.

The input pulses are fed to two voltage comparators which are both arranged so that if the input pulse goes more positive than a given reference voltage then the comparator output changes from logic 0 ($\approx$ 0.2 Volts) to logic 1 ($\approx$ 3.4 Volts). The two reference voltages are controlled by helipots via the voltage reference circuit (Fig. 2.10) which maimtains the voltage levels and the gap between them. A small amount of hysteresis is provided on the comparators by feedback resistors. If the input pulse exceeds both V_{LOW} and V_{HIGH} then both comparators

FIG 2.9 BLOCK DIAGRAM — PULSE HEIGHT ANALYSER.

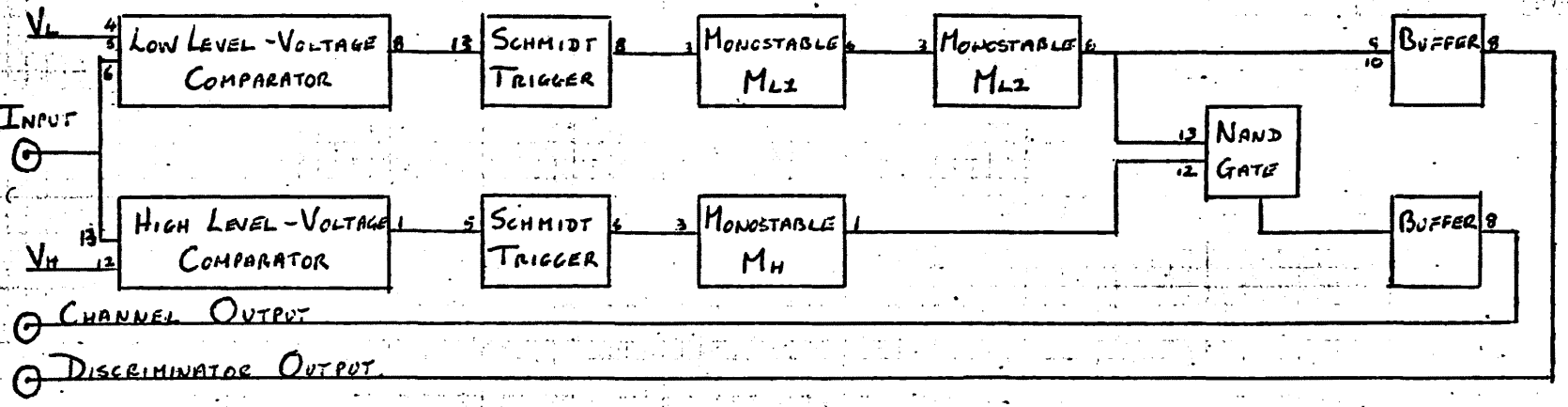

FIG 2.11 ANALYSER ACTION.

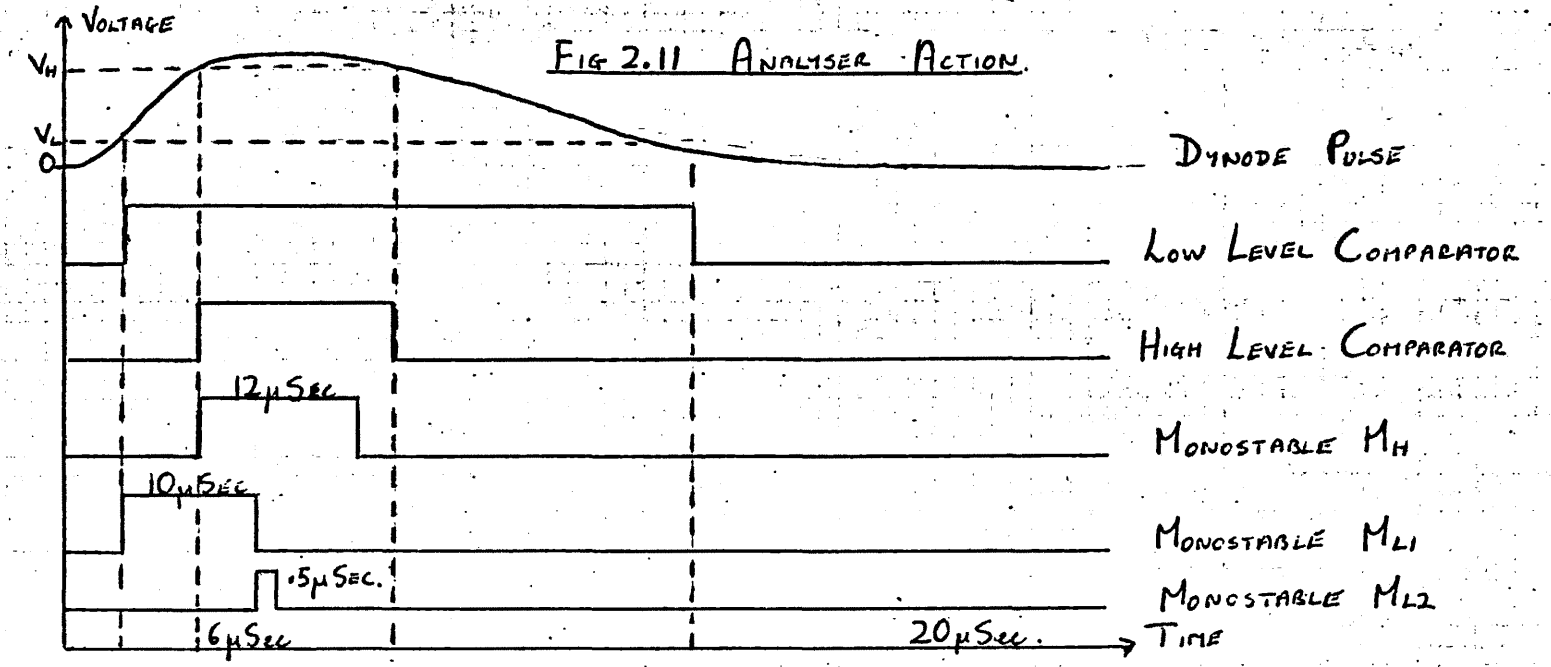

FIG 2.10 DISCRIMINATOR REFERENCE VOLTAGE CIRCUIT DIAGRAM.

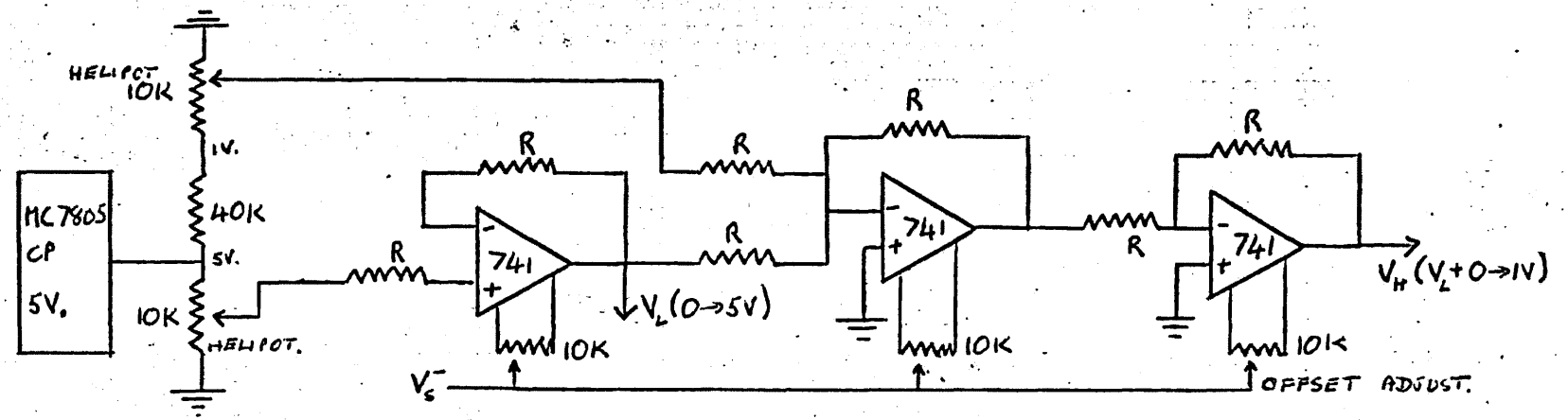

$R = 200K\Omega \pm 1\%$ METAL OXIDE.

output positive pulses which are fed to schmidt triggers which ensure that the time delay through the unit is consistent. The trigger outputs are fed to monostable circuits which provide set length output pulses. The monostable M_{L1} gives a pulse of length greater than the rise time of the photomultiplier pulse. The trailing edge of the M_{L1} pulse triggers the monostable M_{L2} whose output is fed to a nand gate. The other input to this gate is from the monostable M_H which if fired produces a pulse of length greater than those of M_{L1} and M_{L2} combined (Fig. 2.11). Provided M_H has not been fired the pulse from M_{L2} can get through the gate and is output from the unit via a current buffer so that it can be driven down a cable. This pulse from M_{L2} is also output via another buffer before it goes through the gate so that the analyser can be used as a simple discriminator if needed. Fig. 2.12 shows the printed circuit board layout.

2.5 FAST COINCIDENCE UNIT

To determine whether two pulses, one from each detector, are due to two gamma-rays resulting from one annihilation the unit must discover whether the rays were given off simultaneously, i.e. whether the pulses are coincident. Since the response of the detector is very slow, and may vary depending on conditions, the time pick-off device is used to produce a very fast pulse as near to the start of the detector pulse as is possible. There will still be some non-linear time lag through the system due to the limitations of the electronics so that it is

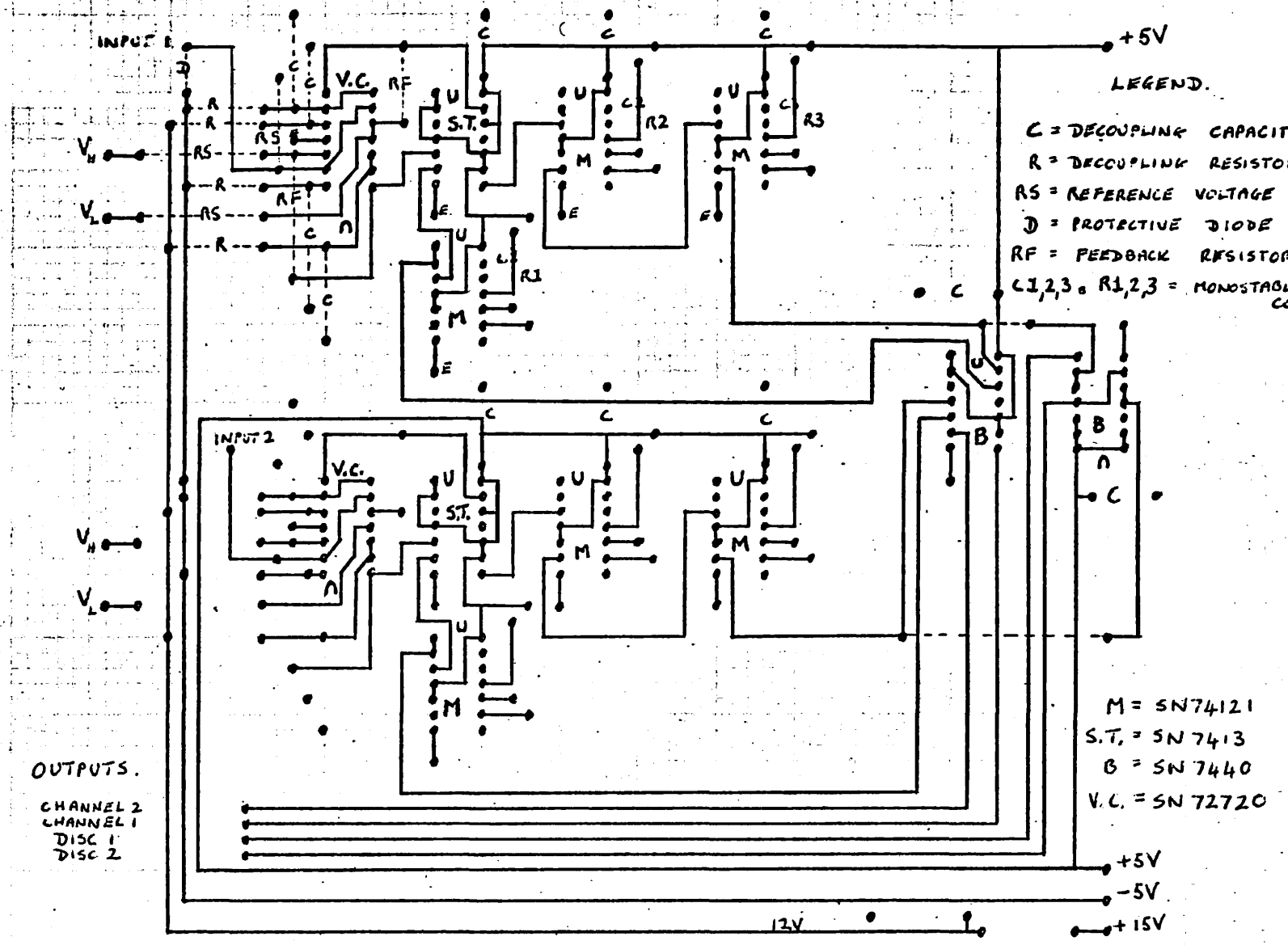

CIRCUIT DIAGRAM — DUAL PULSE HEIGHT ANALYSER. FIG 2.12

only necessary to detect whether the two pulses from the detectors occurred within a few nanoseconds of each other. This test is performed by the fast coincidence unit.

In order to make the unit adaptable to other uses it was designed to accept positive or negative pulses of about 3 Volts and of duration greater than 2 nanoseconds from up to four sources. The unit can determine whether 2, 3 or 4 pulses are coincident (or anti-coincident) with a presettable coincidence resolution time of 3 to 14 nanoseconds. The output pulse occurs after a fixed time from the start of the input pulse although it can be inhibited by a special input signal. There are several output pulses which can be chosen depending on what it is needed for. Fig. 2.13 shows a block diagram of the unit.

Operation

The unit has four input lines any of which can be switched out, when the input is earthed and that line is switched off as far as the coincidence testing is concerned. The input impedence of each line is matched to 100 ohms and protected by fast diodes and each line can be biased via a switch to accept positive or negative pulses. Negative pulses are fed direct to the clock input of a J.K. flip-flop whereas positive pulses are inverted first. Since both the J and K inputs of the flip-flop are tied to logic 1 the outputs Q and $\bar{Q}$ both change. Q goes from logic 0 to logic 1 and $\bar{Q}$ does the opposite. One of these outputs may be selected by the coincidence/anti-coincidence switch for input to the nand gate which performs the coincidence test. The nand gate

requires all its inputs to be at logic 1 to change its output from logic 1 to logic 0 which is only possible if there is a pulse present at all the coincident lines but not at the anti-coincident lines. The output from the nand gate is fed via an inverter to the J and K inputs of another flip-flop.

Another nand gate is arranged so that it is connected to the $\bar{Q}$ outputs of all the input JK flip-flops. Since $\bar{Q}$ changes from logic 1 to 0 then any input pulse will cause this nand gate to change from logic 0 to 1 and this output is fed to an inverter. So far the propagation time of any pulse from input to the output of the inverters in both test lines should be identical. But the pulse in the coincidence line is fed to the J and K inputs of a flip-flop which has a minimum setup time of 3 nSecs. If the information on the J and K inputs has not been there for at least 3 nSecs. before the clock pulse starts then that information is not recognised. So, if the pulse along the second test line is to be used as the clock pulse it must be delayed by at least 3 nSecs. longer than the pulse in the coincidence test line. Let 't' be the propagation delay through the unit to the output of the inverters in both test lines and led 'd' be the delay put in between the second test line inverter and the clock input of the second stage flip-flop. Suppose one pulse is input at time zero then this information will be conveyed to the clock input after time 't + d'. If there has been a coincidence then this information must reach the J and K inputs at time 't + d - 3 nSecs.' for it to be recognised. But this means other input pulses

must have been present between time zero and time 'd-3' nSecs. for a coincidence to be recognised and so d-3 nSecs. is the coincidence resolution time.

The delay in the second line is produced by feeding the inverter output to 3 and gates in series. Each and gate has a propagation delay time of 5 nSecs. so that the resolution may be changed by feeding the output from a different and gate to the clock input of the second stage flip-flop. The output from the and gate is also fed to the clear inputs of all the input stage flip-flops to reset them. Since the delay 'd' can be selected to be 5, 10 or 15 nSecs. then, taking the pulse rise times into consideration, the resolution time may be (d-3 nSecs.) , 3, 8 or 13 nSecs.

If the second stage flip-flop recognises a coincidence and changes, the Q output is fed to a nand buffer and hence output from the unit (A fast pulse). The Q output is also fed to another nand gate whose output is fed to the clear input of the second stage flip-flop to reset it. This nand gate output is also taken to the clock input of the third stage flip-flop whose J and K inputs are also connected to the second stage flip-flop's Q output. Thus every time a coincidence is detected a very fast signal is output and the second stage flip-flop is quickly reset. The third stage flip-flop can however be used to produce a much slower output suitable for most scalers, etc.

When the third stage flip-flop changes the $\bar{Q}$ output is fed to a standard T.T.L. monostable which produces a set length pulse of about 500 nSecs. which is output via a

FIG 2.13 BLOCK DIAGRAM — FAST COINCIDENCE UNIT.

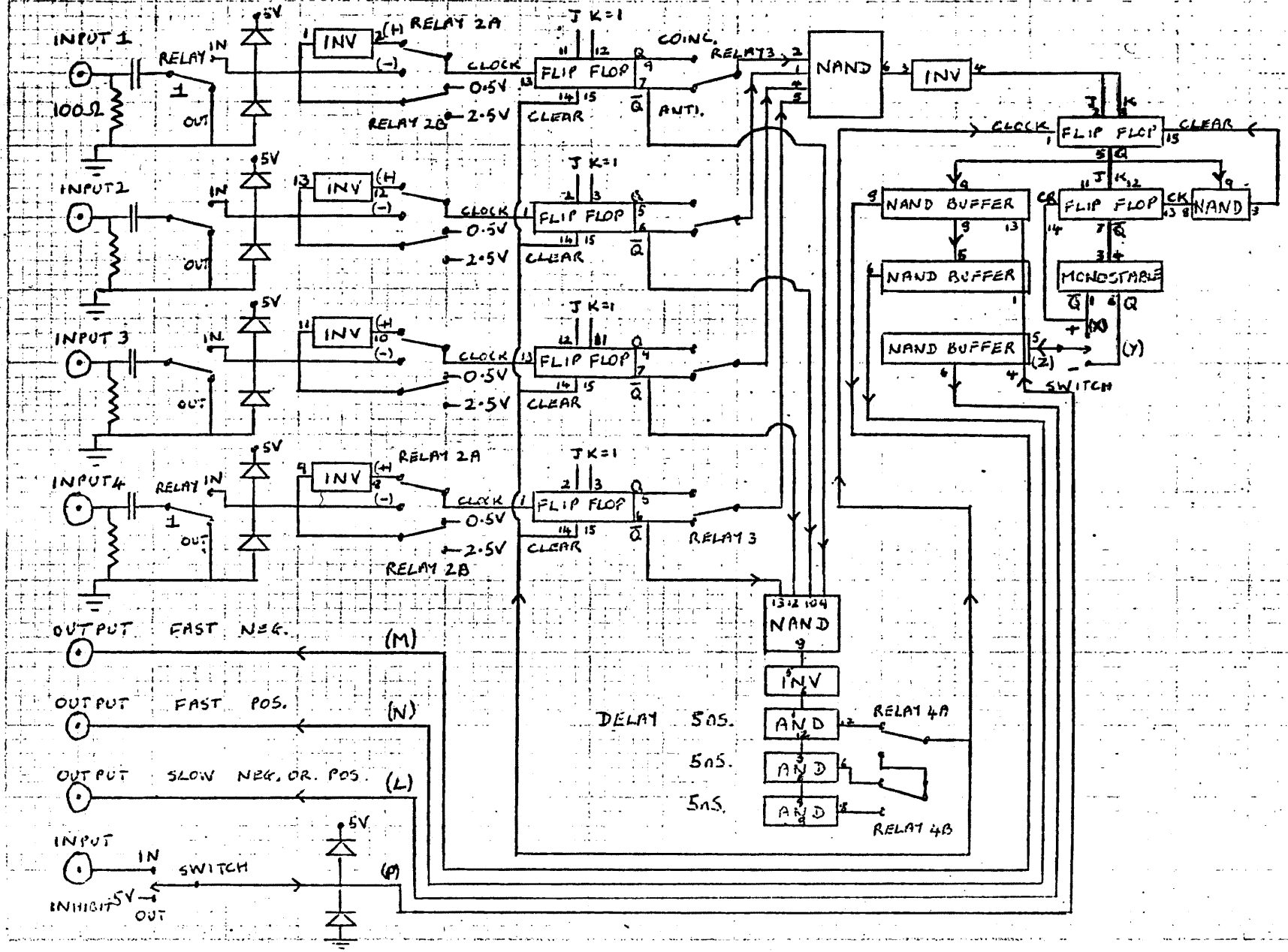

nand buffer and which is also fed back to the clear input of the third stage flip-flop to reset it. There is a fifth input line to the unit which can be used for an inhibit signal or can be switched out. When the negative inhibit signal is present it inhibits all the output buffers and hence there are no output signals.

Unless otherwise stated all the integrated circuits used are Schottky T.T.L. devices which are high speed and have a typical propagation delay time of 3 nSecs. The propagation delay time through the unit is approx. 20 nSecs. for the fastest pulse. Fig. 2.14 is the printed circuit diagram and Fig. 2.15 shows the switching arrangements. The actual switching is done by remote relays mounted on the printed circuit board.

2.6 TRIPLE COINCIDENCE UNIT

The final stage of the triple coincidence system is to test whether the pulses from the pulse height analysers and from the fast coincidence unit are all in coincidence. The unit must accept pulses from three sources and determine whether they occur within a specific period of time. The count rate will not be very high and the input pulses will be 'slow'. Provision must be made to delay pulses in individual lines by varying amounts to compensate for electronic lags in the amplifiers, etc. If the pulses are coincident the unit must output a pulse suitable for counting by a scaler. The typical delay required in each channel is 1 to 10 μ Secs. and the coincidence resolution time should be variable over the range

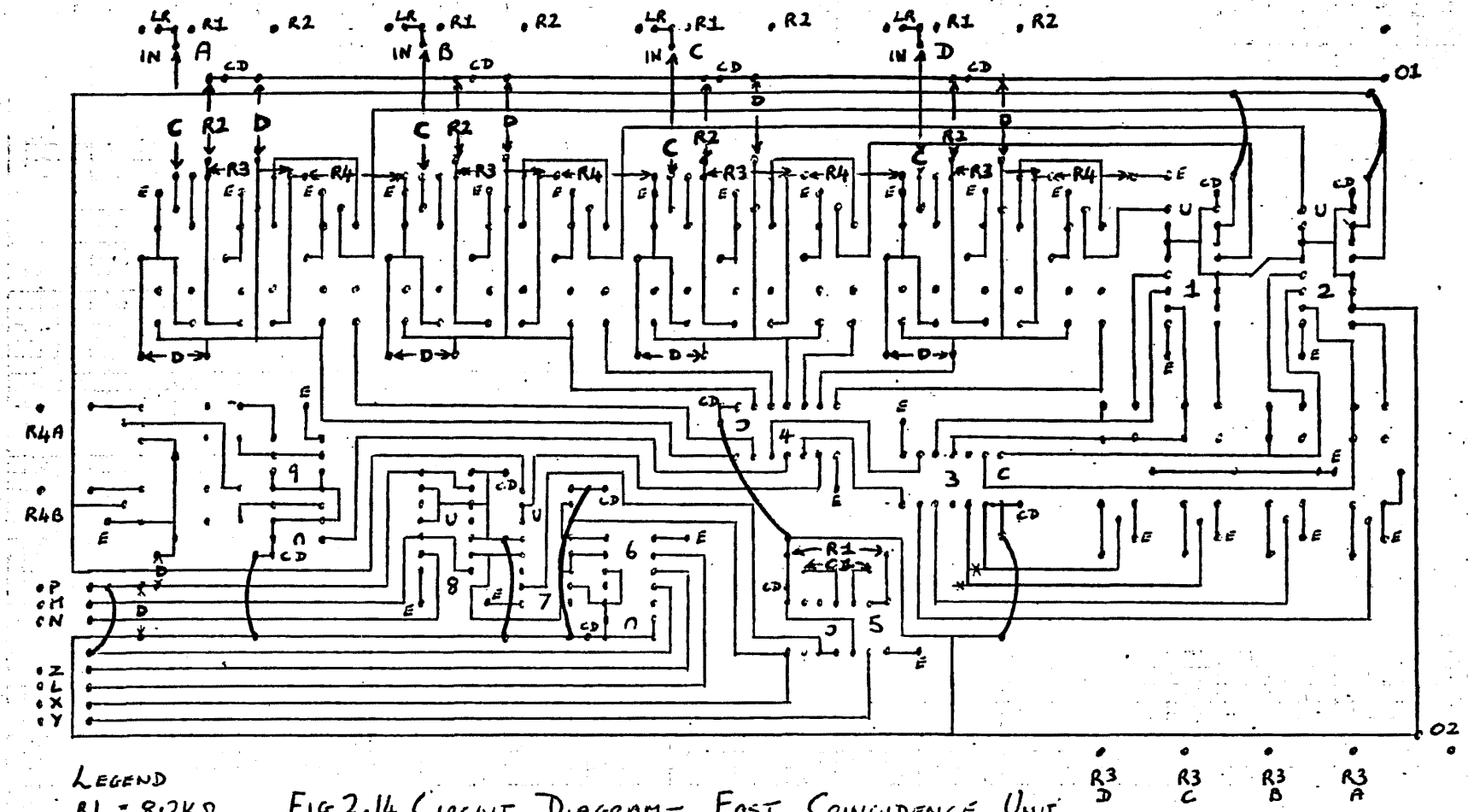

FIG 2.14 CIRCUIT DIAGRAM – FAST COINCIDENCE UNIT.

LEGEND

R1 = 8·2KΩ
R2 = 5·11KΩ
R3 = 4·3KΩ
R4 = 1·0KΩ
LR = 110Ω – LOAD RESISTOR.
C = ·1μF – POLYSTYRENE (100MHz)
C1 = 100pF
D = IN4148 – HIGH SPEED
CD = ·1μF – POLYSTYRENE – DECOUPLING CAPACITOR.
E = EARTHED THROUGH BOARD.

INTEGRATED CIRCUITS.

1,2,7	= SN74S112	FLIP FLOP (S)
3	= SN74S20	NAND GATE (S)
4	= SN74S04	INVERTER (S)
5	= SN74121	MONOSTABLE (N)
6,8	= SN74S40	NAND BUFFER (S)
9	= SN74S11	AND GATE (S)
OTHER UNITS	= RS5	REED RELAY

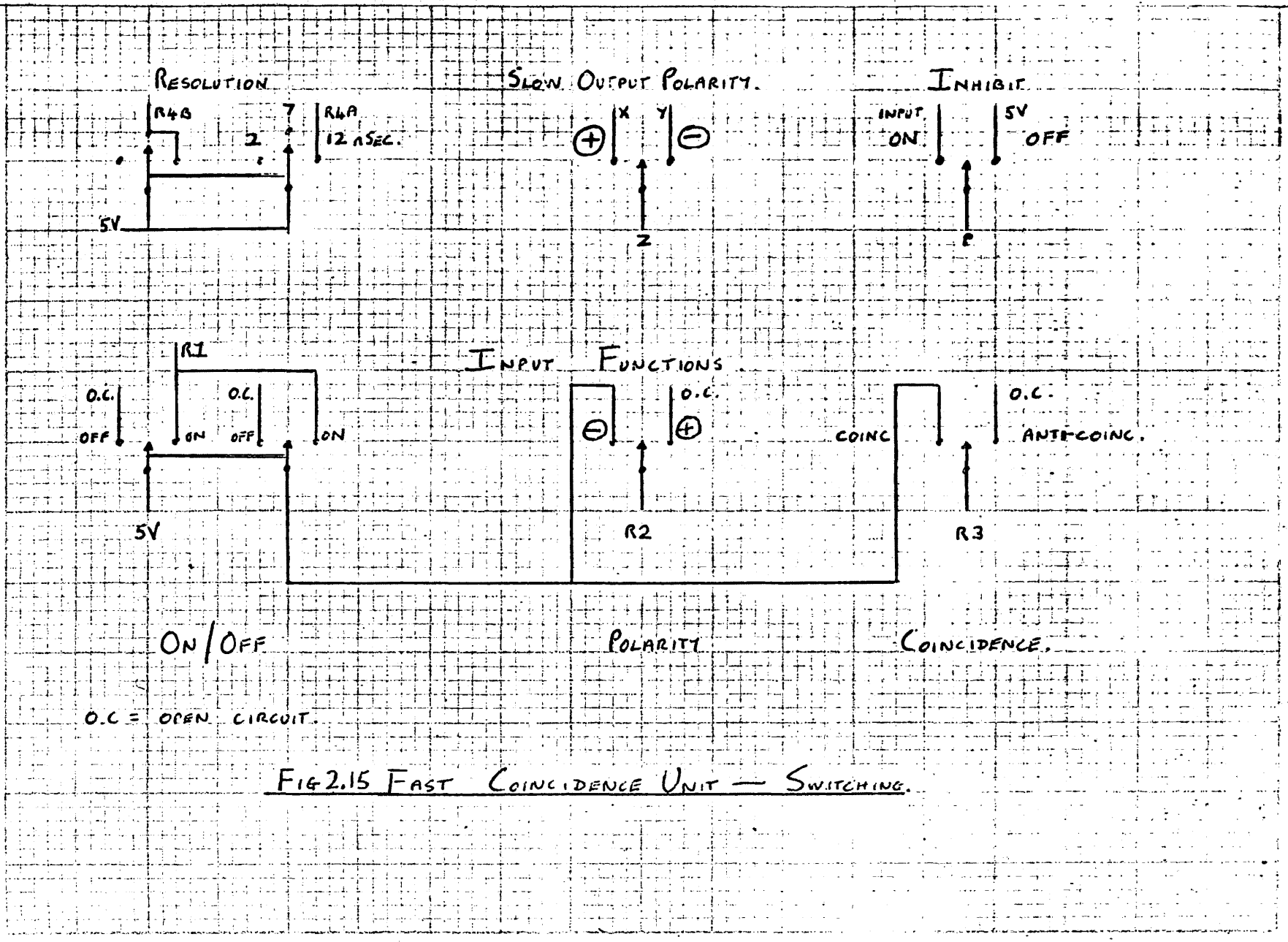

FIG 2.15 FAST COINCIDENCE UNIT — SWITCHING.

.1 to 1μ Sec. The unit must accept negative input signals of 3 to 10 Volts and of 200 to 600 nSecs. duration. The output should be a pulse of about -7 Volts and of about 400 nSecs. duration. To help set up the system the various delay and resolution pulses are output at test points so that they can be displayed on a 'scope. Fig. 2.16 shows a block diagram of the system.

Operation

Input pulses are fed via fast protective diodes to an emitter follower circuit which provides a high input impedence and also limits the pulses to not more than 5 Volts. This protects the integrated circuits which are very vulnerable to large pulses. The pulse from the emitter follower is used to trigger a monostable whose output pulse is variable between 1 and 10μ Sec. in duration, controlled by a variable timing resistor mounted on the front panel of the unit. This pulse is fed to a second monostable which triggers on the trailing edge so that the first monostable effectively produces a 1 to 10μ Sec. delay. The output of the second monostable has a presettable length between .05 and .5 μ Sec. which determines the resolution time for a coincidence. The coincidence test is performed by an and gate and since the output of this gate will be dependent on the overlap of the input pulses it is used to trigger another monostable which gives a suitable length pulse for output to a scaler, etc. A current buffer is employed so that the final shaped pulse can be driven down cables.

Block Diagram - Triple Coincidence Unit. Fig 2.16

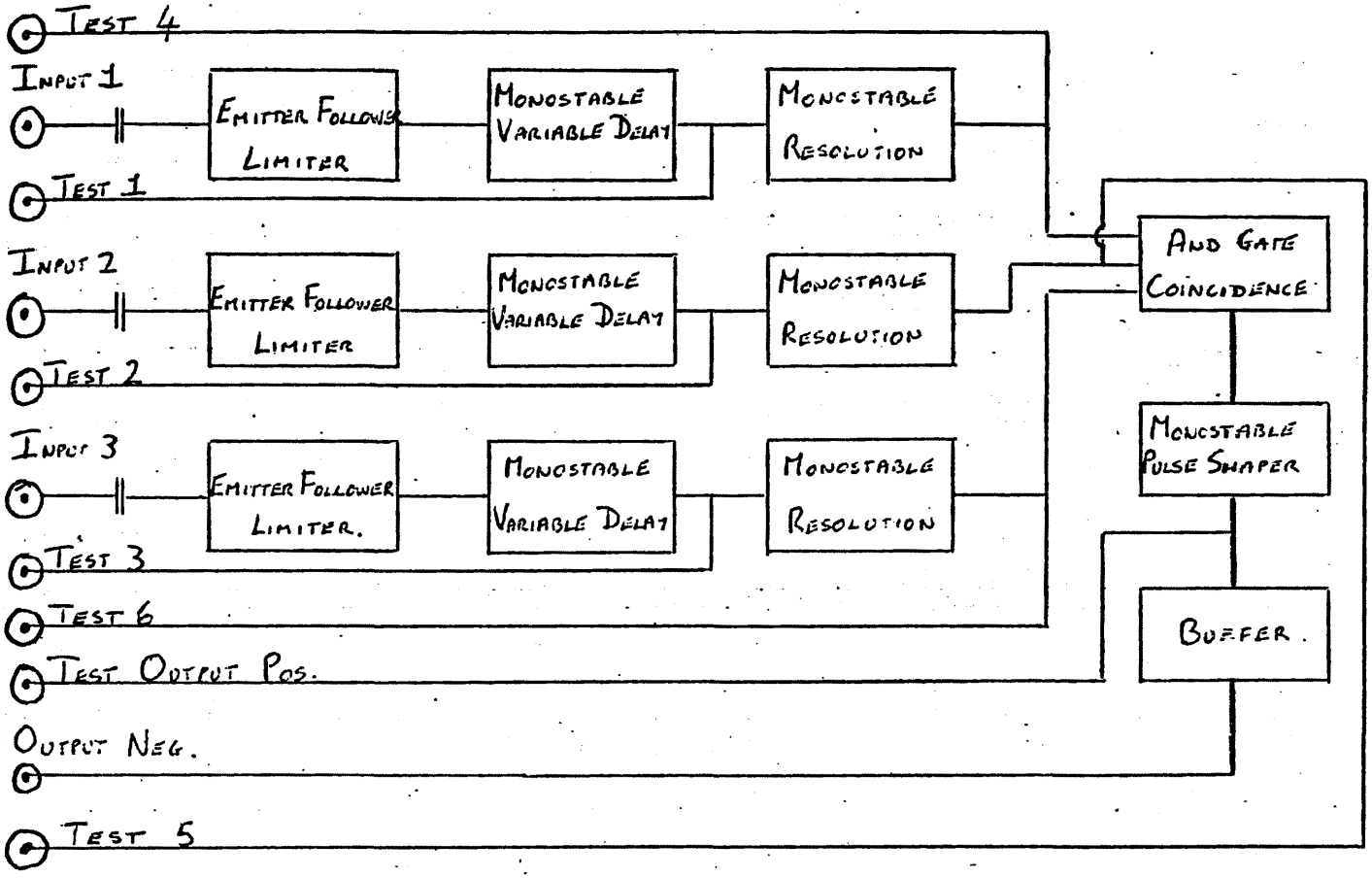

The coincidence resolution time is 2τ where τ is the preset length of the pulses produced by the second stage monostables. Fig. 2.17 is the printed circuit diagram.

2.7 TIMER UNIT FOR '2000' SERIES SCALER

The scalers used to count the slow line pulses for test purposes were Harwell '2000Series' scalers which had no internal timing provision. Therefore the scalers must be controlled by an external timer using the remote gating facilities supplied on the scaler. The scaler gating logic was:

+ 15 Volts implies count

0 Volts implies stop counting

- 30 Volts implies reset counters to zero.

To make the external timer adaptable it must not only produce these logic signals for use with a scaler but it must also respond to similar logic signals itself so that a master controller can be used if necessary. The timing period should be variable from about 1 Second to say 50,000 Seconds (15 hours) and during this period the timer must output + 15 Volts. The timing period must be accurately repeatable and started either manually or by a remote signal. Similarly the timer must output a - 30 Volts signal in response to a similar remote signal or a manual signal in order to reset the scaler. It must reset itself at the same time. Visible indication that the timer is working is necessary. Fig. 2.18 is a block diagram of the unit.

Circuit Diagram- Triple Coincidence Unit. Fig 2.17

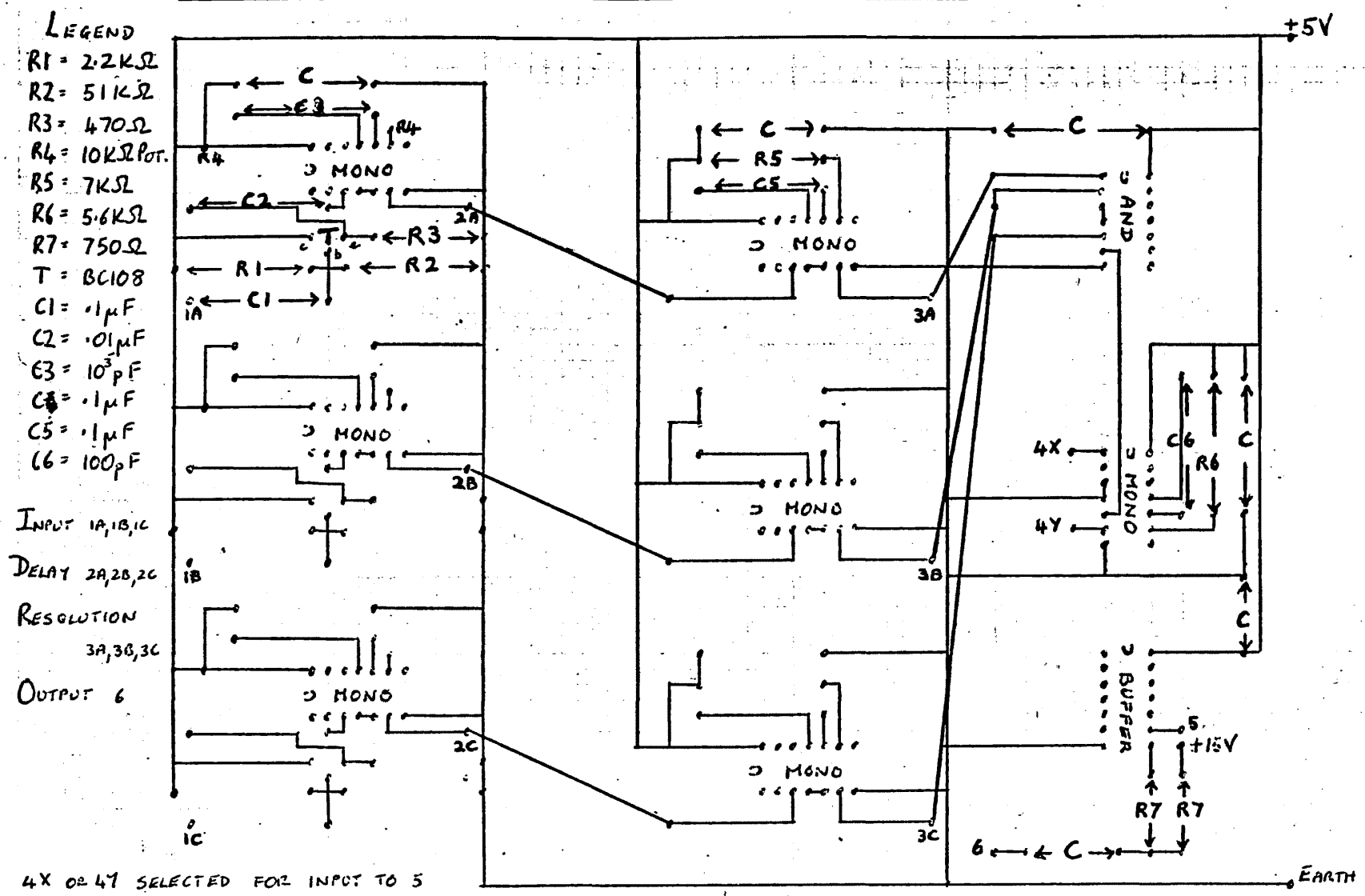

Operation

A small mains transformer produces a 4.5 Volt peak to peak signal which is full wave rectified by diodes 1 which lead to a schmidt trigger which outputs square waves at 100 Hz. When relay 1 is on these pulses are fed to six decade counters in series which are arranged in divide by ten mode. The output from one of the last 5 is selected by a panel switch for input to a seventh decade counter. These outputs occur after 1, 10, 100, 1000, or 10^4 Seconds from the start pulse. The seventh decade counter's mode can be changed by a second panel switch so that the output follows 1, 2, 5 or 10 input pulses. The timing period can thus be 10^0, 10^1, 10^2, 10^3, 10^4 Seconds multiplied by 1, 2, 5 or 10.

The seventh counter's output is fed to a bistable circuit (Fig. 2.19) which then turns a buffer to an 'off' state. This buffer controls relay 4 which is in the output line. When the timer is activated either by switch 4 or a remote signal (providing switch 4 is in the mid position when the remote input line is connected) a + 15 Volts signal is fed via diode 3 to relay 1 and the timing begins. The 15 Volts signal is also output from the timer via relay 4, when this is activated by the start of timing period signal, and is used to illuminate a bulb to indicate that the timer is functioning. At the end of the timing period relay 4 is opened and the output falls to zero.

A - 30 Volts signal either selected manually by

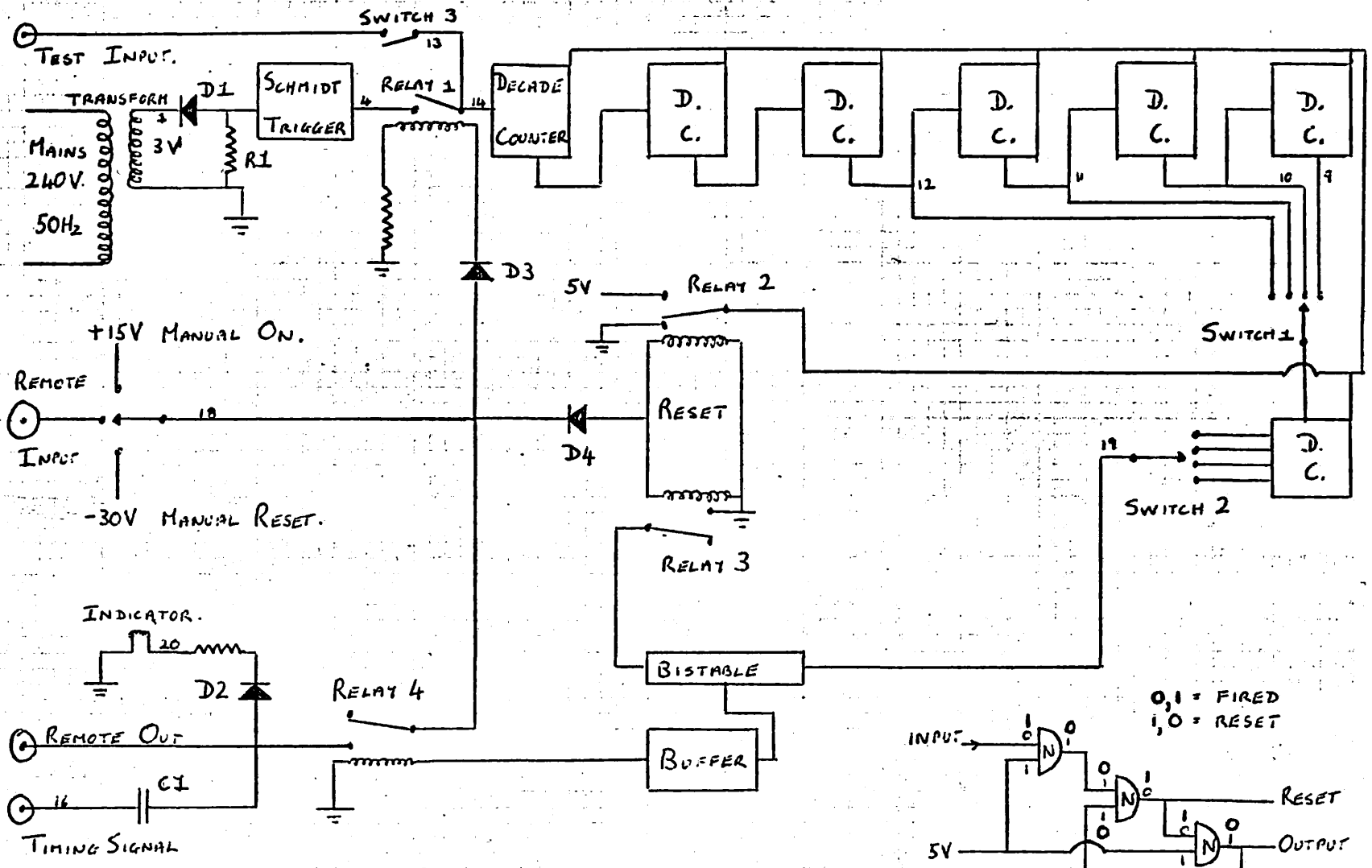

BLOCK DIAGRAM – 2000 SERIES TIMER. FIG 2.18

BISTABLE CIRCUIT (NAND GATES) FIG 2.19

switch 4 or from a remote controller will be fed via diode 4 to relays 2 and 3 which reset the decade counters and the bistable circuit which in turn closes relay 4 (via the buffer) so that the - 30 Volts signal is output from the timer. A decoupled output is provided so that information about the timer can be sent back to the master controller. Fig. 2.20 is the printed circuit layout and Fig. 2.21 shows the switching arrangements.

2.8 TIMER-SCALER

Almost all information about numbers of positrons, fast coincidences, etc. is conveyed by pulses which come from various points in the system and need to be counted. Usually the pulses are counted for a set period of time. A timer-scaler must accept pulses of either polarity of magnitude between 2 and 30 Volts. It must count the pulses for a pre-determined time which should be variable between 1 second and 24 hours and which must be repeatable to within a few μSecs. There must be a variable threshold on the input so that the unit can discriminate against noise and pulses below a certain height. The number of pulses counted must be visibly displayed and if the count capacity of the unit is exceeded it must both give a warning to this effect and output pulses which could be counted by another scaler. The timing period signal should be output so that it can control other units whilst the scaler-timer itself must be controllable by another remote unit. Visible indication should be given of both the timing period and when the input gate is open enabling

CIRCUIT DIAGRAM – HARWELL '2000' SERIES TIMER. FIG 2.20

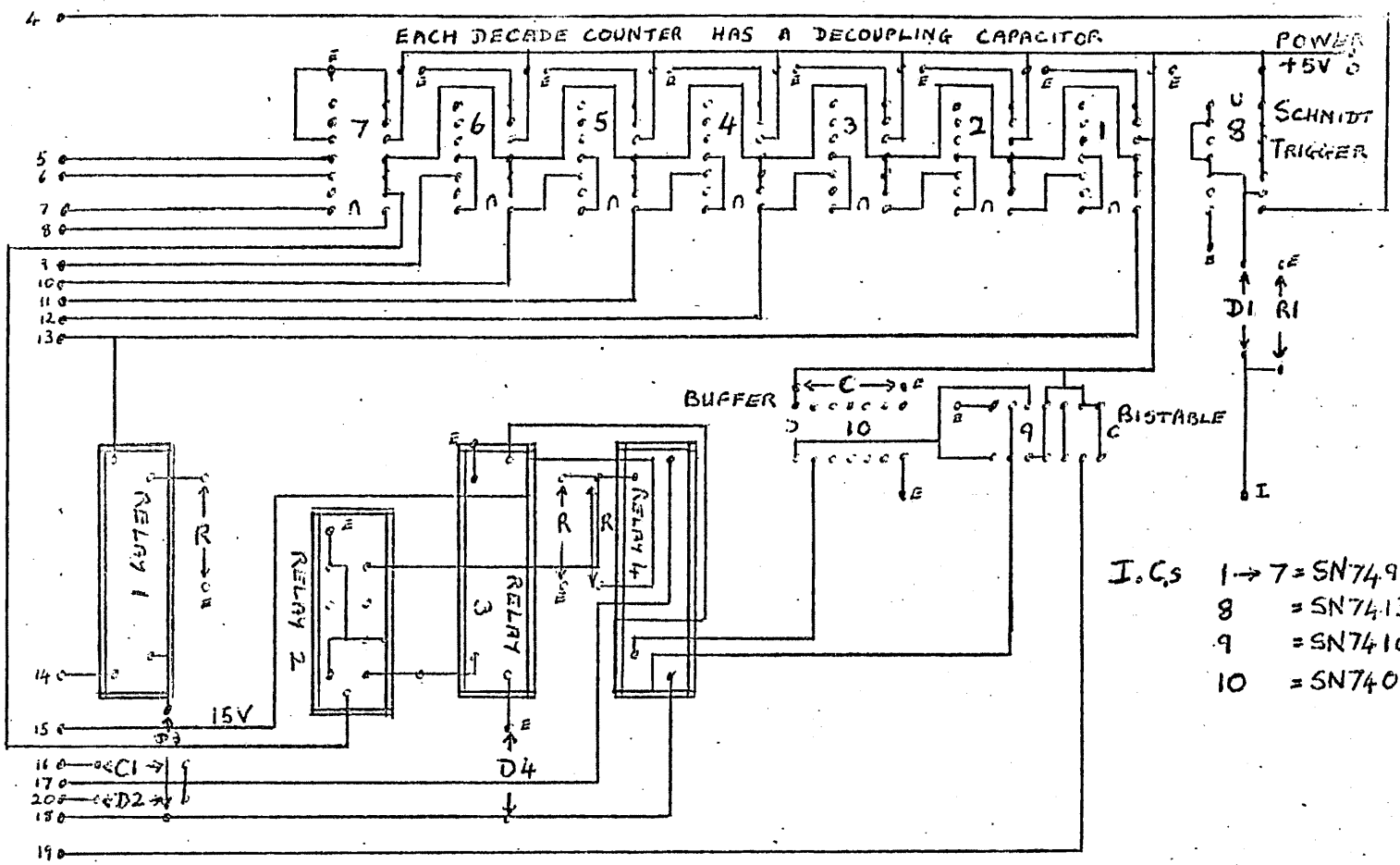

FIG 2.21 '2000' SERIES TIMER SWITCHING.

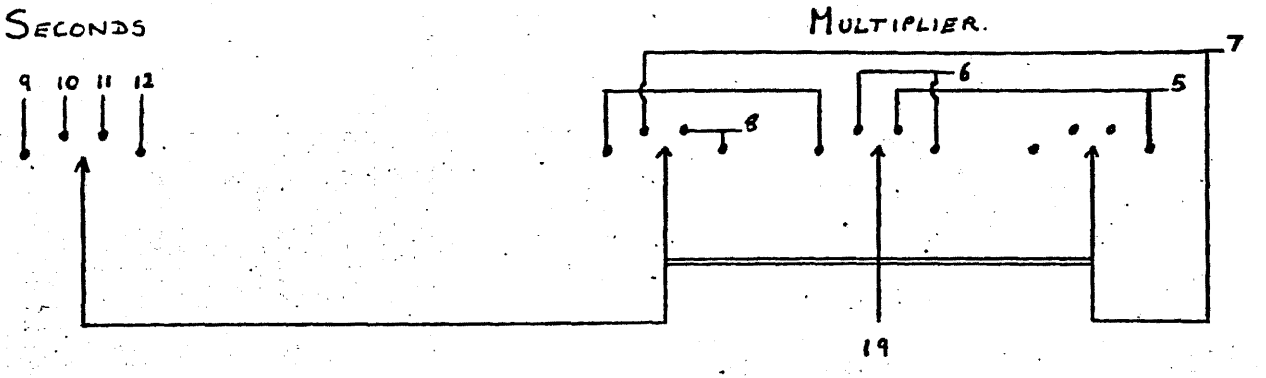

TIMING PERIOD SWITCHES.

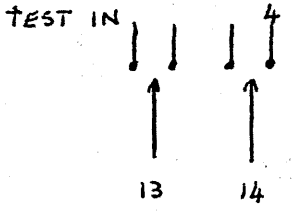

TEST SWITCH

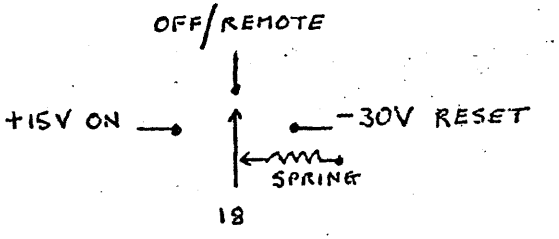

CONTROL SWITCH

the scaler to count. The unit must be capable of timing the length of an external operation to within 1 mSec. All functions of the timer-scaler must respond to the logic:

+ 3.5 Volts = logic 1 = on or start

0 Volts = logic 0 = off or stop.

Operation of Power Supply

A mains transformer produces 12 Volts a.c. which is full wave rectified by a bridge rectifier. This signal is then smoothed by a 10,000 μF capacitor and then input to two 5 Volt regulators type LM309K (National Semiconductor) which are capable of delivering up to 1.5 amps of ripple free output. One regulator powers the scaler section and the other powers the console and timer sections. Fig. 2.22 is a block diagram of the power supply.

Operation of Scaler Section

Input pulses are fed through a 10KΩ potentiometer which taps off a fraction of the pulse to provide the adjustable threshold in conjunction with the schmidt trigger which follows. The signal is fed to an emitter follower which also acts as a limiter, and the line is protected by fast diodes on both sides of the emitter follower. The signal is then fed to a schmidt trigger whose input d.c. bias is selected by a switch so that positive or negative pulses can be accepted. Fig. 2.23 shows the input circuit.

The schmidt trigger is also a nand gate and so inverts the pulses which go through the gate to another

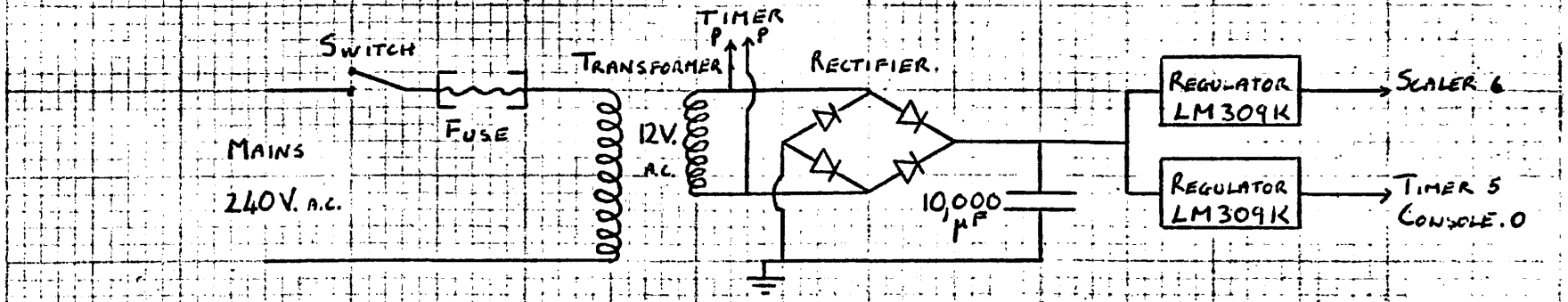

FIG 2.22 CIRCUIT DIAGRAM — TIMER-SCALER POWER SUPPLY.

FIG 2.23 CIRCUIT DIAGRAM — TIMER-SCALER INPUT CIRCUIT.

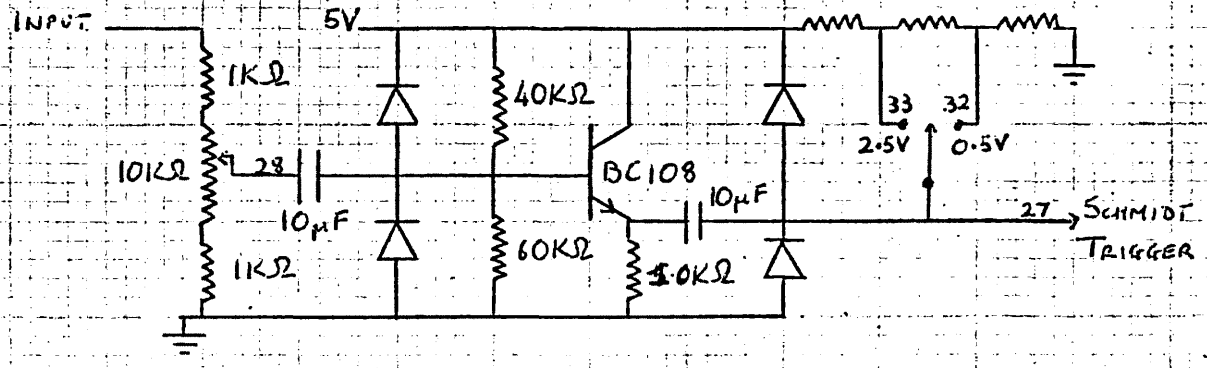

DIODES ARE FAST TYPE IN4148.

inverter. The polarity switch selects either the schmidt nand gate output or the inverter output or the internal timing signal for input to a gate which is controlled by the console. The console allows the gate to open and shut in response to a signal from the timer or from an external manual switch or from a remote source. When open the gate passes the pulses through to the decade counters which count the pulses and give a binary coded output. This is fed to the decoders/buffers whose output is compatible with the seven segment readout devices used to display the count in denary. If the sixth decade counter reaches the count of 10 a signal is sent to a monostable which produces a set length pulse which is fed back to the console where it is output from the unit via a buffer for counting by another scaler. The monostable pulse is also used to trigger a bistable circuit which illuminates a bulb to indicate that overflow has occurred. Fig. 2.24 shows a block diagram of the scaler section and Fig. 2.25 is the printed circuit.

Operation of Timer Section

The 12 Volt a.c. signal from the mains transformer is full wave rectified by a second bridge rectifier and the amplitude reduced by a potential divider. This signal is fed to a schmidt trigger which produces a square wave at 100 Hz. which is fed to a nand gate controlled by the console. When open the gate allows the square wave to go through to the main timing circuit which consists of 7 decade counters. The first six produce 'divide by 10' outputs in sequence, one of which is selected by a switch

for input to the seventh counter which is arranged to give a separate output for 1, 2, 4 or 8 pulses in. One of these outputs is selected by another switch for returning to the console section as the stop signal. The first decade counter produces a special pulse which is also sent back to the console as the start/stop signal. The use of two pulses in this way ensures that the timing period is accurately repeatable. Timing periods are 10^0, 10^1, 10^2, 10^3, 10^4 seconds multiplied by 1, 2, 4 or 8. By disconnecting the timer the scaler will count indefinitely. Figs. 2.26 and 2.27 show the block diagram and printed circuit of the timer section.

Operation of Console Section

This consists of the controlling logic circuits mostly made up from gates and the buffers which are required in connection with output signals and warning indicators. The special timer bistable circuit (Fig. 2.28) controls the timed counting period of the scaler and indicates when it is on by illuminating a bulb. It responds to start and stop signals from the timer section and can only be reset manually. A start signal affects the lower three gates and the outputs A and B cause:

(1) a logic 1 signal to be sent to the scaler input gate opening it;

(2) an indicator bulb to glow via a buffer;

(3) the remote timing output to go to logic 1.

A stop signal affects the upper three gates so that they turn the lower three gates off, i.e. outputs A and B off. The bistable will not respond to any more signals until it has been reset.

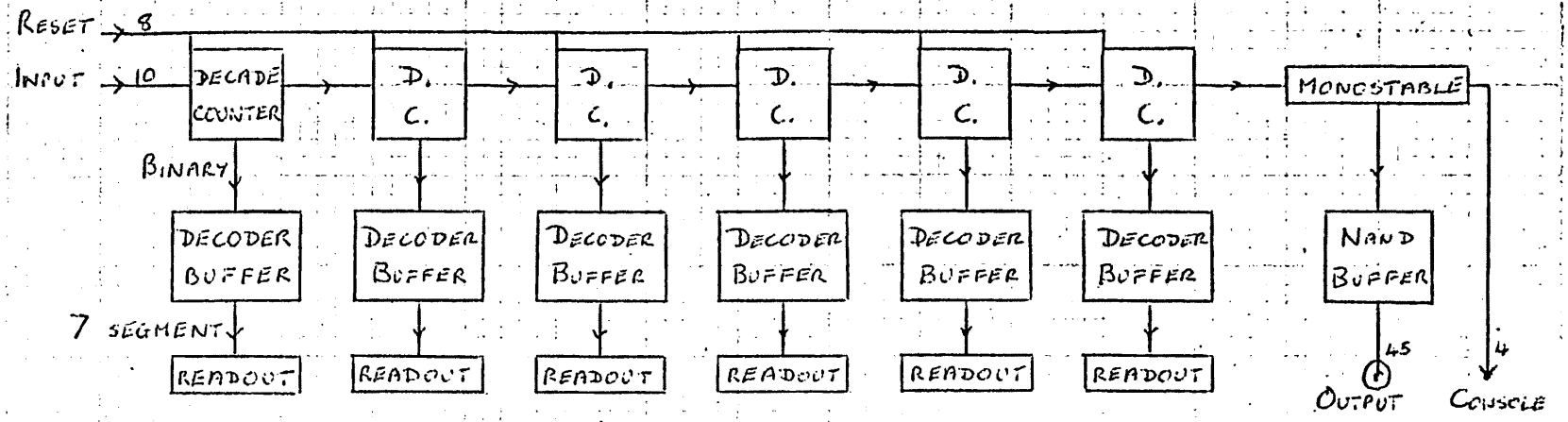

FIG 2.24 BLOCK DIAGRAM – SCALER SECTION.

TIMER – SCALER

FIG 2.26 BLOCK DIAGRAM — TIMER SECTION.

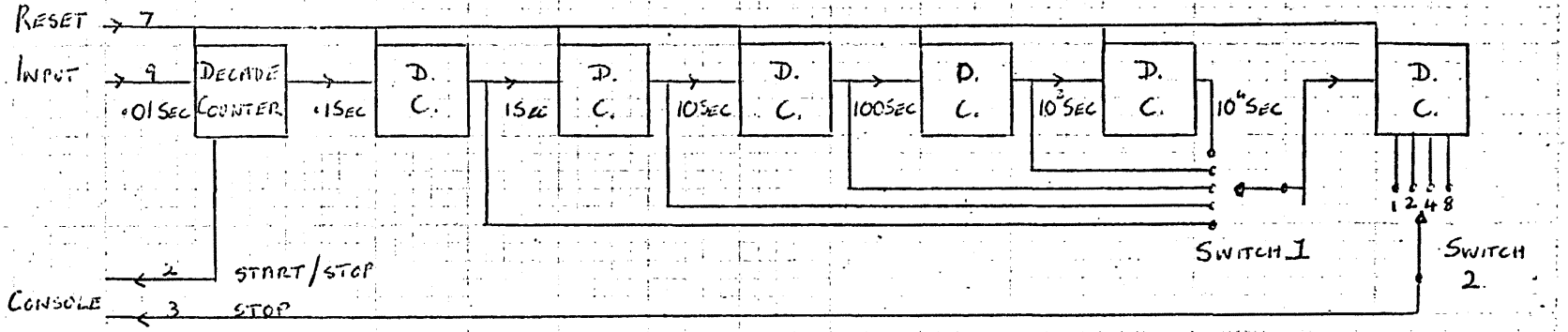

Circuit Diagram — Timer Circuit. Fig 2.27

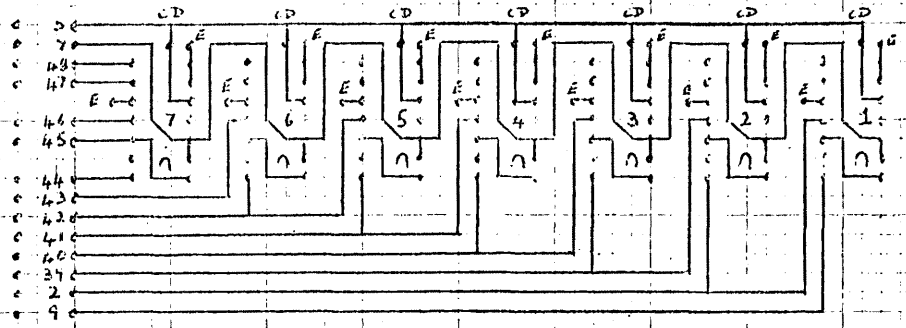

Integrated Circuits 1→7 are SN7490

Decade Counters arranged in binary

count mode.

E = earthed through board.
CD = decoupling capacitor
— = wire connection.

Circuit Diagram — Scaler Circuit. Fig 2.25

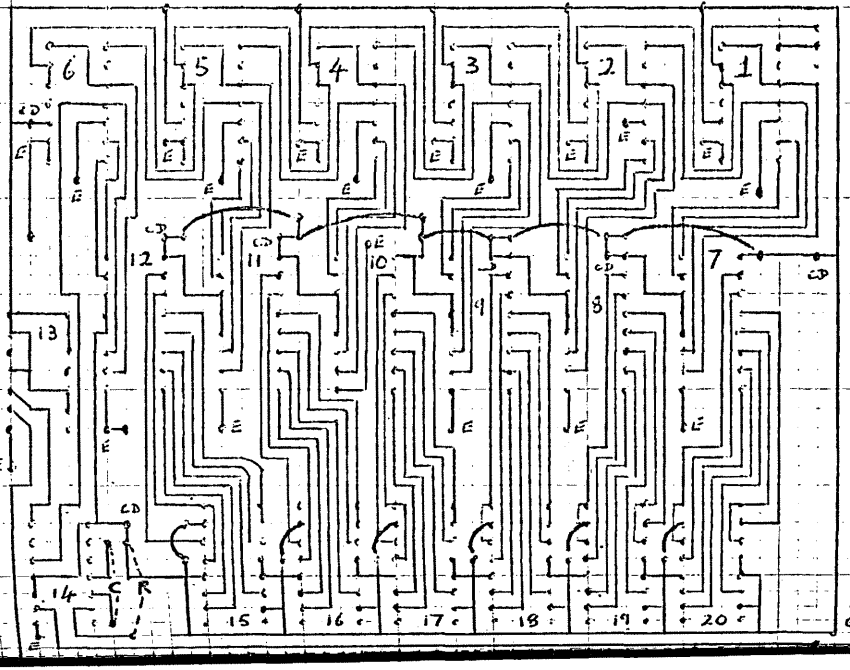

Integrated Circuits

Nos 1→6 = SN7490 Decade Counters.
7→12 = SN7447 Decoder/Buffer.
13 = SN7440 Nand Buffer.
14 = SN74121 Monostable.

Indicators

Nos 15→20 = Minitron Type 3015F

C = Monostable timing capacitor — 100pF
R = Monostable timing resistor — 6·8 KΩ.

The scaler overflow bistable circuit (Fig. 2.29) is turned on by a pulse from the scaler section when it causes an overflow warning indicator to glow. It is reset manually.

The console section contains all the switching for the various modes of operation and in some cases contains interface devices between both the unit and external links and between sections where a current boost is necessary, e.g. reset lines. Figs. 2.30 and 2.31 show the block diagram and printed circuit of the console section. Fig. 2.32 shows the switching arrangements.

FIG 2.31 CIRCUIT DIAGRAM — TIMER-SCALER CONSOLE.

LEGEND.

R1 = 500Ω
R2 = 2·2KΩ
R3 = 40 KΩ
R4 = 60 KΩ
R5 = 10 KΩ
R6 = 2·7KΩ
R7 = 2·2KΩ
R8 = 500Ω.
C = 10μF
D = SLOW DIODE
FD = FAST DIODE IN1148
RR = REED. RELAY RS5
T = BC108.

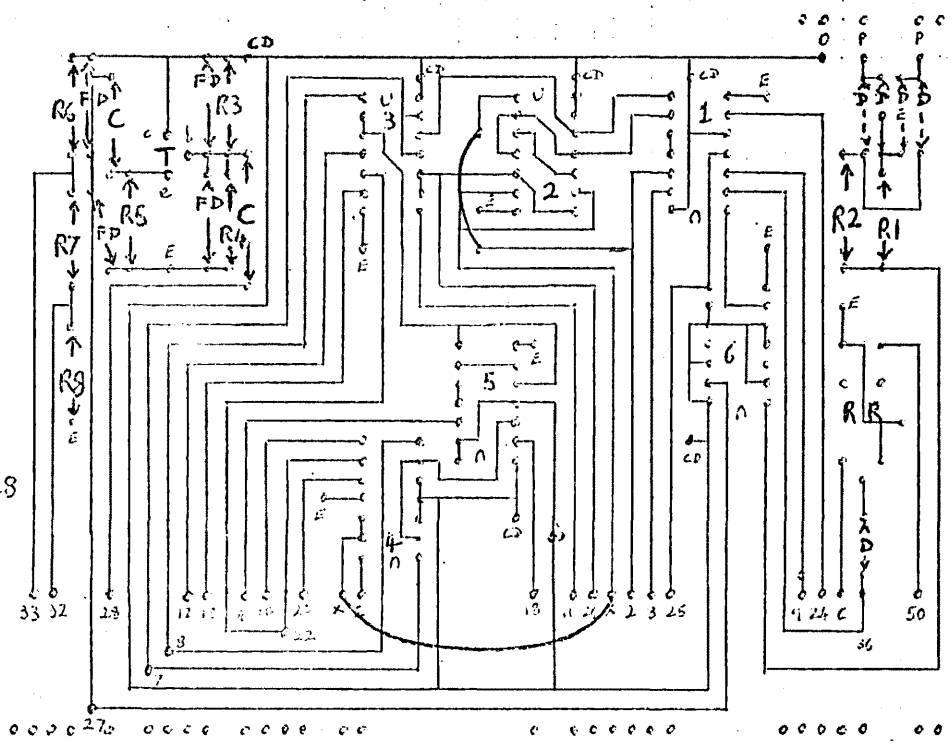

INTEGRATED CIRCUITS.

1,2,5 = SN7400 NAND
3 = SN7416 INV. BUFFER.
4 = DM8091 NAND BUFFER
6 = SN7413 SCHMIDT NAND.

E = EARTHED THROUGH BOARD.
CD = DECOUPLING CAPACITOR.
⌒ = WIRE CONNECTION.

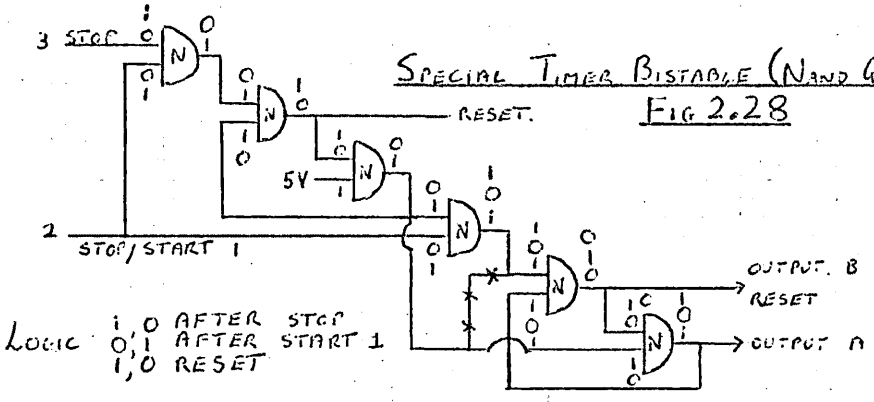

SPECIAL TIMER BISTABLE (NAND GATES)
FIG 2.28

LOGIC 1,0 AFTER STOP
0,1 AFTER START 1
1,0 RESET

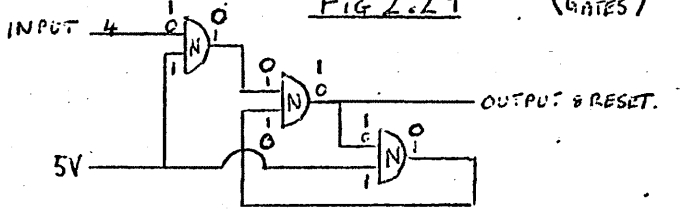

SCALER OVERFLOW BISTABLE. (NAND GATES)
FIG 2.29

LOGIC 0,1 AFTER INPUT
1,0 RESET

FIG 2.30 BLOCK DIAGRAM — TIMER-SCALER CONSOLE.

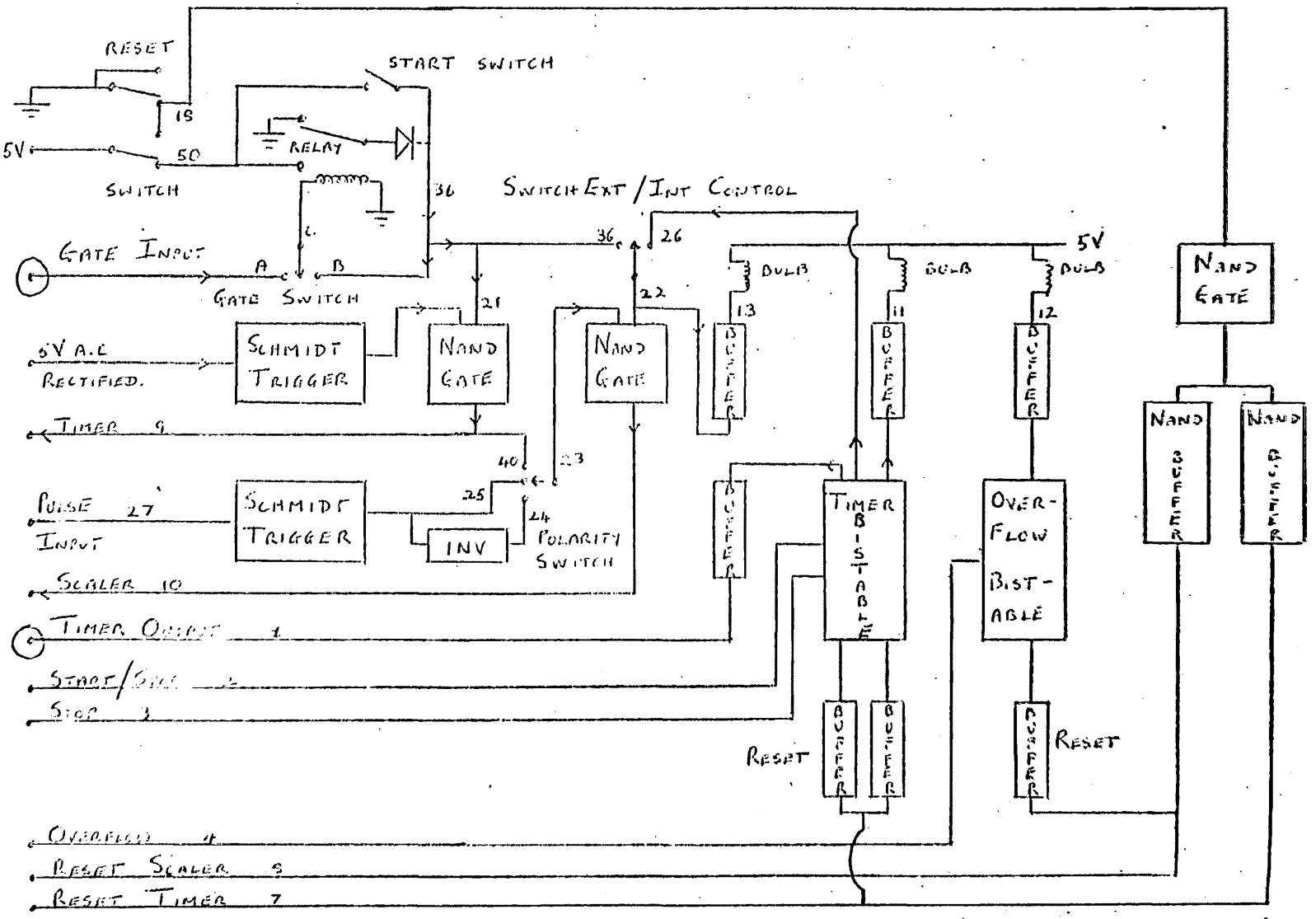

TIMER - SCALER —— SWITCHING. FIG 2.32

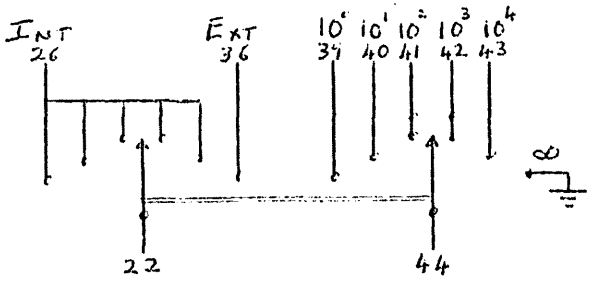

SECONDS ← TIMING PERIOD →

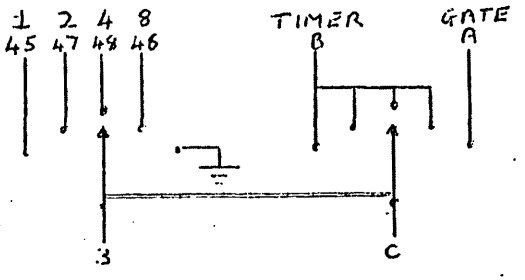

MULTIPLIER OR GATE CONTROL.

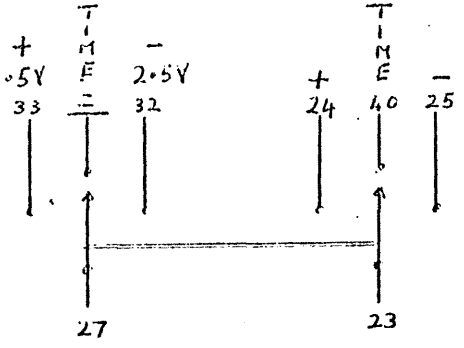

INPUT POLARITY OR TIMING MODE.

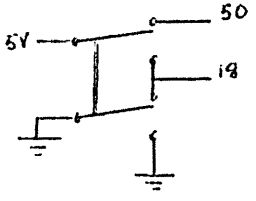

RESET

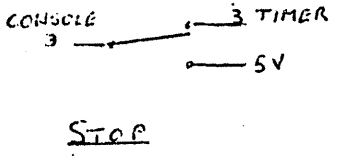

STOP

PUSH SWITCHES BIASED UP.

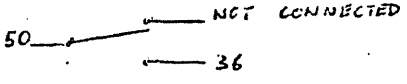

START

CHAPTER 3

CHANNELLING

3.1 INTRODUCTION

Stark predicted in 1912 that protons would show anomalous penetration in an ordered crystal providing that the crystal lattice was in such a direction that it presented open 'channels' to the proton beam. A computer was used to simulate the channelling effect (Robinson and Oen, 1963) before the first direct evidence was published (Nelson and Thompson, 1963). The experiment described consisted of projecting an ion beam on to a gold single crystal foil 3000 A° thick and then collecting the transmitted ions. The current due to the collected ions was found to be dependent on the relative angle between the beam and one of the major axes of the crystal. The conclusion drawn was that the ion trajectory might be led into the open channels in the crystal structure by a series of small angle collisions provided that the ion energy was such that the mean free path between wide angle collisions was much larger than the lattice spacing. Channelling would only occur if the cross section for small angle collisions was large enough to make the process effective.

The results were confirmed by showing that the reflected ion yield decreased when the incident beam was parallel to a crystal axis and that both effects ceased if the crystal lattice structure was damaged. The

channelling ion had its trajectory deflected by glancing collisions with lattice atoms giving a zig-zag motion down the channel. At the ion energies used energy loss was due to ion-electron collisions which would decrease in low electron density channels so that the range would increase. However, distortions of the lattice periodicity caused by radiation damage or thermal vibrations would interfere with the effect.

An analytical range-energy relationship for a copper ion channelling in a copper lattice was obtained by assuming that the channels were bordered by close-packed atomic chains (Lehmann and Liebfried, 1963). The zig-zag motion was based on collision forces which were either Coulomb interations for high ion energies and small interaction distances or Born-Mayer interactions for low ion energies and large interaction distances.

The idea of an atomic chain was extended in the first comprehensive treatment of channelling (Lindhard, 1965). It was suggested that if the lattice interatomic distance was small enough, and if the angle between the particle's trajectory and the string of atoms, i.e. the channel wall, was less than a critical value, then the potential associated with the atoms could be regarded as a continuum. If the particle had insufficient transverse energy to break through the potential barrier channelling would occur. This would mean that the cross-sections for inelastic collisions with both nucleii and electrons would be reduced resulting in increased range.

The particle would remain in the channel provided it did not gain enough transverse energy from a collision to break out. The critical angle Ψ_c was given as

$$\left[\frac{2Z_1 Z_2 e^2}{Ed} \right]^{1/2}$$

Many experiments were conducted on proton channelling using different target materials, e.g. mica (Hamilton and Quinton, 1966). One method of demonstrating proton channelling was to measure the gamma ray yield due to the p, γ reaction. The incident proton beam energy was just above the resonant reaction energy so that some energy had to be lost before the reaction took place. The target crystal thickness was of the order necessary for the correct loss of energy so that when channelling occurred the gamma ray yield decreased (Bøgh et al., 1964).

Lindhard had suggested that there would be two types of channelling, axial and planar, depending on whether the channel was two or one dimensional. Later results showed that ions may wander across from one planar channel to another quite freely and there might be a relationship as well as competition between the two types of channelling (Dearnaley et al., 1968). It was also apparent that for high particle energies quantum-mechanical corrections to the classical theory would be necessary.

The first demonstration of positron channelling was achieved by injecting ^{64}Cu atoms into a copper single crystal along the <100> axis. The yield of positrons as a function of emission angle with respect to the <100>

axis was measured to show that particles emitted from the centers of atomic strings would have their motion steered by the rows of atoms. (Uggerhøj, 1966). A later method was to observe the drop in back-scattering yield when the ⟨110⟩ plane of a KCl crystal was parallel to a positron beam (Didenko et al., 1970). Since channelling implies increased penetration it must also imply less positron back-scattering and a 40% drop in yield was obtained.

This experiment also showed that channelling efficiency increased with the target's atomic number and that the critical angle increased with both the lattice parameter, d, and the effective atomic number, all of which agreed with Lindhard's theory. Kumakhov showed that the back-scattered channelling yield was dependent on impurities in the channels so that the method could be used to find the exact location of an impurity.

Channelling of relativistic (16 - 28 MeV) positrons was found to be correlated with the forward Brehmstrahlung intensity (Walker et al., 1970). Both the intensities of transmitted positrons and photons showed a marked variation when the ⟨111⟩ or ⟨110⟩ lattice planes of the target crystal were parallel to the incident beam. The F.W.H.M. of the positron peak was however 40% smaller than predicted by Lindhard's theory due to relativistic effects. A dip was obtained in the forward Brehmstrahlung intensity which was ascribed to the increased probability of small impact parameter events during channelling. Shoulders were observed on the dip due to low energy gamma rays which were attributed to coherent radiation produced by channelling positrons.

This radiation would be produced by any charged particle which moved in a straight line in a medium having a periodic varying dielectric if its energy loss was minimal. The radiation is similar to Cerenkov radiation and consists of a few fundamental frequencies and their integer harmonies which are less intense (Belyakov, 1971). These frequencies and their respective magnitudes were calculated by Nip and Kelly.

A general condition for charged particle channelling applicable to fairly complicated crystals has been obtained (Martynenko, 1971). This assumed that the motion was one of small oscillations along the trajectory when the transverse energy remained fairly constant. Another attempt to improve Lindhard's theory used the Debye model for lattice vibrations (Pathak and Yussouff, 1971). The theory assumed that quantum-mechanical effects for light fast particles were not negligible and also attempted to explain the thickness dependence of channelling. The Debye approach showed that channelling is dependent on temperature and a thickness dependence was obtained by regarding channelling as the formation of standing waves in a periodic crystal.

Investigation of the temperature dependence of the channelling back-scattering yield of a proton beam showed that this was probably due to the effect of lattic vibrations (Komaki et al., 1971). However, the results also showed that the minimum yield from clean surfaces was independent of the type and energy of the particles.

Channelling of a mono-energetic beam of positrons in thin gold crystals was observed by measuring the intensity

of single Compton scattered positrons as a function of the angle between the positron beam and the crystal axis (Anderson et al., 1971). The thin crystal defined a reaction depth which decreases when channelling occurs resulting in a decrease in the measured intensity. Strong dips were found along the $\langle 110 \rangle$ and $\langle 111 \rangle$ axes. The critical angle was about half that predicted by Lindhard and this was assumed to be due to lattice thermal vibrations.

A positron beam with a divergence of only 2×10^{-4} radians enabled the observation of channelling with positron energies up to 1 GeV (Morokhovskii et al., 1972). Channelling was detected by measuring the forward Bremstrahlung radiation as a function of the beam to crystal axis angle.

3.2 THEORY OF CHANNELLING

Channelling is the anomalous absorption of particles by single crystals because the particles bounce off the sides of a potential tunnel formed by the atoms of the lattice. The range increases because the cross-sections for inelastic collisions decrease under these conditions. The opposite to channelling is blocking when the trajectory of a particle is blocked by an atom in the lattice structure thus completely prohibiting forward motion. Channelling particles may be dechannelled, i.e. knocked out of a channel by collision with impurities in the lattice, lattice atoms or electrons.

Study of the energy loss of protons channelled in silicon and germanium suggested that the loss mechanism could be divided into two types. One due to valence electrons and the other due to core electrons (Appleton et al., 1967). At low energies, ions channelled in silicon have an energy loss which can be described by a logarithmic velocity function similar to the Bethe formula although there is no constant ratio between the stopping power for channelled particles and random particles (Della Mea, 1972). Energy loss due to core electrons is important only when the channels are narrow.

Hyperchannelling is defined for channelling particles which lose even less energy than in normal channelling processes. The critical angle is very small and is probably due to the axially channelled particle remaining in only one channel throughout flight (Appleton et al., 1972). This would only occur if the critical angle, i.e. transverse energy is very small.

Axial channelling (two dimension), due to mutually perpendicular strings of atoms, results in the particles taking up a ring like intensity distribution on emerging from the target crystal. On entering the crystal the particle assumes a transverse energy E_T which is the sum of the transverse kinetic energy ($E \sin^2 \Psi$) and the value of the continuum potential at the point of entry($U(r)$). Channelling implies $E_T < E \sin^2 \Psi_c$ and there will be a distribution of transverse energies for a beam whose incident angle Ψ is between $E \sin^2 \Psi$ and $E \sin^2 \Psi_c$. A sharp peak around the lower value is the result of the entrance geometry and the decrease in continuum potential

gradient with increasing distance from the string.

If the energy is near $E \sin^2 \psi$ then the scattering by the string only rotates the transverse momentum vector P_T. Providing it undergoes many collisions the direction of P_T will become random and the spatial distribution in the energetically allowed regions of the transverse plane for a given E_T is uniform. For the same reason that most particles enter the crystal with $E_T \approx E \sin^2 \psi$, most particles will emerge with angle ψ but with random P_T. A ring shaped intensity distribution results which is centred around the axial direction and with a maximum at angle ψ. Experiments have shown that the intensity is higher in the original beam direction, i.e. P_T is not randomised, which may be due to either the particles being scattered into low index planes in the transverse direction, i.e. dechannelling, or just insufficient collisions.

The rings have a finite width because the incident face of the crystal governs the distribution of transverse energies and hence the largest exit angle. The back surface of the crystal determines the smallest angle of exit because it is a function of the distance from the string, i.e. of U(r), at which the particle escapes. So there is a surface film whose thickness dictates the lower limit exit angle. All this neglects the effects due to multiple scattering and the divergence of the incident beam.

Similar results have been obtained as a by-product of Rutherford scattering experiments using 1.2 MeV positrons channelled through silicon crystals. The yield

of single Rutherford scattered positrons shows a pronounced dip when the particles are channelled but the dip has high shoulders due to correlated collisions with the strings (Pedersen et al., 1972). There was some suggestion in the experimental data that the planar channelling dip might have fine structure due to wave interference .

It has been shown that substitutional impurity atoms should show the same interaction yield attenuation as host atoms for a channelled beam. If the impurity is interstitial then the effect on the channelling yield can be quite marked and if the impurity is sited near the middle of a channel the yield actually increases rather than decreases (Alexander and Poate). This is attributed to 'flux peaking' when the impurity attracts the channelling particles towards the center of the channel to a much greater extent than its blocking effect.

Experiments on flux peaking using Yb atoms in a silicon crystal with helium ions being channelled have shown that although the channelling yield depends on the depth of the impurity, as indicated by computer simulations, the usual depths used are not big enough to allow the channelling particles to obtain a statistical spread across the channel (Eisen and Uggerhøj, 1972). The effect of the particles energy on flux peaking was inconclusive because it is very dependent on the exact position of the impurity atom in the channel even when there is no statistical spread of particles across the channel.

It was postulated that the effect of a substitutional impurity atom would only be the same as a host atom if the two thermal vibration amplitudes were similar, e.g. Au impurity in a Cu lattice. If the amplitudes were different then the location of the impurity in the lattice structure could be determined fairly accurately from its effect on the channelling yield (Anderson et al., 1972). However this requires complete angular scans for several channelling axes and even then the technique can only give the usual lattice site occupied by the impurity atom.

Many channelled particles gain enough transverse energy to overcome the continuum potential of the strings and are dechannelled. Dechannelling may be due to the thermal vibration of both lattice and electrons which may either change the particle's transverse energy due to a collision or distort the continuum potential. Dechannelling can also be caused by crystal defects (the surface of the crystal can be considered as a defect) as well as impurities, stacking faults, dislocations, etc. Thus dechannelling may be caused by collisions with interstitial impurities (although this may also cause flux peaking), encountering lattice distortions and displacements and by disintegration of the lattice periodicity at grain boundaries, etc. In some cases the particle may not be completely dechannelled at an obstruction but may have its channelling direction changed. (Mory and Quéré). Opacity has been defined as the number of such dechannelling faults in a sample.

3.3 DERIVATION OF THE CRITICAL ANGLE

Channelling is defined as particle propagation through a crystal such that the particle's path is near the centre of a channel along a major axis of the crystal giving the path a certain stability. Such particles are subject to periodic harmonic forces of which a focussing force may predominate. Transverse motion is roughly a long wave oscillation combined with short wave vibrations with the lattice period. The long wave oscillation has constant amplitude and wavelength V/W, where V is the particle velocity and W is the period of transverse oscillation (Lindhard, 1965).

If a particle moves along and oscillates about the centre line of a channel then the particle can only escape from the channel if the energy of oscillation exceeds the potential barrier to a neighbouring channel. Ψ is the angle between particle motion and channel direction when the particle is at the channel axis. The particle can therefore escape if the transverse energy $E \sin^2 \Psi$ is greater than the barrier energy say E_c. The critical angle

$$\alpha_c \approx \left(\frac{E_c}{E} \right)^{1/2}$$

The solid angle for channelling becomes

$$\Omega_c \approx \frac{\pi E_c}{E}$$

This shows that the channelling angle increases with

barrier energy, i.e. the packing of the atoms in the strings, but decreases with higher particle energies. It appears to be independent of the particle's mass and charge although E_c is in fact dependent on the particle's atomic number.

This is a simplified picture suitable only for hyperchannelling because channelling in general does not imply that a particle must stay within one channel. Suppose that only particle - atom collisions govern the path of the particle (true for heavy particles) then we can assume:

(1) Scattering angles are small since the atom can be considered as infinitely heavy compared to the particle so the Thomas-Fermi potential V(R) can be used and the scattering angle Φ :

$$M_1 \Phi = \frac{-1}{V^2} \int_{-\infty}^{+\infty} dz \frac{\delta}{\delta p} V\left(\sqrt{z^2 + p^2}\right)$$

where M_1 = particle mass

V = particle velocity

p = impact parameter

(2) A collision means that the particle must come close to an atom and if the particle trajectory makes a small angle with a row of atoms then passing close to one atom must imply passing close to several neighbouring atoms, i.e. the particle collides with a string of atoms interspaced in a straight line called a perfect string. Thus the particle's path is governed by independent

collisions with a number of strings.

(3) Except for very high particle velocities, quantum-mechanical corrections to the classical orbital picture are negligible.

(4) Deviations from perfect lattices and strings due to thermal vibrations are negligible in the ideal crystal.

If many consecutive atoms contribute to the deflection of the particle's trajectory, i.e. many small collisions, then there is a string or continuum approximation which is equivalent to this. Suppose the average potential at distance r from the string is given by:

$$U(r) = \int_{-\infty}^{+\infty} \frac{dz}{d} V\left(\sqrt{z^2 + r^2}\right) \qquad (1)$$

$V(R)$ = particle-atom potential

d = interatomic distance in the string.

The screening length of the particle-atom interaction is given by:

$$a = a_o \times 0.8853 \left(Z_1^{2/3} + Z_2^{2/3}\right)^{-1/2} \quad \text{but } Z_1 \ll Z_2.$$

$$\therefore \quad a = a_o \times 0.8853\, Z_2^{2/3}$$

The Fermi function belonging to one atom is $\Phi_o(\frac{R}{a})$. If R is not very much larger than a, the potential V(R) is of the Thomas-Fermi type given by:

$$V(R) = \frac{Z_1 Z_2 e^2}{R} \Phi_o\left(\frac{R}{a}\right)$$

substitute in (1) gives:

$$U(r) = \int_{-\infty}^{+\infty} \frac{dz}{d} \frac{Z_1 Z_2 e^2}{R} \Phi_o\left(\frac{R}{a}\right)$$

$$= \frac{Z_1 Z_2 e^2}{d} G\left(\frac{r}{a}\right) \qquad (2)$$

For $\frac{R}{a} \ll 1$ then $\Phi_o \approx 1$ and equation (2) shows that G and therefore U(r) must increase logarithmically as r decreases if r is small.

$$\therefore \quad G\left(\frac{r}{a}\right) \approx 2 \log \frac{Ca}{r} \qquad (3) \qquad \text{for } r < Ca.$$

2 log C is a constant of integration determined by the screening. The continuum model implies that scattering at distances around the minimum distance of approach must be due to the string not to a single atom. Thus the velocity parallel to the string V cos Ψ multiplied by the collision time Δt must be larger than the interatomic spacing d.

The collision time is of the order $\frac{r_{min}(1)}{V \sin \Psi}$ where 1 is the impact parameter and $r_{min}(1)$ is the minimum distance of approach.

$$\therefore \quad \Delta t \times V \cos \Psi \approx \frac{r_{min}(1)}{V \sin \Psi} > d \qquad (4)$$

For small Ψ, $\sin \Psi \approx \Psi$ and the minimum distance of approach is obtained from:

$$U(r_{min}) = \frac{M_1 V^2}{2} \sin^2 \Psi \approx E \Psi^2 \qquad (5)$$

E = energy

r_{min} implies $l = 0$ and r_{min} increases rapidly as $\sin\Psi$ ($\approx \Psi$) — decreases, i.e. r_{min} tends to zero for a fixed Ψ if the energy increases so at high energies the average potential is given by:

$$U(r) = \frac{Z_1 Z_2 e^2}{d} \cdot 2 \log \frac{Ca}{r} \qquad (6) \quad \text{from (2) and (3)}$$

But (5) = (6) at high energies so:

$$E\Psi^2 = \frac{Z_1 Z_2 e^2}{d} \cdot 2 \log \frac{Ca}{r} \qquad \text{or}$$

$$\log \frac{Ca}{r} = \frac{2Z_1 Z_2 e^2}{E\Psi^2 d} \qquad \text{or}$$

$$\frac{r}{Ca} = \exp\left[-\frac{E\Psi^2 d}{2Z_1 Z_2 e^2}\right] \qquad \text{or}$$

$$r = Ca \exp\left[-\frac{E\Psi^2 d}{2Z_1 Z_2 e^2}\right]$$

But from (4) $r > d \cdot V \sin\Psi = d \cdot V\Psi$

$$\therefore \quad \Psi d < Ca \exp\left[-\frac{E\Psi^2 d}{2Z_1 Z_2 e^2}\right] \qquad \text{or}$$

$$1 < \frac{Ca}{\Psi d} \exp\left[-\frac{E\Psi^2 d}{2Z_1 Z_2 e^2}\right] \qquad (7)$$

If Ψ increases from zero then, providing $\frac{Ca}{\Psi d}$ remains large, equation (7) becomes untrue if the exponential decreases rapidly so the condition necessary for (7) to be correct is given by:

$$\Psi < \Psi_c = \sqrt{\frac{2Z_1 Z_2 e^2}{Ed}}$$

Provided that $\frac{Ca}{\Psi_c d}$ is larger than unity this formula gives the critical angle, i.e. $\Psi_c \leq \frac{Ca}{d}$ or $E \geq 2Z_1 Z_2 e^2 d/a^2$. Ψ_c obtained thus is usually larger than α_c obtained previously for what is now called hyperchannelling. Any particle moving through a crystal such that its trajectory makes an angle $\leq \Psi_c$ with a crystal lattice direction is subject to the continuum theory and will suffer separate repulsive collisions with atomic strings giving a sort of mirror reflection. The particles do not approach near enough to undergo normal multiple scattering.

A particle beam incident parallel to an atomic string can be divided into:

a) those particles entering the crystal at a distance from the string less than r_{min} so that they will move like those in a random target.

b) those particles entering at a distance from the string larger than r_{min} which can be channelled.

The fraction of 'random' particles is given by:

$$\text{Fraction} = \frac{\pi r^2}{S} = \frac{\pi d^2 \Psi_c}{S}$$

where $S = [Nd]^{-1}$

Ψ_c = critical angle

N = atomic density

d = interatomic distance

The fraction is dependent on particle energy via the critical angle. Corrections to the theory will probably

be required to take account of the four original assumptions.

3.4 ENERGY LOSS MECHANISMS IN CHANNELLING

Channelling is defined as the anomalous absorption of an aligned particle beam by an orientated crystal which implies that the particles penetrate deeper into the crystal because the stopping power, i.e. average loss of energy per unit distance, for a channelled particle is much less. Energy losses are probably due to both collisions with lattice nucleii (nuclear stopping) and collisions with electrons (electronic stopping).

Nuclear Stopping

A particle of energy E may pass one nucleus at a distance r where the average potential is U(r) and suffer a deflection through a small angle Φ. The formula used before for scattering at small angles is given by:

$$M_1 \Phi = \frac{-1}{V^2} \int_{-\infty}^{+\infty} \frac{dz}{} \frac{\delta}{\delta_p} V\left(\sqrt{z^2 + p^2}\right)$$

(Symbols previously defined)

$$\therefore \quad \Phi = -\frac{1}{M_1 V^2} \int_{-\infty}^{+\infty} dz \frac{\delta}{\delta_p} V\left(\sqrt{z^2 + p^2}\right) \qquad (10)$$

The average potential at distance r from the string is given by:

$$U(r) = \int_{-\infty}^{+\infty} \frac{dz}{d} V\left(\sqrt{z^2 + r^2}\right) \qquad (11)$$

Substitute (11) in (10) :

$$\Phi = - \frac{d.U'(r)}{M_1 V^2} = - \frac{d.U'(r)}{2E}$$

Since the collision is elastic the energy transfer is:

$$T = \frac{d^2 [\, U'(r)]^2}{2M_2 V^2} \qquad (12)$$

M_2 = atomic mass

The average energy loss can be obtained by integrating T over the unit cell, which is composed of strings, and over all possible values of r. However, (12) indicates that the energy loss to the nucleus will increase as r decreases. But a condition for channelling is that $U(r) \leq E_T$, the transverse energy of the particle, so there must be a minimum distance of approach r_{min} for channelled particles. This shows implicitly that compared to a random beam of particles a channelled beam's average energy loss is small. Except at low energies the contribution of nuclear stopping to the stopping power will be small anyway.

Electronic Stopping

Decreasing transverse energy means that the electronic stopping decreases but at a slower rate than nuclear stopping so the ratio between electronic and nuclear stopping is higher for a channelled particle beam than for a random beam. For reasonably high velocities the Bethe - Block formula can be used:

$$\frac{dE}{dR} = S_e \cdot N \cdot Z_2 = \frac{4\pi Z_1^2 e^4}{mV^2} Z_2 \cdot N \cdot L_e \qquad (13)$$

where N = number of atoms/unit volume

S_e = stopping cross section / electron

$L_e \sim \log \frac{2mV^2}{I}$

I = average excitation potential.

Collisions with electrons are regarded as quantum - mechanical and can be divided into resonance collisions, which usually occur outside the electronic orbit, and close large momentum transfer collisions which usually occur inside the orbit and are governed by the Rutherford scattering law. The two types contribute asymptotically equally to the total stopping power so that at reasonable penetration depths:

$$\frac{dE}{dR}(\vec{R}) = S_e [(1 - \alpha) NZ_2 + \alpha \cdot \rho(R)] \qquad (14)$$

where $\rho(R)$ = electron density at the point through which the particle is moving

$\alpha \approx 1/2$, α approaches 1/2 as the penetration depth increases. For a very thin foil this shows that the stopping cross section can only be reduced by 1/2 in the most favourable conditions. For a given transverse energy E_T there is an effective charge or atomic number $Z_2^*(E_T)$ such that if $E_T = U(r_{min})$ then $Z_2^*(E_T)$ is the number of electrons per atom of the string outside r_{min}. Given a large number of particles with a large spread of E_T, equation (14) can be averaged:

$$\frac{dE}{dR}(\vec{R}) = S_e [(1-\alpha) NZ_2 + \alpha Z_2^*(E_T) \cdot N] \text{ and}$$

hence we can define the average electronic stopping power

$S_e(E_T)$:

$$S_e(E_T) = S_e \left[(1-\alpha) + \alpha \frac{Z_2^*(E_T)}{Z_2}\right] \qquad (15)$$

If the ratio:

$$\frac{Z_2^*(E_T)}{Z_2} = \frac{d\, r_{min}\, U'(r_{min})}{2 Z_1 Z_2 e^2} \qquad (16) \text{ and}$$

$$\Psi_c^2 = \frac{2 Z_1 Z_2 e^2}{E d} \qquad (17)$$

then combining (16) and (17) in (15):

$$S_e(E_T) = S_e \left[1 - \alpha \exp\left(\frac{-2 E_T}{E \Psi_c^2}\right)\right]$$

The electronic stopping power does decrease for particles making small angles of incidence with the strings although the maximum angle is slightly smaller than the critical angle for channelling. For a single collision with a string with impact parameter 1 and angle Ψ the resonance stopping is independent of the string and can be neglected. The energy loss is then given by:

$$T_e(r) = \frac{S_e}{2} \cdot d \cdot \rho_s(r)$$ where $\rho_s(r)$ is the electron density of the string. The penetration of channelled particles will be enhanced because the average energy loss due to both nuclear and electronic stopping will be less than for random particles. However, the decrease in electronic stopping is much less than the decrease in nuclear stopping.

3.5 THE GAMMA-GAMMA SYSTEM

3.5.1 Introduction

The experiment to observe channelling consisted of allowing a narrow beam of positrons to be incident on the face of a thin silicon slice. Providing that the crystal allowed about half of the positrons through under normal conditions then if channelling occurred many more positrons would get through. The beam must have an angular deviation less than the critical channelling angle for the effect to be noticeable. The number of positrons annihilating in the crystal was to be measured, using the triple coincidence system, as a function of the crystal orientation. If the beam became parallel to a crystal axis then channelling would occur and a fall in the counting rate would be observed.

The first source used was ^{22}Na whose positron spectrum, a gaussian distribution, has an end point at 545 KeV. whilst the maximum number of positrons with one energy occurs at 225 KeV. At this energy the maximum range of positrons in silicon is 194 μm. A silicon single crystal of high purity (5N, i.e. 1 part in 10^6) measuring 2 cm in diameter and 30 μm. thick was supplied by G.E.C. Semiconductors Ltd. The critical angle for positrons of 225 KeV. is about 14 mrads so that the positron beam should have an angular deviation of about 5 mrads. The 1 mCi. source supplied by the Radiochemical Centre at Amersham had an active area of 1 cm. in diameter.

3.5.2 Construction of Thin Silicon Slices

Ten more silicon slices were made at Metals Research Ltd who provided the silicon and the facilities. A large 2 cm diameter single crystal was mounted on a goniometer so that it could be orientated. The crystal was stuck on a wooden support and completely covered with a mixture of Durafix and graphite to keep the crystal firmly in place. X-ray photos taken of the crystal on the goniometer were analysed using a Greninger chart so that the crystal axes could be plotted. The goniometer was adjusted until the X-ray photo showed that the orientation was exactly perpendicular to the < 100 > face. Silicon has a simple cubic structure so that a < 100 > face is one of the sides of the cube.

The orientated crystal was put on a 'Microslice' machine (Fig. 3.1) which consists of a thin diamond edged circular saw which is held under tension. The blade is rotated by an electric motor and the crystal is fed to the blade on a counterbalanced arm which has two functions:

(1) it provides the correct pressure between blade and crystal - usually about 50 gm per cm. of cut;

(2) it allows the crystal to back away from the blade in order to minimise the effects of irregularities in the surface of the blade.

Each cut took approx. two hours using the standard oil as lubricant. Ten slices were obtained and these were kept in their positions by the glue until demounted by dissolving the glue in methanol. The slices of about 500 µm. were cleaned with methanol.

FIG 3.1 MECHANICAL CUTTER

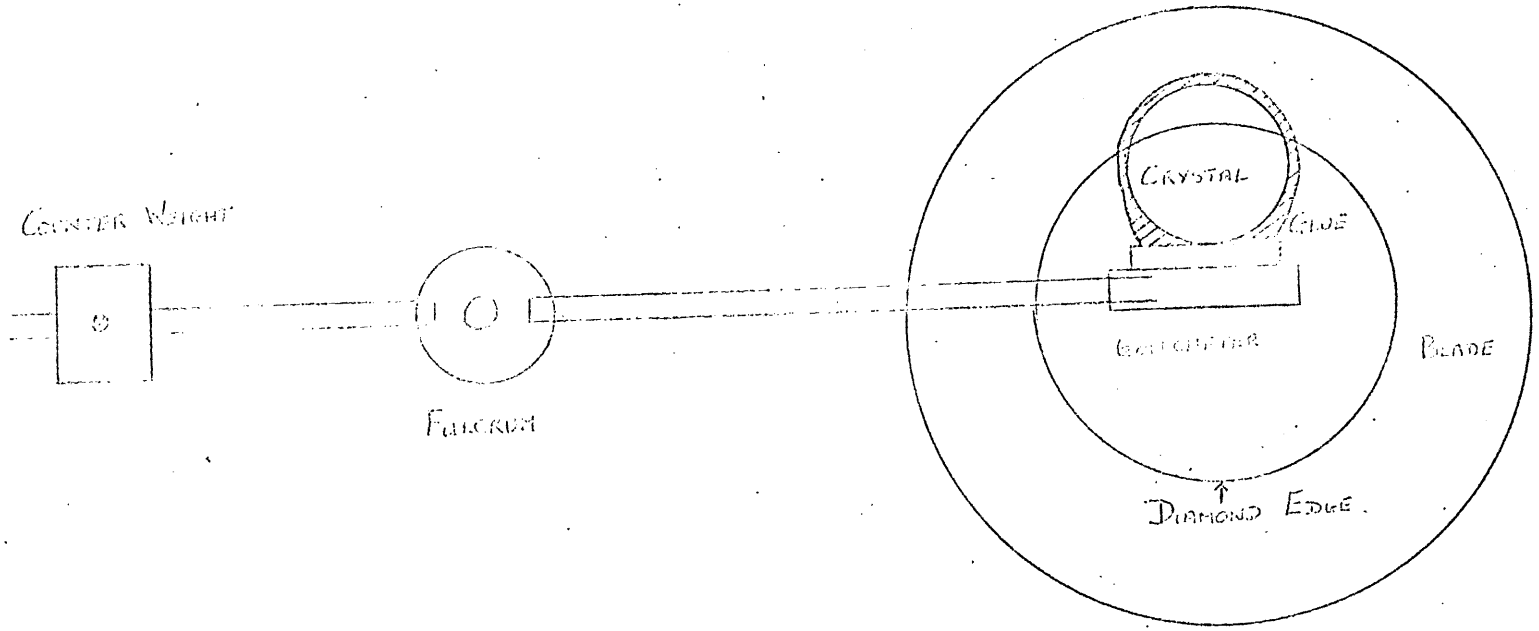

To make the slices thinner they were etched in an acid solution:

30 ccs. of Hydrofluoric Acid +
400 ccs. of Nitric Acid +
200 ccs. of Hydrochloric Acid
} concentrated.

This mixture is potent and dangerous being liable to explode unless kept in an ice bath. There was no available information on the etching rate to be expected so this had to be discovered by empirical methods. The only substance in which the slices could be mounted which was not attacked by the acid solution was Beeswax. A small square of glass was completely covered by molten beeswax and the silicon slice was placed on top. Beeswax was poured round the edges of the crystal which was cleaned with ether when the wax was dry. The slice could be demounted by dissolving the wax in ether.

To find the etch rate one slice was etched for five minute periods at the end of which the slice was demounted and its thickness measured with a micrometer screw gauge. After 30 minutes the slice was reduced to about 200 µm., an etch rate of ten microns per minute. The remaining slices were etched for 30 minutes plus a multiple of two minutes (later 1 minute) so that a range of thicknesses between 200 and 50 µm. were obtained. To ensure an even etch the solution was continuously stirred electrically. The etch rate was not particularly stable especially if the temperature was allowed to vary even over a small range.

On demounting the slices were far too brittle to touch and had to be supported over a large area or they

would break under their own weight. Since the center of the slice must be free for channelling the slices were mounted between two large metal washers stuck together with beeswax. This made the mounting simple since the slices could be floated off the glass plate base onto one of the washers when the second washer could be gently lowered to secure the slice. The sandwich was removed and the wax allowed to harden.

3.5.3 Construction of the Brass Collimator

The channelling experiment requires a well collimated beam of positrons which can only be produced by a simple slits type arrangement if an accelerator is not used. The angular deviation of the beam is restricted to 5 mrads. and to make the number of positrons in the beam as high as possible there were two requirements:

(a) that the target crystal be as near to the source as possible;

(b) that the collimator should contain multiple slits because of the finite size of the source.

Metals Research Ltd had a larger version of the 'Microslice' machine (used on the silicon) which had a blade which was approximately 8/1000 of an inch thick. A test cut with the machine showed that due to blade wobble the cut produced was 10/1000 inch thick. This machine could only be used with certain materials, one of which was brass, which although 'soft' will not clog the cutting edge. The arrangement shown in Fig. 3.2 was produced and ten cuts were put in, each being 10/1000 inch thick spaced

5cm.
1cm.
3cm.
1cm.
5cm.
CUTS
END VIEW
3cm.
1cm.
3cm.

at 1 mm intervals. The collimator length was calculated to be 2 inches for an angular deviation of 5 mrads. After the cutting the two sections of the collimator were screwed together.

3.3.4 Experimental Arrangement

Using the brass collimator the minimum length of the positron beam would be 5 cm, but the mean free path (λ) of positrons is given by:

$$\lambda \approx \frac{0.707}{\pi n r^2}$$

where n = number of air molecules / cc.

r = radius of air molecule since positron radius is negligible.

At S.T.P. $n \approx 2.7 \times 10^{19}$ molecules / cc.

$r \approx 2 \times 10^{-8}$ cm.

$\therefore \quad \lambda \approx 2 \times 10^{-5}$ cm., i.e. a collimated beam cannot be produced.

Consider $$p = \frac{1}{3} nmc^2$$

$$= \frac{1}{3} \frac{0.707\ mc^2}{\pi r^2 \lambda}$$

$\therefore \quad p \propto \frac{1}{\lambda}$ The mean free path is inversely proportional to the pressure. Using a two inch diffusion pump we can easily obtain pressures of 10^{-6} Torr = 10^{-8} atmospheres. At this pressure the mean free path will be 10^8 larger, i.e. $\lambda \approx$ 20 metres which is much larger than required. The experiment must be conducted in a vacuum and a diagram of the arrangement is shown in Fig. 3.3.

Fig 3.3 First Cell of the Experimental Apparatus

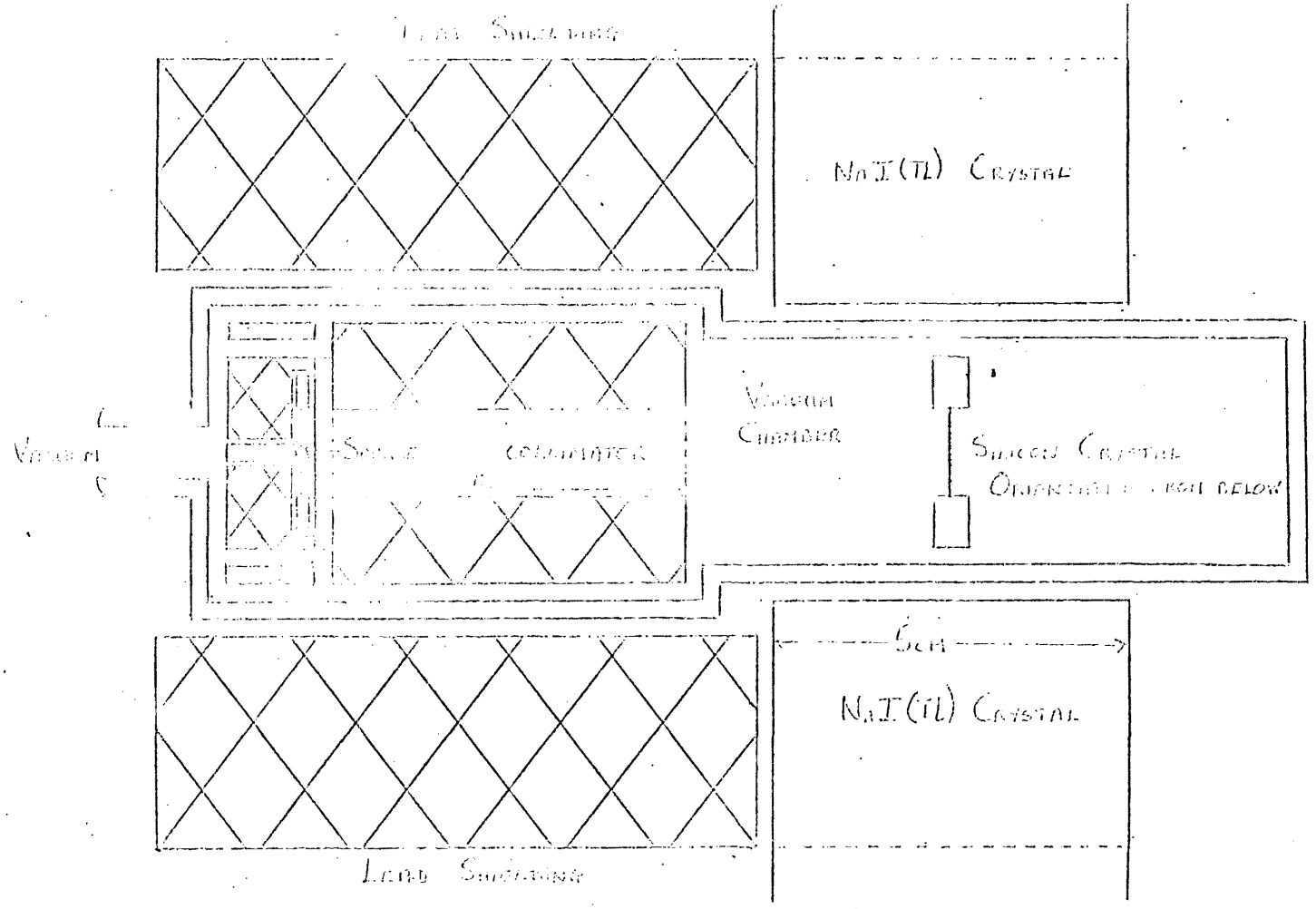

The expected maximum counting rate was calculated using the 1mCi ^{22}Na source with an active area of diameter 1 cm.

a) Effective Source

Since the slits do not cover the whole area of the source part of the source will be lost. If the source is uniformly spread out then the effective source

$$= \frac{\text{area of source covered by slits x source}}{\text{area of source}}$$

To find the approximate area of the source which is covered by the slits; this can be considered to be the area covered on a 1 cm. square multiplied by the fraction of the square covered by the source.

Area of square covered by slits $= 9 \times 1 \times 25.4 \times 10^{-3}$

$= 23 \times 10^{-2}$ sq. cm.

Fraction of square covered by source $= \frac{\pi \times .5^2}{1} = .25\ \pi$

$\therefore$ Area of source covered by slits $= 23 \times 10^{-2} \times .25\pi$

$= .18$ sq. cm.

$\therefore$ Effective Source $= \frac{.18 \times 1}{.25\ \pi} \approx .23$ mCi.

b) Collimated Fraction

Since positrons are emitted in random directions the fraction that will emerge from the slits is given by:

Collimated Fraction $= \frac{\text{Effective area of slits}}{\text{Area of sphere of radius = slit length}}$

$$= \frac{25.4 \times 10^{-3}}{4\pi \times 5.0^2} \approx \frac{10^{-3}}{4\pi} \approx 7.8 \times 10^{-5}$$

c) Number Collimated

The number of positrons which will succeed in emerging from the slits to form the collimated beam is given by:

Number Collimated = Effective Source x Collimated Fraction

$$= .23 \times 3.7 \times 10^7 \times 7.8 \times 10^{-5}$$

$$= 6.6 \times 10^2 \text{ positrons / second.}$$

d) Number Detected

If the photomultiplier crystal is 5 cm. from the crystal in which all of the positrons must annihilate then the fraction of the random direction annihilation gamma rays which will hit the crystal is given by:

$$\text{Fraction} = \frac{\text{Area of Scintillation Crystals}}{\text{Area of sphere of radius = crystal distance}}$$

$$= \frac{2\pi \ 1^2}{4\pi \ 1^2} = \frac{1}{2}$$

So only one half of the gamma rays will hit the counters even when they are at a minimal distance of one inch away. Since the detectors are probably only about 3% efficient then the total number of annihilations detected is

$$6.6 \times 10^2 \times \frac{1}{2} \times \left(\frac{3}{100}\right)^2 \approx .3 \text{ / second.}$$

In practice many of the positrons went through the crystal and did not annihilate as was expected. However, it was found possible to put the detectors slightly nearer to the

crystal to compensate for some of this loss in count rate.

When the experiment was attempted it was found that the 1 mCi source produced extremely high singles count rates in the two counters even with the maximum amount of lead shielding. The attenuation of a broad beam of gamma rays by two inches of lead is a factor of 10^{-3}. The singles rates were measured to be about 2×10^4 counts / second. The chance coincidence rate is given by

$$N_c = N_1 N_2^2 \tau$$ where τ = resolution time $\approx$ 20 nSec.

N_1 and N_2 = singles rates.

$$= (2 \times 10^4)^2 \times 2 \times 20 \times 10^{-9}$$

$$= 4 \times 4 = 16 \text{ counts / second.}$$

The random coincidence rate was a factor of 10^2 larger than the true count rate which was anyway very slow. Given the statistical uncertainty in any number ($\sqrt{N}$) combined with errors associated with the electronics, then the chance coincidence rate would mask the effect due to channelling.

3.5.5 Improvements to the System

The only way to diminish the singles rates and hence the chance rate without decreasing the resolution time which would impair the efficiency of the system would be to take the counters further away so that more shielding could be used. But this would considerably worsen the detection geometry for those positrons annihilating in the

crystal unless the method of collimation was changed. The slits would have to be made longer but wider so that the same angular deviation of the beam was obtained. However, this could not be done with the present source since the effective source would be drastically reduced and the number of positrons in the beam would be too small. After several trial experiments a new source was designed in conjunction with a new beam chamber (Fig. 3.4). A one mCi ^{69}Ga source, whose daughter ^{68}Ge is a positron emitter (1.8 MeV), was ordered from the Radiochemical Centre in October 1972 when a 2 to 3 month delivery delay was quoted. The source was to be recessed into a 2 mm. diameter dip in one end of a 5 mm. diameter, 1 cm. long, stainless steel rod. A 5 μm. thick mica window was to be used to seal the source. The collimating slit was also 2 mm. in diameter constructed from brass plates between lead shielding. This apparatus was built and used for positron range measurements. The ^{69}Ga source was not delivered until June 1973 when its strength was found to be 40 μCi, and not the 1 mCi ordered.

3.6 THE SILICON DETECTOR SYSTEM

3.6.1 Introduction

It had been decided that the gamma-gamma scintillation counting system might not be good enough because drifts in the amplifiers in conjunction with the very low counting rates would make the channelling effect very difficult to see. If the positrons were detected directly

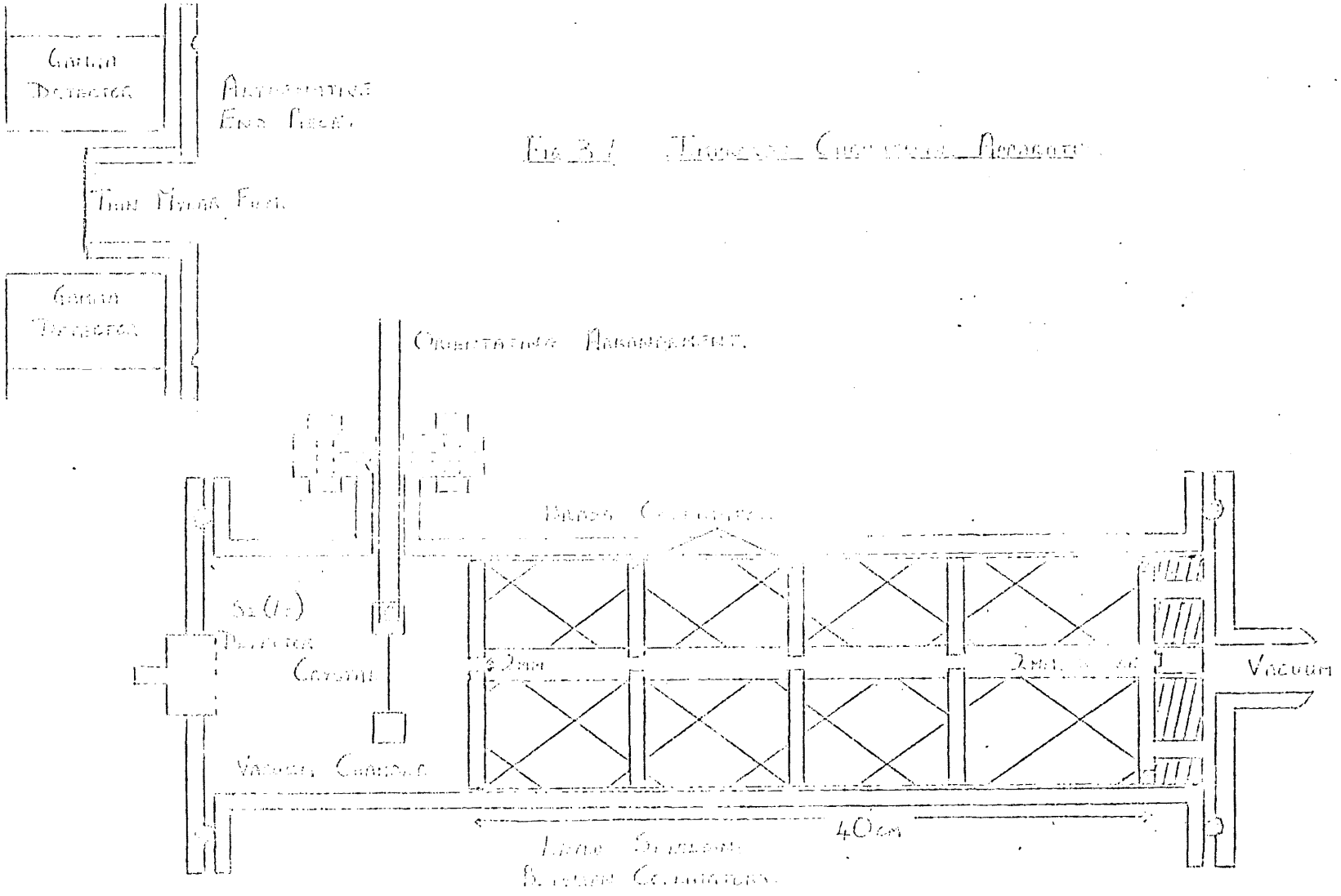
Vacuum
40cm

with a Si (Li) detector as they emerged from the target crystal then the results would yield much more information about the effect of channelling on positron energies.

The end point energy of a ^{68}Ge positron source is 1.8 MeV. so in order to stop all the positrons the detector would have to be 3 mm. thick, i.e. more than the maximum range of 1.8 MeV. positrons in silicon. A detector with area 200 $mm.^2$ was ordered together with a high voltage power supply from Nuclear Enterprises Ltd. A low noise pre-amplifier was obtained from Tennelec Ltd and the complete system is shown in Fig. 3.5.

To increase the resolution and prevent damage to the entry window of the detector and to prevent positrons being absorbed in the air the detector was operated in vacuum. However, as the detector is easily damaged if the vacuum fails when the H.T. is on, a safety device was designed and built. This device automatically switched off the H.T. if the vacuum fell below a certain level.

3.6.2 Detector Bias Supply Controller

The unit is required to turn off the bias supply to the Si (Li) detector if the vacuum falls below a pre-determined level. Since the detector can be used in air the controller must have a bypass facility. The unit must indicate visibly when the correct vacuum has been reached so that the bias supply can be turned on and it must also indicate visibly when the vacuum fails.

Operation

A thermistor is used to sense whether a vacuum is

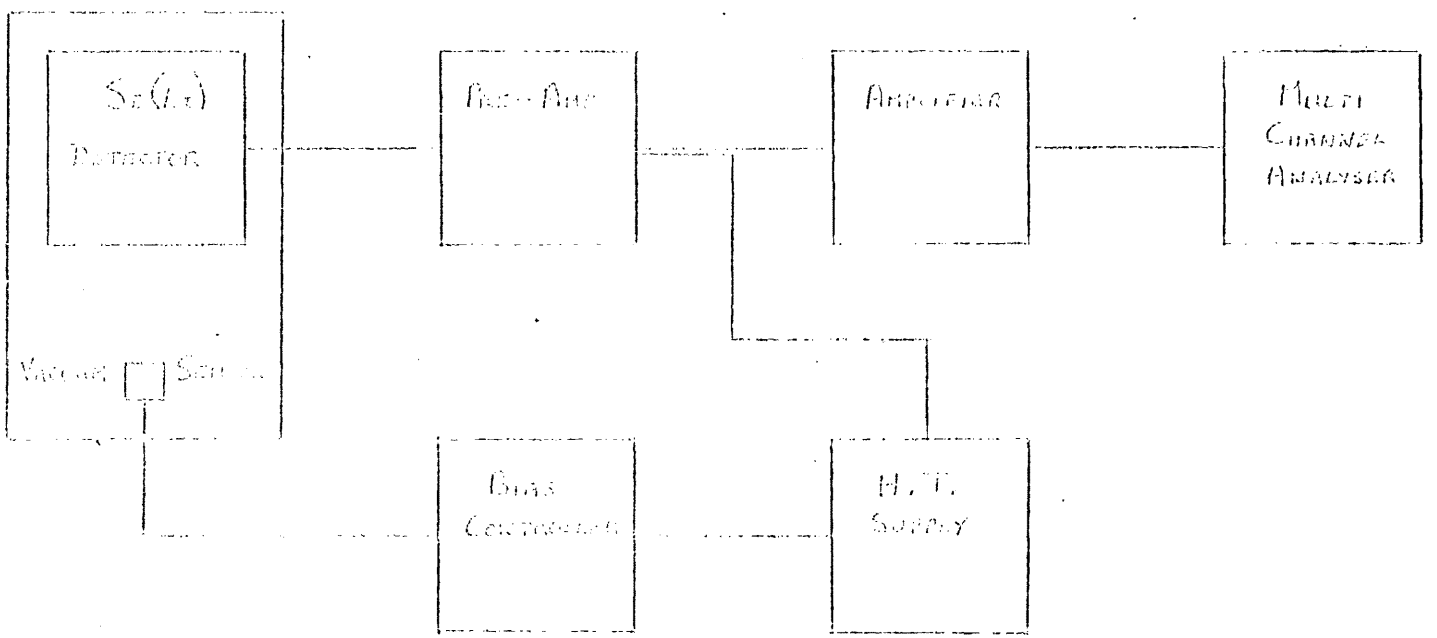
Si(Li) Detector
Pre-Amp
Amplifier
Multi Channel Analyser
Vacuum
Bias Supply
H.T. Supply

present or not. The thermistor is self-heating and will lose heat at a rate dependent upon the state of the vacuum. Hence, its temperature and therefore its resistance depend upon the vacuum. At high vacuum little heat will be lost and its resistance will be low. If the vacuum fails the thermistor will rapidly cool down causing its resistance to increase. The change in p.d. across the thermistor is detected by a voltage comparator and if the p.d. rises above a set value the comparator output changes state from logic 0 to logic 1. The reference voltage, current through the thermistor and the vacuum gauge zero level are all variable.

When the comparator output changes it triggers a bistable circuit which in turn cuts off the relays carrying the power supplies from the N.I.M.S. rack to the H.T. supply unit whose output must fall to zero. The bias will fall slowly to earth because of residual charge on its capacitors - a sudden drop would damage the detector. The bistable also illuminates a warning bulb to indicate that the vacuum has failed. When the vacuum is restored a green light shows that the bias can be restored by pressing the reset button. The bias will, of course, have to be slowly wound up to the correct level. The controller can be bypassed by connecting the comparator input directly to the 5 Volt supply instead of to the thermistor. A block diagram of the unit is given in Fig. 3.6 and Fig. 3.7 is the printed circuit.

Detector Bias Supply Controller.

Block Diagram Fig 3.6

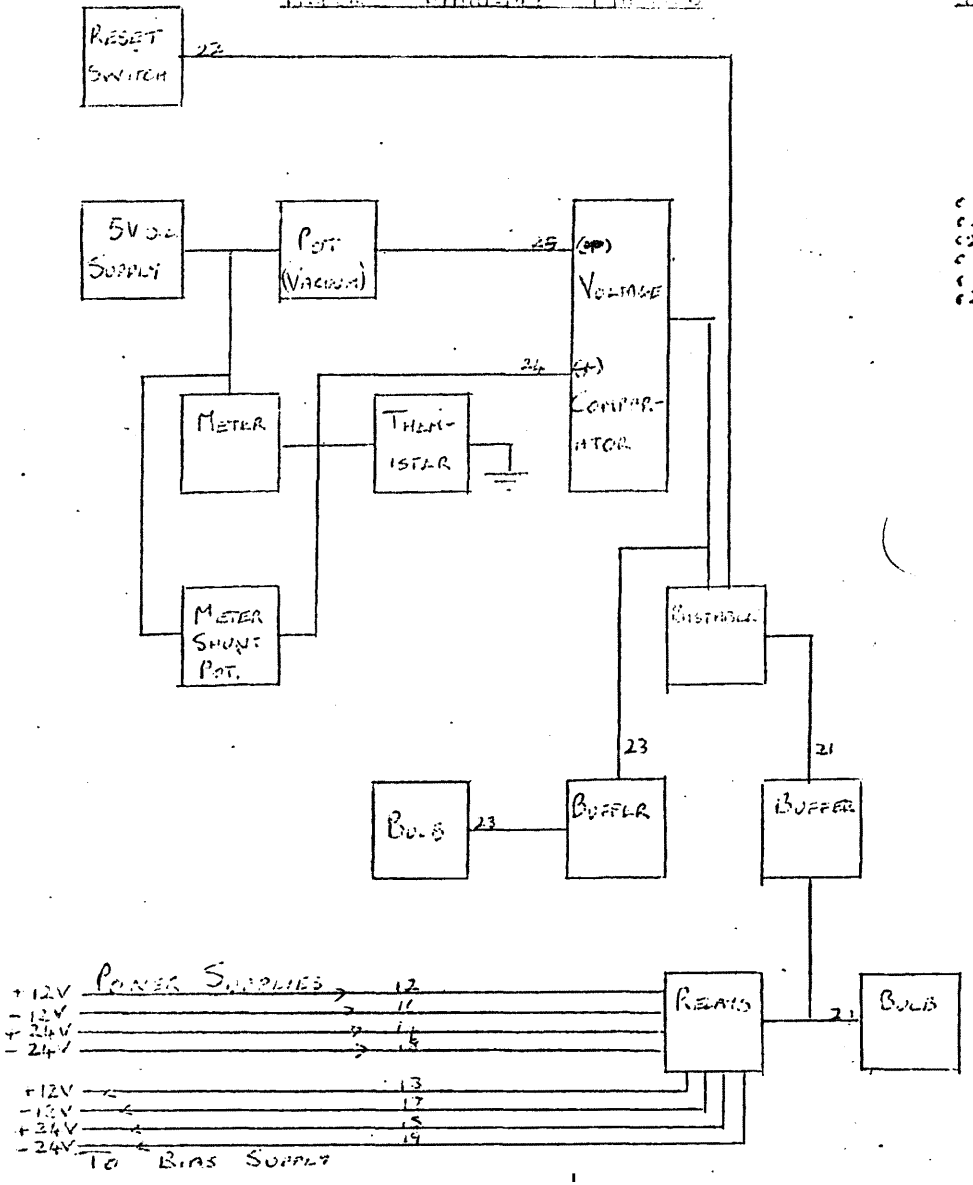

Logic Circuit Diagram Fig 3.7

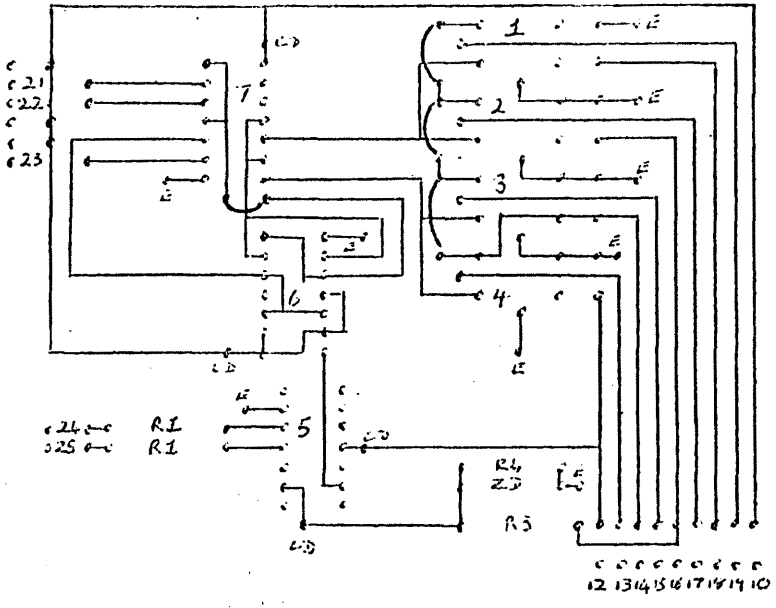

Legend

1 → 4 = Reed Relays Type RS24

5 = SN72710 Comparator

6 = SN7400 Quad Nand

7 = SN7416 Hex. Inv. Buffer.

R1 = 50KΩ R2 = 5KΩ

R3 = 1·5KΩ R4 = 10KΩ

ZD = 5·6V Zener.

CD = Decoupling Capacitor.

E = Earthed.

3.6.3 Discussion

No data was obtained from this experiment so a graph of the sort of behaviour expected from the first experiment - detecting the number of positrons annihilating in the silicon crystal - is shown in Fig. 3.8. The shoulders are postulated as being due to correlated collisions with the strings (Pederson et al., 1972). The bottom of the dip would depend on the target crystal thickness, i.e. the fraction of the positron beam which is absorbed by the crystal. The critical angle is given by:

$$\Psi_c = \left(\frac{2Z_1 Z_2 e^2}{Ed} \right)$$

where $Z_2 = 14$, $d = 5.428 \times 10^{-8}$ cm. } for silicon

$e = 4.802 \times 10^{-10}$ erg$^{1/2}$ cm$^{1/2}$

$E = 1.602 \times 10^{-12} \times 250 \times 10^{3}$ erg } for 250 KeV positrons (^{22}Na)

$Z_1 = 1$

$$\therefore \quad \Psi_c = \left(\frac{2 \times 1 \times 14 \times 4.802^2 \times 10^{-20}}{1.602 \times 10^{-12} \times 2.5 \times 10^{5} \times 5.428 \times 10^{-8}} \right)^{1/2}$$

$$\approx 17 \text{ mrads.}$$

The observed critical angle would be less than this because of the large angular divergence of the positron beam.

Fig. 3.8 Expected Channeling Experiment Results - Source ^{22}Na

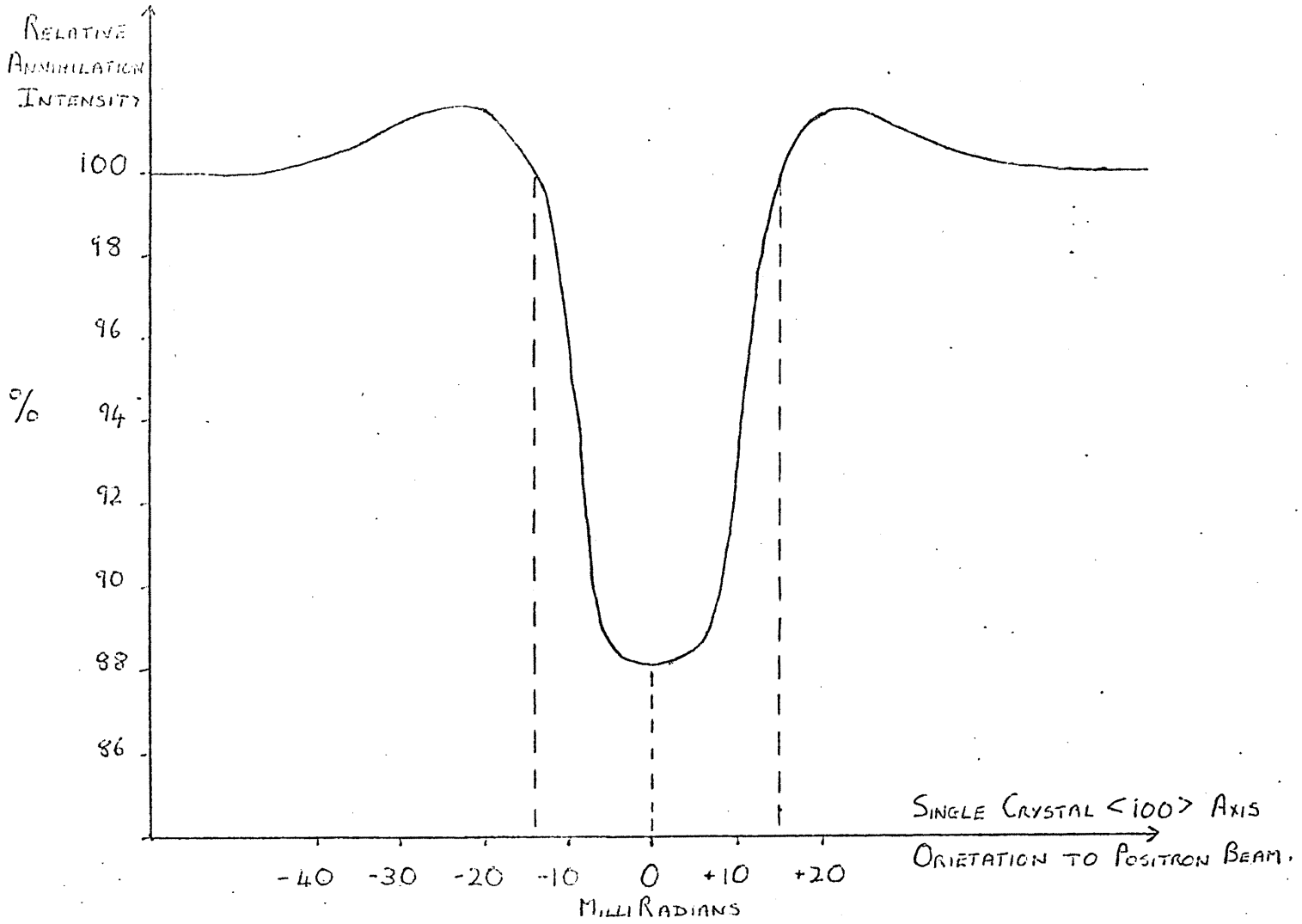

CHAPTER 4

ABSORPTION OF LOW ENERGY POSITRONS AND ELECTRONS

4.1 INTRODUCTION

Although the absorption of electrons had been shown to be dependent on the atomic number (Z) of the absorber (Husain and Putman, 1957), there were few attempts to investigate the difference in absorption of positrons and electrons until 1966 (Takhar). These differences had been discussed by Rohrlich and Carlson in 1954. Takhar compared the absorption of 1.88 MeV positrons with that of 1.77 MeV electrons. The positrons from a ^{68}Ge source which had passed through the absorber were annihilated in a thick aluminium slab and the gamma rays detected by a triple coincidence system. The same absorbers were used for the electrons from a ^{86}Rb source which were detected directly by a geiger-muller counter. Positron and electron absorption curves for various materials were found to be exponential, $I = I_o e^{-\mu x}$, where I = intensity, I_o = initial intensity, μ = absorption coefficient, x = penetration depth, and an absorption coefficient was calculated for each material, one for each particle. The relative ranges showed that the positrons went approximately 20% farther than the electrons.

The results were explained in a later paper (1967) in terms of the atomic number of the absorber and its thickness. The equivalent thickness (t) was defined as the thickness in mg/cm^2 multiplied by Z/A, where A was the mass number. The equivalent thickness was therefore

proportional to the number of electrons per unit area. A plot of the percentage transmission (T) for either positrons or electrons showed an exponential form for all absorbers. A plot of the log of the equivalent thicknesses, which gave equal transmission (T) values, as a function of the atomic number raised to the power 1/3 gave a family of straight lines confirming the relationship given by:

$$\ln t^{\pm}(T) = m^{\pm} Z^{1/3} + c^{\pm}(T) \qquad (1)$$

where m and c are constants. The increased range of positrons with respect to electrons agreed with the theory of Rohrlich and Carlson and the relationship between absorption and the atomic number was ascribed to nuclear scattering, since if the positrons lose energy mainly by collisions with electrons the thickness t should be the same for all materials for a given transmission intensity T.

Nuclear scattering would result in the following conditions:

(a) the probability of a given angle of scatter is proportional to Z^2;

(b) the number of nucleii encountered is proportional to $\frac{1}{Z}$ for absorbers with the same number of electrons per unit volume;

(c) the energy loss per unit path length is proportional to the electron density only. The effect of nuclear scattering, therefore, was to increase the mean free path length for a given penetration depth and the increase would bear a simple relationship to Z and hence

the equation (1).

Similar results for β particles with energies about 320 KeV were obtained for lead, copper and tin absorbers although the positrons did not penetrate as far as predicted by the multiple scattering theory of Rohrlich and Carlson. Furthermore, the positrons at this energy penetrated less far in aluminium than the electrons (Rupaal and Patrick, 1972). These results agreed with those of Seliger (1955) and it was concluded that low energy positrons have a lower transmission than electrons in low atomic number materials.

Takhar had concluded that the ratio of penetration depths increased with increasing atomic number of the absorber in agreement with the multiple scattering theory. Thontardarya and Unakantha (1971) questioned his results and showed that the difference in the ranges observed was due to the different end point energies of the sources used. This suggestion had been put forward first by Cook (1969) who also suggested that the decay spectra of the sources used by Takhar were complex and not suitable for comparison. Thontadarya also explained that the absorption coefficients would be influenced by geometrical factors and therefore repeated the experiments with several suitable sources using a constant geometrical arrangement for detection.

The absorption curves obtained for all the sources and all the absorbers showed an exponential character but only over finite ranges of absorption, e.g. 80% to 99% for aluminium and 90% - 99.5% for tin. The mass absorption coefficients μ/ρ for these ranges showed that for

electrons the coefficients followed a law given by:

$$\mu/\rho = AE_o^{-B}$$ where A and B are constants

E_o is the spectrum end point energy.

The positron absorption coefficients followed a similar law although they were less than the electron coefficients, i.e. positrons had a greater range. The difference between the electron and positron coefficients was much less than that observed by Takhar.

4.2 POSITRON ELECTRON DIFFERENCES IN STOPPING POWER

The range of a particle is determined by the scattering undergone in the absorber. Differences in ranges between electrons and positrons can be explained in terms of different scattering cross sections. Estimating the quantitative differences in energy losses in an absorber allows an estimate of the respective ranges of positrons and electrons to be given.

a) Consider Inelastic Collisions where the Bethe-Block formula assumes that above a certain fractional energy transfer ε_1, the atomic electrons can be considered free so that in a collision Møller's cross section for scattering of free electrons by free electrons is applicable:

$$\left(\frac{d\sigma}{d\varepsilon}\right)^{-} = \frac{\chi}{T}\left[\frac{1}{\varepsilon^2} + \frac{1}{(1-\varepsilon)^2} + \left(\frac{\gamma-1}{\gamma}\right)^2 - \frac{2\gamma-1}{\gamma^2}\cdot\frac{1}{\varepsilon(1-\varepsilon)}\right]$$

where $\chi = 2\pi e^4/mv^2$ (1)

$E = \gamma mc^2$ the total incident energy

$T = (\gamma - 1)mc^2$ the kinetic energy

ε = energy transferred in units of T

Z = atomic number.

The higher energy outgoing electron is by definition the primary electron so that the maximum possible energy transfer $\varepsilon_m = 1/2$. Consider an atom of Z electrons then the average energy loss due to such hard collisions is given by:

$$ZT \int_{\varepsilon_1}^{1/2} \varepsilon \left(\frac{d\sigma}{d\varepsilon}\right)^{-} d\varepsilon = Z\chi \left[\ln \frac{1}{4\varepsilon_1} + 1 - \frac{2\gamma - 1}{\gamma^2}.\ln 2 + \frac{1}{8}\left(\frac{\gamma - 1}{\gamma}\right)^2\right] \qquad (2)$$

If the fractional energy transfer is less than ε_1 so that the atom has only been excited then the average energy loss is given by a summation over all the probable excitations given by:

$$ZT \int_{0}^{\varepsilon_1} \varepsilon\sigma(\varepsilon, \gamma)d\varepsilon = Z\chi \left[\frac{\ln ZT^2 \varepsilon_1(\gamma + 1)}{I^2} - \beta^2\right] \qquad (3)$$

where σ = the cross section for a given excitation (ε, γ)

I = average ionization energy

$\beta = \frac{V}{c}$

For all possible energy transfers the two are combined to obtain the average energy lost due to collisions per unit path length x in a medium with N atoms per unit volume given by:

$$-\left(\frac{dE}{dx}\right)^{-} = NZ\chi \left[\ln\left(\frac{T^2}{I^2}\frac{\gamma + 1}{2}\right) + f^{-}(\gamma)\right] \qquad (4)$$

$$\text{where } f^{-}(\gamma) = 1 - \beta^2 - \frac{2\gamma - 1}{\gamma^2}.\ln 2 + \frac{1}{8}\left(\frac{\gamma - 1}{\gamma}\right)^2 \qquad (5)$$

For positrons the process is the same but because positrons are distinguishable from electrons the upper limit for energy transfer becomes 1. Similarly, when the energy transfer is large the appropriate cross-section is Bhabba's given by:

$$\left(\frac{d\sigma}{d\varepsilon}\right)^{+} = \frac{\chi}{T}\left[\frac{1}{\varepsilon^2} - \frac{\gamma^2-1}{\gamma^2}\cdot\frac{1}{\varepsilon} + \frac{1}{2}\left(\frac{\gamma-1}{\gamma}\right)^2 - \left(\frac{\gamma-1}{\gamma+1}\right)Q + \left(\frac{\gamma-1}{\gamma+1}\right)^2 Q'\right] \tag{6}$$

where $$Q = \frac{\gamma+2}{\gamma}\cdot\frac{1}{\varepsilon} - 2.\frac{\gamma^2-1}{\gamma^2} + \varepsilon\left(\frac{\gamma-1}{\gamma}\right)^2 \tag{7}$$

$$Q' = \frac{1}{2} + \frac{1}{\gamma} + \frac{3}{2\gamma^2} - \left(\frac{\gamma-1}{\gamma}\right)^2\cdot\varepsilon(1-\varepsilon) \tag{8}$$

Assuming that the average energy loss due to atom excitation is the same since it is primarily a function of the atom and not the exciting particle, the average energy lost due to collisions per unit path length x as above is given by:

$$-\left(\frac{dE}{dx}\right)^{+} = NZ\chi\left[\ln\left(\frac{T^2}{I^2}\cdot\frac{\gamma+1}{2}\right) + f^{+}(\gamma)\right] \tag{9}$$

where $$f^{+}(\gamma) = 2\ln 2 - \frac{\beta^2}{12}\left[23 + \frac{14}{\gamma+1} + \frac{10}{(\gamma+1)^2} + \frac{4}{(\gamma+1)^3}\right] \tag{10}$$

At energies around 212 KeV the rate of loss of energy is initially the same but this does not last long. In general, the difference in collision loss is dependent only on the incident energy through the factors $f^{\pm}(\gamma)$ and it is not really dependent on the atomic number of the absorber. Below about 345 KeV. positrons will lose energy more rapidly than electrons but less rapidly above this level. This difference of several percent will only be detectable in

terms of ranges if the effect of multiple elastic scattering is the same for both particles.

b) Consider Elastic Collisions

The cross section for elastic scattering of positrons and electrons by the coulomb field of a charge Ze was given by Mott in the form of a series of Legendre Polynomials which can be expanded in terms of $\frac{Z}{137}$ to give:

$$\sigma_{\pm}(\Theta, \gamma) = \frac{1}{4}\left(\frac{r_o Z}{\beta^2 \gamma}\right)^2 \left(\frac{1}{\sin^4 \Theta/2}\right)\left[1 - \beta^2 \sin^2 \frac{\Theta}{2} \mp \frac{2\pi\beta}{137} \sin\frac{\Theta}{2} \cdot \left(1-\sin \frac{\Theta}{2}\right)\right] \qquad (11)$$

The ratio $\frac{\sigma_+ - \sigma_-}{\sigma_-}$ is zero at scattering angles of 0° and 180° and is otherwise negative with a minimum

$$-2\left[\frac{2 \times 137}{\pi Z}\left(\frac{\gamma+1}{\gamma-1}\right)^{1/2} + 1\right]^{-1} \quad \text{at } \sin\frac{\Theta}{2} = \frac{\gamma}{\gamma+1}$$

This means that the minimum goes from 60° to 180° as the energy increases from 0 to ∞, i.e. σ_- is always bigger than σ_+ and may be as much as three times bigger depending on the energy and the angle.

The difference in multiple scattering between positrons and electrons is only important if it results in a different average penetration depth at which the original direction is completely lost, i.e. particle direction is random. The solution of Boltzmann's equation for an infinite medium is that the path length x is given by:

$$x = \int_0^x dx' = \int_E^{E_o} \left|\frac{dx'}{dE}\right| dE \qquad (12)$$

where E = particle energy

E_o = initial particle energy.

From the elastic cross sections we can determine the likelihood of the particle undergoing a specific deflection and by suitable integration discover the probable average angle Θ through which it has been deflected for a given path length. If the loss of initial orientation is defined as $\langle \cos \Theta \rangle_{\text{Average}} = 1/e$, when the average total energy $E_d = \gamma_d mc^2$, then the average penetration depth Z_d is given by:

$$Z_d = \int_o^x \langle \cos \Theta \rangle_{Av} dx' = \int_d^o \langle \cos \Theta \rangle_{Av} \left| \frac{dx'}{d\gamma} \right| d\gamma \quad (13)$$

But $\langle \cos \Theta \rangle_{Av}$ is a function of the elastic cross section per unit solid angle (for particles of total energy E) as well as the path length x. But the elastic cross sections for positrons and electrons are different so for a given path length the energy lost must be different, which in turn must affect $\langle \cos \Theta \rangle_{Av}$ (a function of the energy γ). Therefore, $\langle \cos \Theta \rangle_{Av}^{+}$ and $\langle \cos \Theta \rangle_{Av}^{-}$ must be different just as $(\frac{d\gamma}{dx})^{+}$ and $(\frac{d\gamma}{dx})^{-}$ are different and:

$$Z_d^{\pm} = \int_d^o \langle \cos \Theta \rangle_{Av}^{\pm} \left| \frac{dx'}{d\gamma} \right|^{\pm} d\gamma \quad (14)$$

At the average penetration distance Z_d the intensity distribution can be described by the diffusion theory. Using Boltzmann's theory the intensity at distance S due to a uniform plane source at $x = Z_d$ is given by:

$$I(x) = I(Z_d)\,[1 - \mathrm{erf}(\frac{x - Z_d}{1.225 r_{Av}})] \qquad (15)$$

$$\text{where } r^2_{Av} = 1.05 \int_0^{\gamma d} \frac{1}{\langle \cos\theta \rangle_{Av}} \left| \frac{ds}{d\gamma} \right| d\gamma \qquad (16)$$

which takes the energy loss into account. The theoretical range is thus given by:

$$R_{TH} = Z_d + r_{Av} \qquad (17)$$

So on passing through matter the statistical behaviour of positrons and electrons reflects their single scattering differences through:

a) the cross section for inelastic scattering by atomic electrons;

b) the maximum possible energy loss in such a collision;

c) the elastic cross section.

The stopping power or average rate of energy loss is affected by a) and b) although the effect may be masked in range measurements because of c). Range differences would be marked in heavy elements because the cross sections and multiple scattering differences are dependent on the atomic number.

This theory has been updated to give a better explanation of experimental results especially in the region below 100 KeV (Batra and Sehgal, 1970). Both inelastic and elastic collisions were considered by using an empirical relation for the total stopping power of the absrober and the results were corrected for the multiple

scattering effect. The average range of a charged particle energy E is given by:

$$R(E) = \int_0^E \left[\frac{1}{\rho}\left(\frac{dE}{dx}\right)_{TOTAL}\right]^{-1} dE \qquad (18)$$

where ρ = density, and:

$$\left(\frac{dE}{dx}\right)_{TOTAL} = \left(\frac{dE}{dx}\right)_{COLLISION} + \left(\frac{dE}{dx}\right)_{RADIATION} \qquad (19)$$

This shows that positrons and electrons will lose energy by collision and excitation and by bremstrahlung radiation. In the same way as in the previous method the average collision loss per unit path length is given by:

$$-\left(\frac{dE}{dx}\right)^{\pm}_{COLLISION} = NZ\chi\left[\ln\left(\frac{T^2}{I^2}\cdot\frac{\gamma+1}{2}\right) + f^{\pm}(\gamma) - \delta\right] \qquad (20)$$

where $f^{-}(\gamma) = 1 - \beta^2 - \frac{2\gamma-1}{\gamma^2}\cdot\ln 2 + \frac{1}{8}\left(\frac{\gamma-1}{\gamma}\right)^2$ for electrons

$$f^{+}(\gamma) = 2\ln 2 - \frac{\beta^2}{12}\left[23 + \frac{14}{\gamma+1} + \frac{10}{(\gamma+1)^2} + \frac{4}{(\gamma+1)^3}\right]$$

for positrons.

These reflect the difference between the Møller and Bhabba cross sections and δ is a density effect correction, where N = number of atoms per unit volume

$\chi = 2\pi e^4/mv^2$

I = average ionization energy

$E = \gamma mc^2$ the total incident energy

$T = (\gamma-1)mc^2$ the kinetic energy of the moving electron.

The energy loss due to radiation was derived by Bethe and Heitler and was corrected by Koch and Motz to give:

$$-\left(\frac{dE}{dx}\right)_{\text{RADIATION}} = N \int_0^T k \, d\sigma_K \qquad (21)$$

where k = energy of the emitted photon in units $m_e c^2$

m_e = mass of electron (The equation is only strictly true for an electron.)

$d\sigma_K$ = differential form of the Bremstrahlung cross section.

If the reciprocal of (21) ÷ (20) is the range then this is very complex so an empirical relation for the total stopping power may be used given by:

$$-\frac{1}{\rho}\left(\frac{dE}{dx}\right)^{\pm}_{\text{TOTAL}} = (mZ+c)\, F^{\pm}(\gamma) \qquad (22)$$

where ρ = density of absorber

$$\left.\begin{aligned} F^{+}(\gamma) &= \gamma^{2.4} / \gamma^{1.9} - 1 \\ F^{-}(\gamma) &= \gamma^{2.56} / \gamma^{2} - 1 \end{aligned}\right\} \text{ For } T \leq 500 \text{ KeV}$$

The factors m and c can be calculated and hence the stopping powers. Comparison of experimental data and theoretical data justifies the empirical relation because the errors are never more than 4% and it is possible to compute a smooth error curve which allows corrections to be made to the range as estimated by (22).

Because of the multiple scattering effect which becomes important at very low energies the theoretical range is always greater than the measured value. At low energies multiple scattering angles may become large and the motion becomes random so that the true range is given by:

$$R = R(E) - R(E_r)$$

where R(E) is the theoretical range

$R(E_r)$ is the theoretical range at the energy at which random motion can be said to start provided that random motion straggling is small.

4.3 EXPERIMENTAL METHOD

It was intended to compare the energy losses and therefore the ranges of positrons and electrons using the silicon detector and the ^{68}Ge positron source. In order to equalise the energies of the particles from the positron source and the ^{86}Rb electron source a thin absorber would be placed in front of them until their β ray spectra were identical as seen by the silicon detector. The effect of further absorbers could therefore be investigated to give quantitative information about the numbers of particles absorbed and the energy lost.

A preliminary experiment was conducted to investigate Takhar's results using the ^{22}Na positron source and a range of aluminium absorber thicknesses. The positron beam was collimated to one cm. in diameter and angular deviation 40 mrads. by lead collimators. The beam then passed through a thin mylar window into the absorber and the number of positrons annihilating in the absorber was detected by the triple coincidence system. A diagram of the apparatus is given in Fig. 4.1. The absorbers ranged between 0 and 256 mg./cm.^{2} and the minimum count over a 35 minute period was 180,000 giving a statistical error of about .25%. The results adjusted for background count are shown in Fig. 4.2 where the errors in the points are smaller than the size of the point.

Fig. 1.1 Absorption Experiment Arrangement

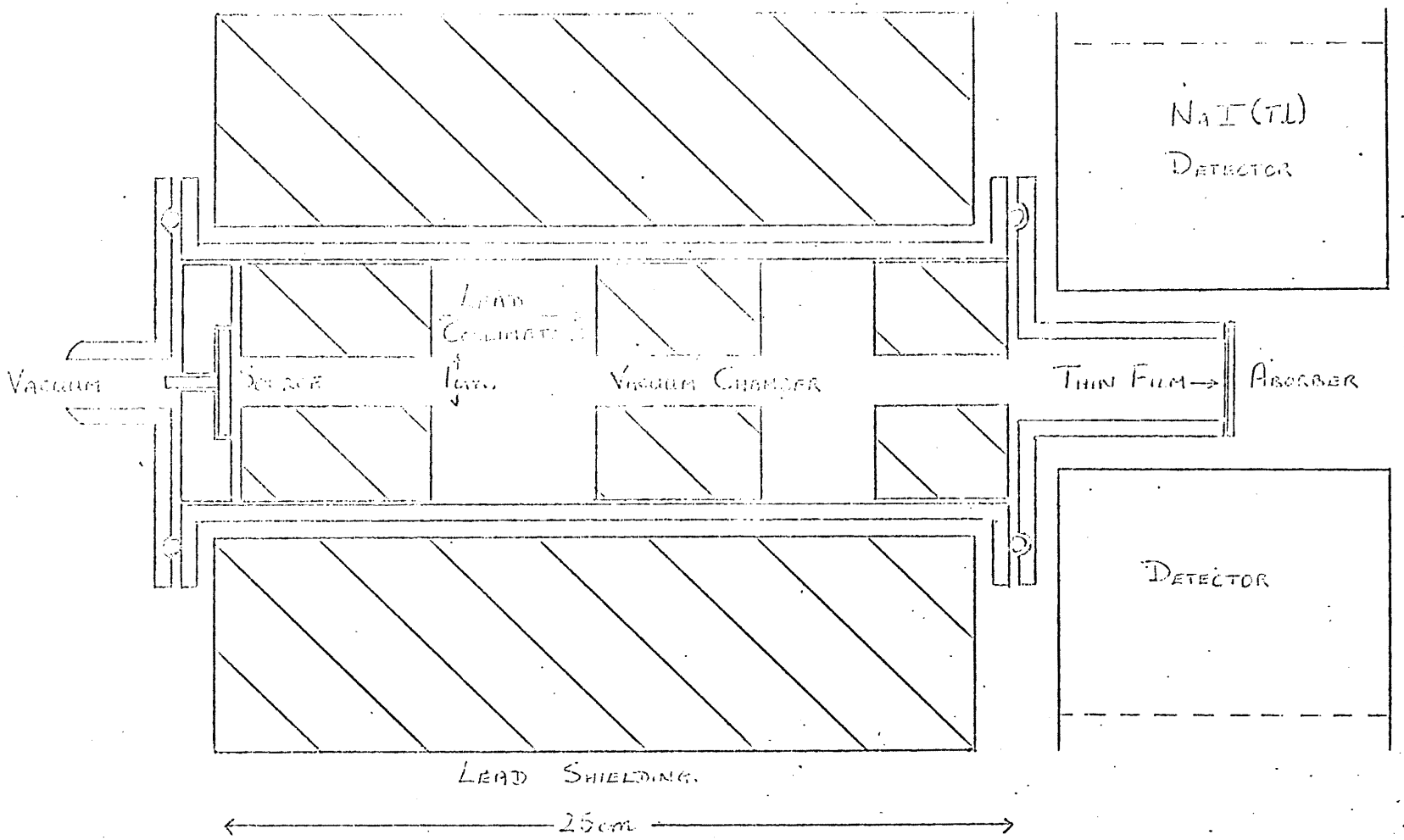

Fig. 1.2 Transmission of Protons through Aluminium.

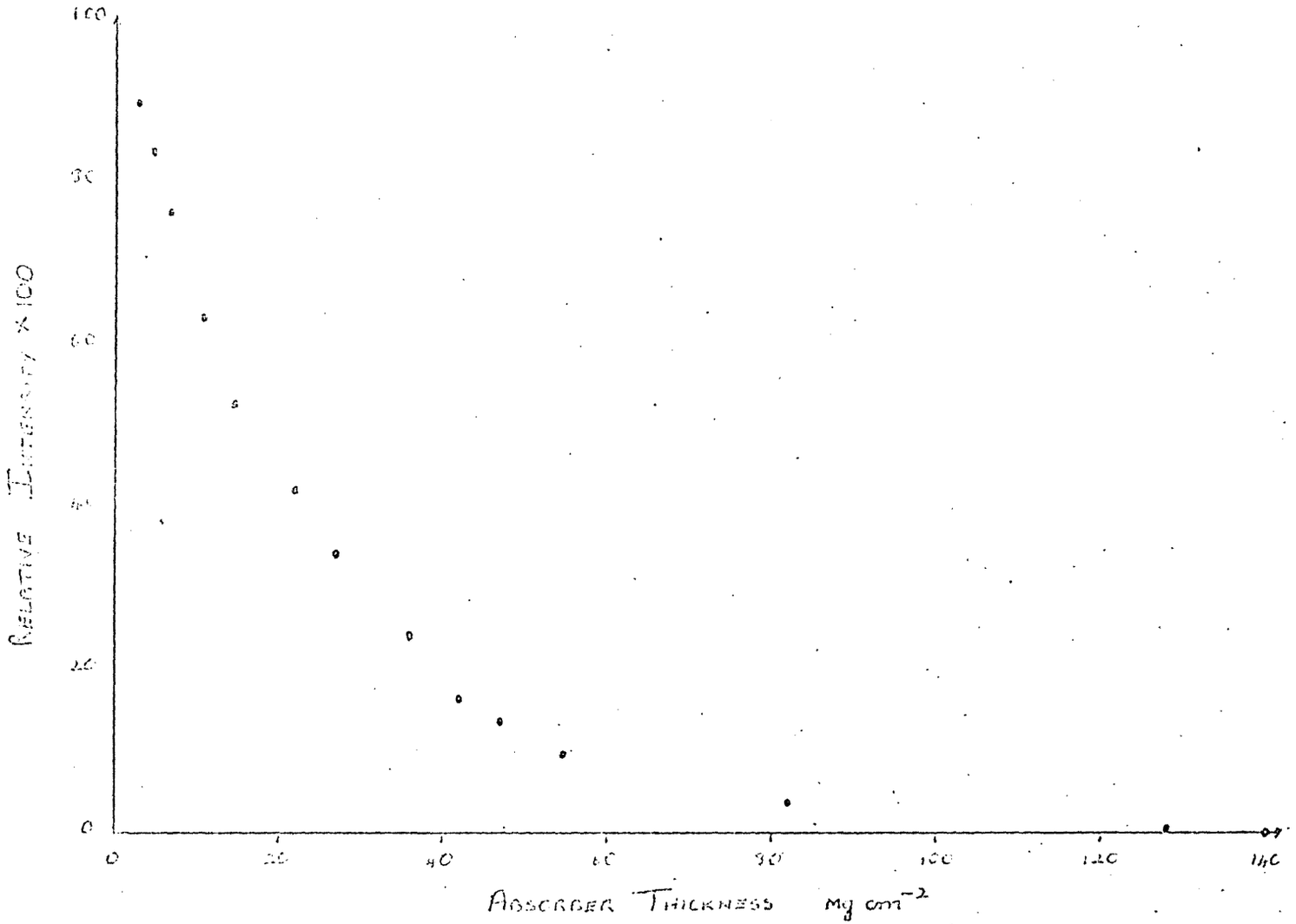

4.4 DISCUSSION OF RESULTS

Fig. 4.2 shows the relative intensity of the transmitted beam as a function of absorber thickness measured in mg./cm.^{2}. The curve appears fairly exponential which might indicate either:

1) that the ^{22}Na positron spectrum has a shape whose area increases exponentially so that if a given absorber thickness absorbs all the positrons up to a certain energy then the transmission curve would have an exponential shape;

2) or that the absorption follows a law of the form

$I = I_o e^{-\mu x/\rho}$ (1) (Takhar)

where I = the transmitted intensity at absorber thickness x mg./cm.^{2}

I_o = the initial intensity of the positron beam

μ/ρ = the mass absorption coefficient.

To use Takhar's 't' thickness ($= \frac{Zx}{A}$) instead of x will only change the x axis scale and will not affect the relative positions of data points. From this equation (1) $\ln I = \ln I_o - \frac{\mu x}{\rho}$ and a plot of ln I versus thickness x should give a straight line with gradient equal to the absorption coefficient μ/ρ, Fig. 4.3. From the graph the absorption appears not to be strictly exponential except over the transmitted range 20% to 0% which agrees with Thontadarya and Umakantha. However, they compared their results with those of Chang et al. and Baskova and Gorbachev who used monergetic beams of particles which is comparable with considering the last 20% of positrons transmitted which will be the most energetic and will all

FIG. 6.3 LOGARITHMIC PLOT OF NEUTRON TRANSMISSION THROUGH ALUMINIUM.

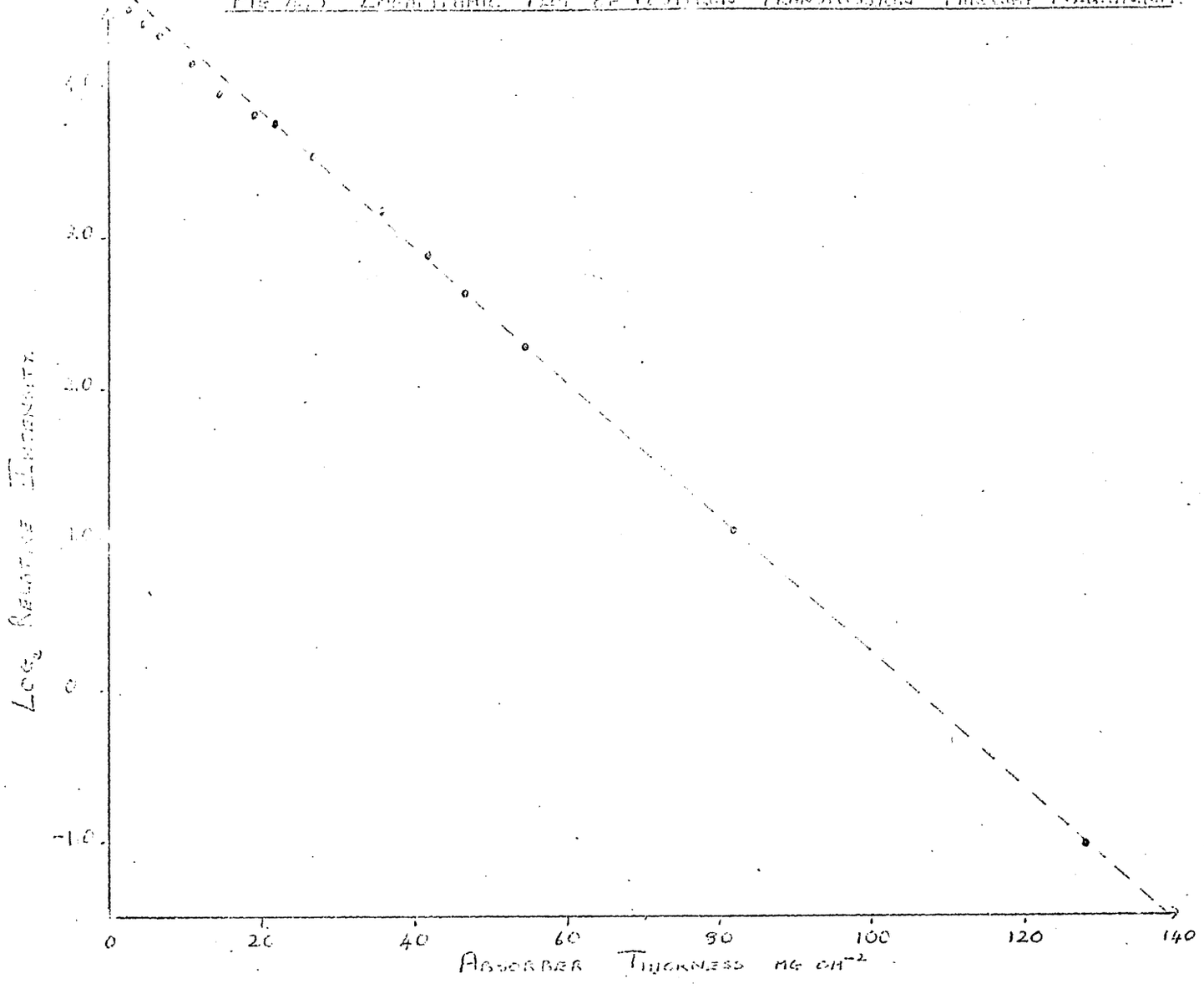

fall within a narrow energy band. From the curve a mass absorption coefficient for the last 20% of 44.9 $cm.^2g^{-1}$ can be obtained which compares with 46.7 $cm.^2g^{-1}$ obtained by Thontadarya et al.

Gleason et al. postulated that the value for for beta particles would follow a law of the type:

$$\mu/\rho = AE_o^{-B}$$

where A and B are constants and in this case Eo is the end point energy. For negative beta particles the constants are A = 17.6 and B = 1.39 which gives $\mu/\rho = 40.92\ cm^2g^{-1}$. Thontadarya et al. suggest that for positrons the constants should be A = 22 and B = 1.33 which gives $\mu/\rho = 49.32\ cm^2g^{-1}$. The error between the calculated absorption coefficient and the experimental value increases with end point energy which may be because as the end point energy increases the energy band comprising the top 20% energetic positrons widens and deviates more and more from the ideal monoenergetic source.

The range of positrons in matter is given by the equation:

$$R^+(E) = \int_0^{E_T} \left[-\frac{1}{\rho} \left(\frac{dE}{dx}\right)^+_{TOTAL} \right]^{-1} dE$$

Batra and Sehgal have suggested the empirical relation:

$$-\frac{1}{\rho} \left(\frac{dE}{dx}\right)_{TOTAL} = (KZ + L)\, F^+(\gamma)$$

where $K = -0.00595$ gm cm^{-2} MeV^{-1}
$L = +0.9280$ gm cm^{-2} MeV^{-1} } constants

$Z = 13$ the atomic number of the absorber aluminium

where $F^+(\gamma) = \gamma^{2.4} / \gamma^{1.9} - 1$

$E = \gamma mc^2$ the total incident energy

$T = (\gamma - 1)mc^2$ the kinetic energy

$= .545$ MeV max. for ^{22}Na.

$$\therefore \quad R^+ = \int_E^{E_o} [(KZ+L) F^+(\gamma)]^{-1} dE = \frac{1}{(KZ+L)} \int_E^{E_o} \frac{\gamma^{1.9-1}}{\gamma^{2.4}} .dE$$

However, comparing the two sides of this equation shows that it is dimensionally incorrect. We suggest that the original empirical relation should have been

$$-\frac{1}{\rho} \left(\frac{dE}{dx}\right)_{TOTAL} = (KZ+L)^{-1} F^+(\gamma) \qquad \text{and therefore:}$$

$$R^+ = (KZ+L) \int_E^{E_o} \frac{\gamma^{1.9-1}}{\gamma^{2.4}} . dE$$

Now $E = \gamma mc^2$ $\therefore$ $dE = mc^2 d\gamma$ and the integration limits are due to the most energetic positron losing all of its kinetic energy. Thus when $E = E_o$ the end point energy $\gamma = \gamma_o$ and when the kinetic energy is zero $E = mc^2$ and $\gamma = 1$.

$$\therefore R^+ = (KZ+L)mc^2 \int_1^{\gamma_o} \frac{\gamma^{1.9-1}}{\gamma^{2.4}} . d\gamma = (KZ+L)mc^2 \left[\frac{\gamma^{.5}}{.5} + \frac{\gamma^{-1.4}}{1.4}\right]_1^{\gamma_o}$$

But $T = (\gamma - 1)mc^2$ or $T_o = (\gamma_o - 1)mc^2 = .545$ MeV

where $m = 9.109 \times 10^{-28}$ g, the electron mass

$c = 2.998 \times 10^{10}$ cm.sec^{-1} the velocity of light

$1eV = 1.602 \times 10^{-12}$ erg.

$\gamma_o = T_o/mc^2 + 1 = 2.06647$

$$\text{and } R^{+} = \frac{(81.872 \times 10^{-8})(.85065)}{1.602 \times 10^{-6}} \left[\frac{\gamma^{.5}}{.5} + \frac{\gamma^{-1.4}}{1.4}\right]_{1.0}^{2.06647}$$

$$= 43.473 \times 10^{-2} \times .419 = 182.22 \text{ mgm cm}^{-2}$$

This range will be overestimated because the multiple scattering effect has been neglected. The concept of a definite range is anyway peculiar because the absorption is considered to be exponential. To get round this Armstrong quotes the range as being the distance at which the transmitted intensity is less than 0.01% and has measured the range of 545 KeV β particles to be 120 mgm.cm^{-2}. Our experiment would yield an 0.01% range of 136.72 mgm.cm^{-2} which compares with the calculated range within 30.0%.

Our conclusion is that the exponential absorption of the whole ^{68}Ge positron source spectrum reported by Takhar was an accident caused by the shape of the spectrum and/or the geometry of his apparatus. This would be particularly true for an ordinary β source since the shape of the spectrum is bound to have a major effect on the transmission curve. Furthermore, Takhar's conclusion that the transmission is Z dependent follows from conventional energy loss considerations which, in general, seem to explain his results better than he does himself.

CHAPTER 5

VACANCIES IN METALS

5.1 INTRODUCTION - POSITRONS IN METALS AND TEMPERATURE EFFECTS

The first account of the effect of temperature on positron motion in metals was published in 1966 (Stewart and Shand). The contemporary theory was that positrons were thermalised by scattering with electrons at a rate much faster than they were annihilated. The average positron energy at annihilation would be less than 1eV. and this would result in the annihilation photons' angular distribution having a sharp cut-off corresponding to the Fermi momentum. It was now shown that at high temperatures this cut-off became smeared out because the positron energy at annihilation was much greater. However, analysis of the data obtained by a standard angular correlation technique showed that there was an effective positron temperature 1.9 times the real temperature, i.e. the positrons were not completely thermalised before annihilation. An alternative suggestion was that in an electron sea the positron's effective mass was 1.9 times the rest mass.

The same technique was used on several metals by Kim et al. (1967) who concluded that the optical resolution of the apparatus would cause the cut-off to appear smeared out equivalent to a positron thermalisation energy 60°K above the true temperature. Furthermore, the effective positron temperature was linear with specimen temperature at high temperatures suggesting that the positron

probably thermalised. At low temperatures this linearity was lost, i.e. no thermalisation, and the calculated low temperature thermalisation time was found to be longer than the annihilation time.

Apparatus with much better resolution was used to investigate the suggestion that positrons might tend to annihilate in low electron density regions around dislocations and vacancies (Connors and West, 1969). The angular distribution curve of photons resulting from annihilation in deformed aluminium had been found to be narrower than that due to annihilation in annealed aluminium. A similar effect was expected, along with a change in the lifetime, if vacancies produced by heating the sample attracted the positrons. Assuming a very short thermalisation time then a positron could either annihilate freely or be trapped and annihilate with a different lifetime. The measured lifetime would be a combination and would depend on the number of positrons annihilating at vacancies. This would mean that the measured lifetime would depend on the temperature via the activation energy for vacancy formation. The effect of temperature on the lifetime was plotted theoretically assuming a Maxwell-Boltzmann distribution of positron energies and a screened potential interaction between positrons and vacancies and showed good correlation with experimental results.

A very similar effect was demonstrated by Bartenev et al. (1970) who showed that the lifetime and annihilation photon angular distribution depended on the state of aggregation of a substance. In non-metals annihilation usually occurs from a state of positronium and

the main two methods are orthopositronium pick-off (annihilation with an electron other than the one in the positronium 'atom') and orthopositronium decay to parapositronium quickly followed by annihilation. If a positronium 'atom' can only exist stably in a certain minimum 'free' volume which is greater than the interatomic spacing then the positronium must usually be contracted resulting in a smaller lifetime. Also, the angular correlation F.W.H.M. will be larger because of the increased kinetic energy. If defects bigger than the minimum 'free' volume are introduced, e.g. vacancies or pores, then the positronium will be favourably captured there. Not only is the positronium able to exist stably in such a defect but the electron density will be lower so that the annihilation rate due to orthopositronium pick-off falls. The percentage of parapositronium annihilation will increase and overall the lifetime will be longer and the angular correlation curve narrower. Experiments on samples in various states of aggregation showed that annihilation depended on the number and type of defects in the sample.

A special electronic system was developed to measure the F.W.H.M. of the angular correlation curve directly in order to show that the width was related to the number of trapped positrons (Mackenzie et al., 1970). Using pure copper and an aluminium alloy the line width was found to be proportional to the number of dislocations i.e. sample hardness measured with a special meter. Providing that the trapping did not become saturated the width of the angular correlation curve was a good measure of the

sample hardness.

Positrons are attracted to vacancies etc. because of the difference between the bottom of the positron energy band in a solid and the potential felt by a positron inside a vacancy, i.e. a vacancy is a positron potential well (Hodges, 1970). The capture process is sufficiently fast to cause saturation even at low vacancy concentrations c. 10^{-5}.

Working backwards Tagaki et al. (1971) showed that the electron distribution at a lattice defect is anomalous by comparing the angular correlation curves obtained from two samples of copper, one of which had been plastically deformed.

Dekhtyar and Cizek attempted to show that the fraction of positrons trapped is proportional to the root of the temperature by comparing angular correlation curves obtained at 77°K and 300°K. The fraction of positrons trapped should depend on the annihilation rates at dislocations and at perfect regions, the number of dislocations, and the rate of trapping which is dependent on the trapping cross-section. However, measurement of the angular correlation curves obtained from an initially annealed sample over a range of temperatures from 100°K to 520°K showed that the main cause of the temperature dependence of positron lifetimes is the trapping of positrons in vacancies. Any differences in the curves must have been due to the temperature and structural differences via the activation energy for vacancies (Connors et al., 1971). The experimental results correlated well with a theoretical curve obtained from a more rigorous statistical treatment

than that employed by Dekhtyar and allowed a value for the vacancy activation energy to be obtained. It was suggested that the effects due to vacancies could easily be confused with either changes in non-local electronic properties, i.e. impurities, or the possible preference of positrons for one component in an alloy.

The lifetimes of positrons in various alkali metals over a very large range in temperatures did not vary, implying that there was no trapping (Mackenzie et al., 1971). Since the theory of positron annihilation had been based on the free electron gas assumed in alkali metals it would no longer have been viable if vacancy trapping had been important in these metals. No trapping was probably a result of the vacancies being too small or not attractive to positrons.

Working at very low temperatures Dekhtyar found that the total area under the 2 γ angular correlation curve increased with temperature. He suggested that at low temperatures there was an increased probability of diffractional reflection from internal faces of the crystal long before thermalisation. Subsequent channelling would enable some of the positrons to escape from the crystal resulting in fewer annihilations and a smaller area under the curve. Another suggestion was that there was increased annihilation in flight at low temperatures as well as channelling in single crystals (Faraci et al., 1972). Both effects would be destroyed at higher temperatures by lattice vibrations. However Campbell et al. (1972) concluded that Dekhtyar and Faraci were mistaken since they could find no change in the intensity of the 511 KeV gamma ray peak with

temperature.

Thermally generated lattice defects or vacancies have a large effect on positron lifetimes in Al, Cd, Zn, In, etc. At low temperatures the vacancy concentration is too small to affect the lifetime, but at ordinary temperatures the effect becomes more marked as the concentration increases. Above a certain temperature saturation occurs when all the positrons are trapped and annihilate from vacancies. McKee et al. (1972) were, however, unsuccessful in proving the trapping model by studying the annihilation rates at various temperatures because their results were inconclusive. Later workers (McKenzie, 1973) have shown that the trapping model will successfully explain their experimental results.

5.2 METHODS OF MEASURING THE VACANCY FORMATION ENERGY

The vacancy concentration can be obtained from:

1) direct measurement under equilibrium conditions. Such experiments show that the predominant thermally generated defect in metals are monovacancies and theoretically any property affected by the presence of point defects which can be measured at high temperatures may be used to study the concentration of defects;

2) quenched in high temperature defects which can then be studied at lower temperatures;

3) the production and study of defects at lower temperatures by cold working the sample.

Theoretical estimates of the vacancy formation energy have been based on the model of a metal proposed by Huntingdon and Seitz (1942) which consists of ions repelling

their nearest neighbours according to a Born-Mayer or Morse potential. The metal stays together because of an elastic matrix or by springs outside the imperfect crystal unit. Zero-point and thermal motion of the ions is neglected. However, depending on the method of calculation the vacancy formation energy for copper has been given in the range 0.8 to 1.8 eV.

The value of E_F^V may be obtained from the quenched in resistivity as a function of the quenching temperature T_Q. The results are not very satisfactory because the equilibrium vacancy concentration quenched in is very small (e.g. $<$ 1 part per million below 600°C) and is much less than typical impurity concentrations. Airoldi et al. quenched 0.04 mm. diameter wires in gaseous argon at 5×10^3 degree/second and the resistivity increments indicated that $E_F^V \approx 1.0$ eV. However by isothermally annealing out the extra resistivity they obtained another value of $E_F^V \approx 1.3$ eV. In general the experiment does not give reproducible results.

Monovacancies and interstitial atoms are the main defects produced by bombarding metals with energetic particles. These defects are mainly annealed out at room temperature by monovacancy migration although this does depend on the samples history, e.g. irradiation dose. Thermal annealing experiments show two peaks for copper near room temperature and their associated activation energies are 0.65 eV and 1.2 eV. Since these are migration energies which are simply related to the vacancy formation energies, but not similar, neither value seems to predict a good value for E_F^V.

The same sort of defects can be produced by cold working and at low temperatures the annealing is again expected to be a monovacancy process although the effect would be impeded by the many dislocations produced. None of the annealing peaks can be identified with a particular migrating defect but the decrease in internal friction and increase in elastic modulus found when annealing slightly strained samples is attributed to defects migrating to dislocations which are then unable to move. The kinetics of this reaction gives a copper vacancy migration energy of 1.0 eV. which is nearer the expected value.

If self-diffusion in metals is a monovacancy mechanism then the data should yield information on the vacancies. The activation energy of self-diffusion is defined in terms of the temperature dependence of the true self-diffusion coefficient D^T by:

$$Q^{SD} = d(\ln D^T) / d(1/kT) \quad \text{and} \quad Q^{SD} = E_F^V + E_M^V$$

where E_M^V = migration energy of a monovacancy.
The method is to inject a radioactive tracer atom into a large thermal gradient in the metal and observe its motion as a function of the temperature. Seeger and Mehrer (1970) used this method and obtained a vacancy formation energy for copper of 1.05 eV.

According to statistical thermodynamics the concentration of vacancies in thermal equilibrium in a crystal is given by:

$$C^{IV} = \exp(-G_F^{IV}/kT)$$

where G_F^{IV} = the Gibbs free energy of monovacancy formation

$= H_F^{IV} + TS_F^{IV}$

where H_F^{IV} = the enthalpy for formation which is usually given the symbol

E_F^{IV} = the 'energy' of formation at atmospheric pressure

S_F^{IV} = the entropy of formation.

Strictly E_F^{IV} is the work done at atmospheric pressure and constant temperature in creating a single vacancy, keeping the total number of atoms in the crystal constant. This disregards the possibility that there is a binding energy between near vacancies which could cause the formation of divacancies so that the total vacancy concentration is given by:

$$C_V = C_{IV} + C_{2V} + C_{3V} \cdots$$

In general the concentrations of di and higher order vacancies is negligible with respect to the concentration of monovacancies and throughout this discussion vacancy implies monovacancy.

Equilibrium experiments usually produce the best results which are accurately repeatable but they may suffer from two major disadvantages. One is that the effect of unit concentration of defects is unknown and therefore so is the proportionality factor between effect and defect concentration and the other is that the true vacancy contribution to an effect is hard to assess since it is impossible to compare it with a defect free crystal. Calorimetric measurements do not suffer from these disadvantages when the specific heat or heat content is

determined as a function of temperature. The heat absorbed by vacancies formed after a small temperature change is obtained from the difference between the measured temperature change and the expected temperature change which would occur if no vacancies were formed. The increase in vacancy concentration can be calculated although the concentrations are usually very high, probably due to errors in estimating the expected temperature change.

Electrical resistivity of metal at high temperatures shows a progressive increase above the expected values for a defect free metal. Resistivity measurements suffer from the disadvantages above but are easy to accomplish and can give good results if the background defect free effect is small. The increase in resistivity is probably due to additional scattering of the electrons by the defects.

Simultaneous measurement of the X-ray lattice parameter (a) and the specimen length (l) as a function of temperature was first suggested by Berry in 1956. If a vacancy is created in a rigid crystal by taking an atom away from an internal site and putting it on the surface, the dimensions of the unit cell measured by the X-rays will remain unchanged whereas the volume of the crystal will increase. An interstitial atom would have the opposite effect on the crystal volume. Similarly, elastic relaxation due to temperature increase will affect both volume and X-ray parameter equally. Hence, the difference between macroscopic volume and X-ray parameter is proportional to the number of vacancies - number of

interstitials. For a cubic crystal:

$$3(\Delta L/L - \Delta a/a) = \Delta N/N$$

where $\Delta N/N$ = net added concentration of substitutional sites - predominantly vacancies. If the left hand side is measured to an accuracy of 10^{-5} and the concentration of vacancies at the melting point is a maximum in the range 10^{-3} - 10^{-4}, then the best experimental error is of the order 1 - 10%. Impurities may also affect the results by producing lattice dilation or by causing a binding energy between vacancy and impurity. The method has been extensively used by Simmons and Balluffi and co-workers.

The equilibrium concentration of vacancies can be measured directly from its effect on positron annihilation. If the positrons are attracted to vacancies where the electron density is anomalous then the annihilation parameters will change.

5.3 POSITRON TRAPPING AT VACANCIES

The atomic nucleus will repel positrons and so the positron's potential energy is smallest in the interstices of the lattice because the core electrons partially shield the nucleus from the positron. Therefore the positron will probably spend most of its time between the nucleii. In the noble metals the ion cores of neighbouring atoms touch each other and so the strongly repulsive potentials around the lattice sites extend far into the unit cell. The varying potentials seen by a positron in copper etc. whose path is parallel to the crystal axis is

shown in Fig. 5.0 (a, b). The positron path may be through the atom sites or between them, when the potential energy at the saddle point can be quite high.

The positron wave functions are Block waves in a periodic lattice:

$$\Psi_k(\underline{r}) = \exp(i\,\underline{k}.\underline{r})u_k(\underline{r})$$

where $u_k(r)$ has the periodicity of the lattice. In f.c.c. or b.c.c. Bravais lattices the wave function with the lowest energy ε_o has wavevector $\underline{k} = 0$ and

$$\Psi_o(r) = u_o(\underline{r})$$

This has the periodicity of the lattice and tunnels through the saddle point from unit cell to unit cell, i.e. ε_o just less than saddle point energy. The wider the core the higher the saddle point energy and consequently the harder it is for the positron to tunnel through. The value of ε_o has been calculated to be 4 eV for copper (Hodges, 1970).

Suppose that one of the ion cores is removed so that a vacancy results then the neighbouring cores will be inwardly displaced (relaxed) and the vacancy's effective negative charge will be screened somewhat by a redistribution of the conduction electrons (Fig. 5.0d). The additional potential well at the location of the missing ion core is quite deep and will depend on the width of the core. If the positron falls into the vacancy the combination of the potential well plus the necessary tunnelling

FIG 5.0 POSITRON POTENTIAL ENERGY IN NOBLE METALS.

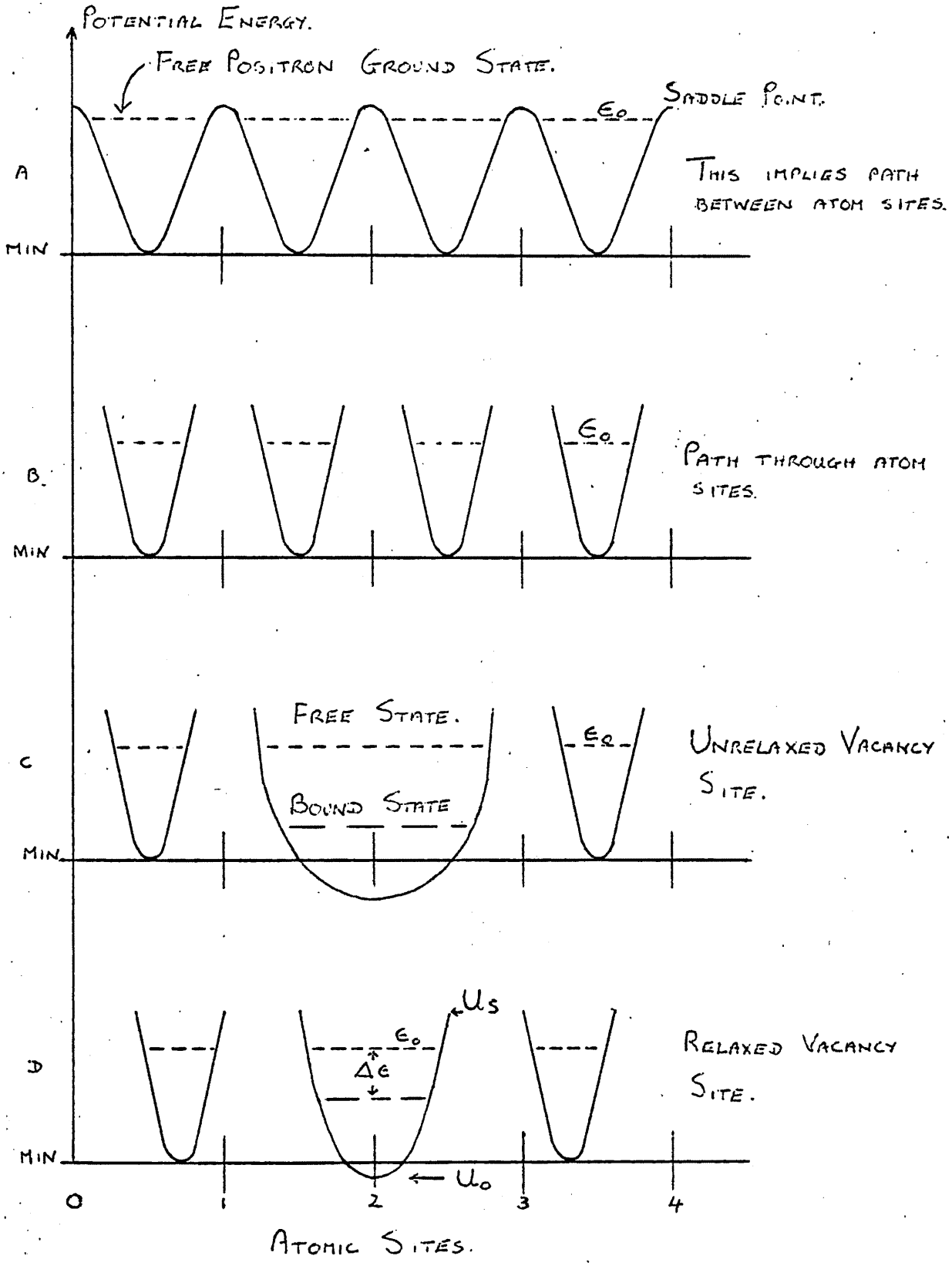

energy may be much greater than its energy and it cannot escape, i.e.

$$U_o + U_S \gg 4 \text{ eV (say)}$$

where U_o = depth of potential well

U_S = tunnelling energy.

A vacancy will be attractive to positrons because of its net negative charge and a positron which falls into the vacancy may become trapped because it has insufficient energy to escape, i.e. $\Delta\varepsilon$ too large. Annihilation can occur in the free state or in the trapped state where the positron experiences an anomalous electron density which will cause the annihilation parameters to change. For example, the annihilation rate at zero angle will be the weighted mean of the two methods given by:

$$I = I_F P_F + I_V P_V \qquad (1)$$

where P_V = probability of annihilation at a vacancy

P_F = probability of annihilation in free state

I_V = count rate from trapped state

I_F = count rate from free state

I = total count rate from crystal.

Let n_F be the number of positrons in the free state then:

$$\frac{dn_F}{dt} = - \lambda_F n_F - \mu C_V n_F + N$$

where λ_F = free annihilation rate

C_V = vacancy concentration

μ = trapping rate

N = number of positrons entering crystal/second.

Similarly n_V is the number of positrons in the trapped state and:

$\frac{dn_v}{dt} = - \lambda_v n_v + \mu C_v n_F$ where λ_v = vacancy annihilation rate.

In the steady state $\frac{dn_F}{dt} = 0$ and $\frac{dn_v}{dt} = 0$ giving:

$$n_F = N/(\lambda_F + \mu C_v)$$

$$n_v = n_F \mu C_v / \lambda_v = N \mu C_v / (\lambda_F + \mu C_v) \lambda_v$$

$$\frac{n_F}{n_v} = \frac{\lambda v}{\mu C_v}$$

I_F is the number of annihilations from the free state

$$= n_F \lambda_F$$

I_v is the number of annihilations from the trapped state

$$= n_v \lambda_v$$

$$\therefore \frac{I_F}{I_V} = \frac{\lambda_v \lambda_F}{\mu C_v \lambda_v} = \frac{\lambda_F}{\mu C_v}$$

From equation (1):

$$I = I_F \left(\frac{n_F \lambda_F}{N}\right) + I_v \left(\frac{n_v \lambda_v}{N}\right) = \frac{I_F \lambda_F}{\lambda_F + \mu C_v} + \frac{I_v \lambda_v \mu C_v}{(\lambda_F + \mu C_v) \lambda_v}$$

$$= \frac{I_F \lambda_F + I_v \mu C_v}{\lambda_F + \mu C_v} \qquad (2)$$

$$\therefore I (\lambda_F + \mu C_v) = I_F \lambda_F + I_v \mu C_v$$

or $$\lambda_F (I - I_F) = \mu C_v (I_v - I)$$

$$\frac{I - I_F}{I_v - I} = \frac{\mu C_v}{\lambda_F} \qquad (3)$$

The concentration of vacancies at thermal equilibrium is given by:

$$C_v = C_o \exp(- E_F^V / kT)$$ where C_o = constant

E_F^V = vacancy formation energy

k = Boltzmann's constant

T = temperature [^oK]

The trapping rate is given here as a constant although possibly:

$$\mu = aT^{1/2} \qquad (4)$$ i.e. is a function of temperature.

From (2) we get:

$$I = \frac{AI_F + I_v \exp[- E_F^V / kT]}{A + \exp[- E_F^V / kT]}$$ where $A = \lambda_F / aT^{1/2} C_o$

$$\text{or } I = \frac{BI_F + I_v T^{1/2} \exp[- E_F^V / kT]}{B + T^{1/2} \exp[- E_F^V / kT]}$$ where $B = \lambda_F / aC_o$

From (3) we get:

$$\frac{I - I_F}{I_v - I} = D \exp[- E_F^V / kT] \qquad (5)$$ where $D = aT^{1/2} C_o / \lambda_F$

Errors are introduced into the results because of possible temperature dependencies of I_F, I_v, E_F^V and a, i.e. trapping may be harder at high temperatures. Using standard angular correlation apparatus set at zero angle McKee et al. (1972)

were able to show that the peak height was a function of temperature. At room temperatures when there are few thermally generated vacancies the value of I approximates to I_F and at very high temperatures when nearly all the positrons are trapped I approximates to I_V. A plot of

$$\ln \left[\frac{I - I_F}{I_V - I} \right] \text{ VS } \frac{1}{T}$$

gives a straight line whose slope yields the vacancy formation energy.

An improvement to the theory takes account of thermal detrapping (Doyama, 1972). If λ_R is the rate of detrapping then:

$$\frac{dn_v}{dt} = - \lambda_v n_v + \mu C_v n_F - \lambda_R n_v \qquad \text{and}$$

$$\frac{dn_F}{dt} = - \lambda_F n_F - \mu C_v n_F + \lambda_R n_v + N$$

working through the same method as before we get:

$$\frac{I - I_F}{I_V - I} = \frac{\lambda_v \mu C_v}{\lambda_F \lambda_v + \lambda_F \lambda_R} \qquad (6)$$

If the detrapping energy barrier is E_D^V ($\approx$ 0.2 eV) then the detrapping rate is:

$$\lambda_R = \lambda_o \exp (- E_D^V / kT) \qquad \text{where } \lambda_o \text{ is a constant.}$$

$$\therefore \frac{I - I_F}{I_V - I} = \frac{\lambda_v a T^{1/2} C_o \exp (- E_F^V / kT)}{\lambda_F \lambda_v + \lambda_F \lambda_o \exp (- E_D^V / kT)}$$

$$= \frac{\lambda_v D \exp(-E_F^V / kT)}{\lambda_v + \lambda_o \exp(-E_D^V / kT)} \qquad (7)$$ Compare with (5).

The detrapping is only important at higher temperatures especially at, or near, saturation when all the positrons are being trapped. λ_R is negligible for positrons trapped by dislocations at temperatures around 300°K (Hautojärvi et al., 1970).

In say aluminium the time spent by a vacancy at one lattice site (14 psec) is much shorter than the life-time of a positron at a vacancy (246 psec). This may be due to the positron following the vacancy's migration or alternatively the presence of the positron may inhibit the migration.

The effect of monovacancies is detectable at concentrations around 10^{-7}. From equation (2):

$$I = \frac{\lambda_F I_F + \mu C_v I_v}{\lambda_F + \mu C_v} \qquad \text{where } C_v = \exp\left(\frac{S_F^V}{k}\right) \exp\left(\frac{-E_F^V}{kT}\right)$$

S_F^V = vacancy formation entropy.

Suppose I_F changes linearly with temperature and becomes constant at high temperatures because it is sensitive to the overlap of the positron and interstitial electron wave functions which shows this sort of character. Then, if λ_F and μ are assumed independent of temperature, the critical temperature T_c is the temperature at which the I parameter curve deviates from the linear background. The temperature dependence of μ will probably be cancelled out by thermal detrapping and the increase in the positrons' residual momentum. Therefore, if the concentration of

monovacancies at T_c where their effect is barely noticeable is a constant in all f.c.c. metals and alloys then E_F^V is proportional to T_c, i.e. the formation entropy is a constant (Karbayashi and Doyama, 1972). In angular correlation experiments the effect of vacancies does not depend upon the valency or size of the missing ion and the entropy is characteristic of the close packed crystal structure. Hence in f.c.c. metals S_F^V is (1.6 ± 0.1) k but in b.c.c. crystals S_F^V is much larger around 2.2 k. H.c.p. crystals are not really comparable because although they are close packed they are nearly always distorted which increases the vacancy formation entropy.

5.4 VACANCY FORMATION ENERGY BY POSITRON METHOD

Both the mean lifetime of positrons and the angular correlation of the annihilation quanta were found to be reversibly temperature dependent (MacKenzie et al., 1964, 1967) in certain metals. If there is an equilibrium concentration of monovacancies in these metals which is a function of temperature then as the temperature increases, i.e. more energy is given to the metal, the vacancy concentration increases. Positrons are attracted to and may be trapped in vacancies where there is an anomalous electron wavefunction due to the lack of core electrons. Usually a positron may annihilate either with core electrons whose considerable potential energy is taken away by the annihilation quanta, or with valence electrons which have little potential energy. If the probability of a trapped positron annihilating with a core electron is

reduced then the core electron annihilation rate will decrease and it will continue to decrease as the concentration of vacancies, i.e. trapped positrons, increases until saturation when nearly all the positrons are trapped before annihilating. Any parameter which differs depending on whether the positron annihilates with a core electron or a valence electron may be used to study the increase in vacancy concentration with temperature.

For the trapping to be effective the binding energy $\Delta\varepsilon$ (the depth of the positron bound state energy level in the vacancy potential well from the ground Block state in the crystal lattice) must be sufficiently large that the probability of the positron escaping into the conduction band (Block state) within its lifetime is extremely small. If the rate of escape is of the order $kT \exp(-\Delta\varepsilon/kT)/h$ where k = Boltzmann's Constant

h = Plank's Constant

T = Temperature (^{o}K)

then the condition for positron trapping in vacancies is given by:

$$\Delta\varepsilon > kT \ln(kT\,\tau/h) \quad \text{where } \tau \text{ is the lifetime.}$$

McKee et al. measured the change in angular correlation coincidence count rate between annihilation gamma rays at zero angle, i.e. zero component of momentum. As more positrons annihilate with valence electrons so the high momentum core electron tails to the correlation curve diminish and the peak rate increases. The method used by us was to measure the change in the width of the 511 KeV annihilation gamma ray energy spectrum peak with a high

resolution Ge(Li) detector. The peak is broadened because the gamma rays take away the total energy of the annihilating pair. If the positron is thermalised, i.e. has energies of a few eV, then the major contribution must come from the electrons. Core electrons have more potential energy than valence electrons so that a decrease in the core electron annihilation rate narrows the peak considerably.

The doppler broadening technique is much less sensitive to changes in the electron momentum distribution than the angular correlation technique because of the inherent resolution of the Ge(Li) detector. The method does however have the advantage that only one detector and no coincidence circuitry is needed and the data can be rapidly obtained so that the counting statistics are usually very good.

If the annihilation gamma ray peak at 511 KeV is observed at various temperatures then the change in the F.W.H.M. can be used to predict the vacancy concentration. Consider the equation (5) from section 5.3:

$$\frac{I - I_F}{I_V - I} = D \exp(- E_F^V / kT)$$

where I_F is the F.W.H.M. of the annihilation gamma ray energy peak when all the positrons annihilate from the free state, i.e. with both core and valence electrons. I_V is the F.W.H.M. when all the positrons are trapped before annihilation and therefore have a very low probability of annihilating with a core electron. I is the F.W.H.M. at

an intermediate temperature $T^{o}K$ and k is the Boltzmann constant and E_F^V the vacancy formation energy.

Given a set of data for I versus T the computer can be used to generate the best values for the parameters I_F, I_V, D and E_F^V which give the best possible fit to the experimental data. The programs used are described in detail in the appendix. Included in the program is provision for the intrinsic resolution of the system 3.84 KeV, measured on the 569.6 KeV 'standard' gamma ray line from Bi-209 source, to be deducted from the measured peak widths.

The sort of curves expected from the experiment can be calculated given that the energy distribution of the annihilation quanta will be an inverted parabola centred on $E = m_o c^2$. This assumes that the positrons are at rest in a Fermi sea of electrons, Fermi velocity V_F, before annihilation. The doppler shift due to the electron motion can be calculated assuming that the annihilation quanta emerge from the centre of mass of the electron positron system which will have a maximum velocity of $V_F/2$.

Consider a stationary source distance d from an observer, then the time taken for the wave to reach the observer is given by:

$$t = d/c \quad (1)$$ where c = velocity of light.

Suppose the source emits a wave of length λ then the number of wavelengths in the distance d is given by:

$$n = d/\lambda \quad (2)$$

Now consider a source moving towards the observer with

velocity v and suppose it emits the wave when distance d away from the observer. When the wave reaches the observer the source will have moved a further distance x towards the observer given by:

$$x = vt \qquad (3)$$ where t is given above.

This means that the n wavelengths now cover a distance of d-x so there is a new apparent wavelength seen by the observer given by:

$$\lambda' = (d-x)/n$$

or $$n\lambda' = d-x$$

and if $c = \nu\lambda$ then substituting (2) and (3):

$$\frac{nc}{\nu'} = \frac{nc}{\nu} - vt$$ and substituting (1)

$$\frac{\not{n}\not{c}}{\nu'} = \frac{\not{n}\not{c}}{\nu} - \frac{v}{c}\frac{\not{n}\not{c}}{\nu}$$

$$\therefore \quad \nu = \nu' - \frac{v\,\nu'}{c}$$

$$\text{or} \quad \nu - \nu' = \frac{-v\nu'}{c}$$

The change in frequency $\nu - \nu' = -\frac{v}{c}$ and for small changes when $\nu \approx \nu'$ this change is given by $\frac{v\,\nu}{c}$. From chapter 1 we find that in two quanta annihilation each quanta takes half of the total electron positron rest mass energy away. Since they have the same rest mass m_o then the energy of the gamma ray is given by:

$$E = m_o c^2 = h\nu$$

This energy will be changed by the doppler effect to:

$$E = h\nu \pm h.(\frac{v\,\nu}{c})$$

where the $\pm$ determines whether the motion is towards or

away from the observer. The maximum doppler shift will be caused by the maximum source velocity, i.e. V_F / 2. The gamma ray spectrum is therefore given by:

$$E = h\nu \pm h\left[\frac{V_F}{2}\frac{\nu}{c}\right]$$

$$= m_o c^2 \left(1 \pm \frac{V_F}{2C}\right)$$

If the Fermi energy is 5 eV then the Fermi velocity is given by:

$$5 \text{ eV} = \frac{1}{2} m_o V_F^2$$

$$\text{or} \quad V_F = \sqrt{\frac{2 \times 5 \text{ eV}}{m_o}} = \sqrt{\frac{2 \times 5 \times 1.602 \times 10^{-19}}{9.109 \times 10^{-31}}}$$

$$= 1.326 \times 10^6 \text{ m sec}^{-1}$$

The maximum change in gamma ray energy is given by:

$$E_{CHANGE} = \frac{m_o C V_F}{2} = \frac{9.109 \times 10^{-31} \times 2.998 \times 10^8 \times 1.326 \times 10^6}{2 \times 1.602 \times 10^{-19}}$$

$$= 1.13 \text{ KeV}$$

The tails of the parabola will thus extend to $E = m_o c^2 (1 \pm V_F / 2C)$ due to the higher velocity core electrons. For a Fermi energy of 5 eV this will result in a maximum shift of 1.13 KeV so that the peak should have a maximum width of 2.26 KeV. This shows that changes in the energy distribution of the annihilating electrons will be effectively amplified 500 times in the gamma ray energy spectrum.

5.5 EXPERIMENTAL METHOD

Pure copper (99.999%) wire with a diameter of .25 mm. was wound into a .75 mm. diameter coil of about ten turns. The coil was etched in concentrated nitric acid for five minutes to reduce the diameter to less than .1 mm. The coil was rinsed and dried and then sent to the London University reactor to be irradiated for seven hours in a flux of 10^{12} n/cm^2/sec. When delivered the next day it was a ^{64}Cu positron source of approximately 1 mCi. The coil was etched again to clean the surface for about 10 seconds in concentrated nitric acid, rinsed and dried.

The prepared positron source was then placed inside a small airtight metal calorimeter, 1 cm. high and 5 mm. in diameter, with a 1 mm.^{3} cavity, Fig. 5.1. The calorimeter was placed inside an electric furnace so that it rested on top of a thermocouple junction. The power to the furnace, which was made from an electric fire element, was controlled by a variac. The furnace was placed in a small chamber 2 m. x 1/2 m. x 1/2 m. whose walls were made of aluminium foil, the top being left open, which was used to produce a stable temperature enclosure for the furnace, Fig. 5.2.

The majority (90%) of the positrons would escape from the coil and annihilate in the metal calorimeter whose temperature was recorded by the thermocouple linked to a digital multimeter accurate to .1 mV. The source and calorimeter were annealed for several hours at a temperature of 900°C. unless the melting point of

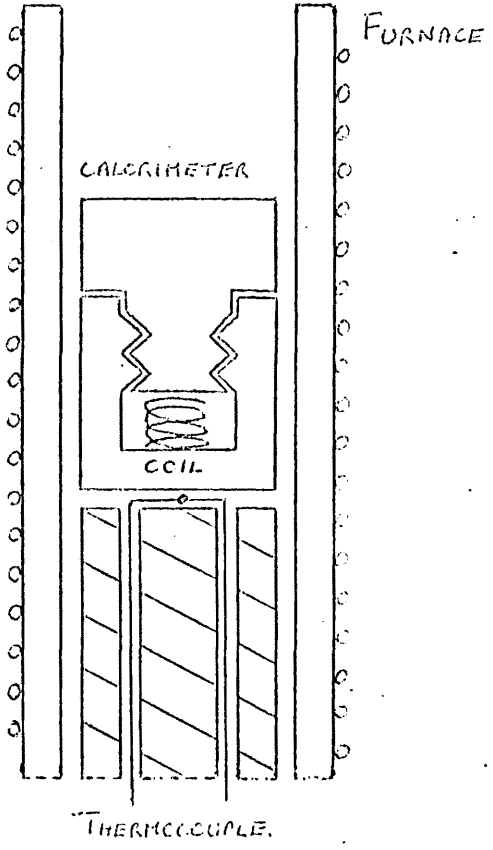

FIG 5.1 CALORIMETER INSIDE FURNACE

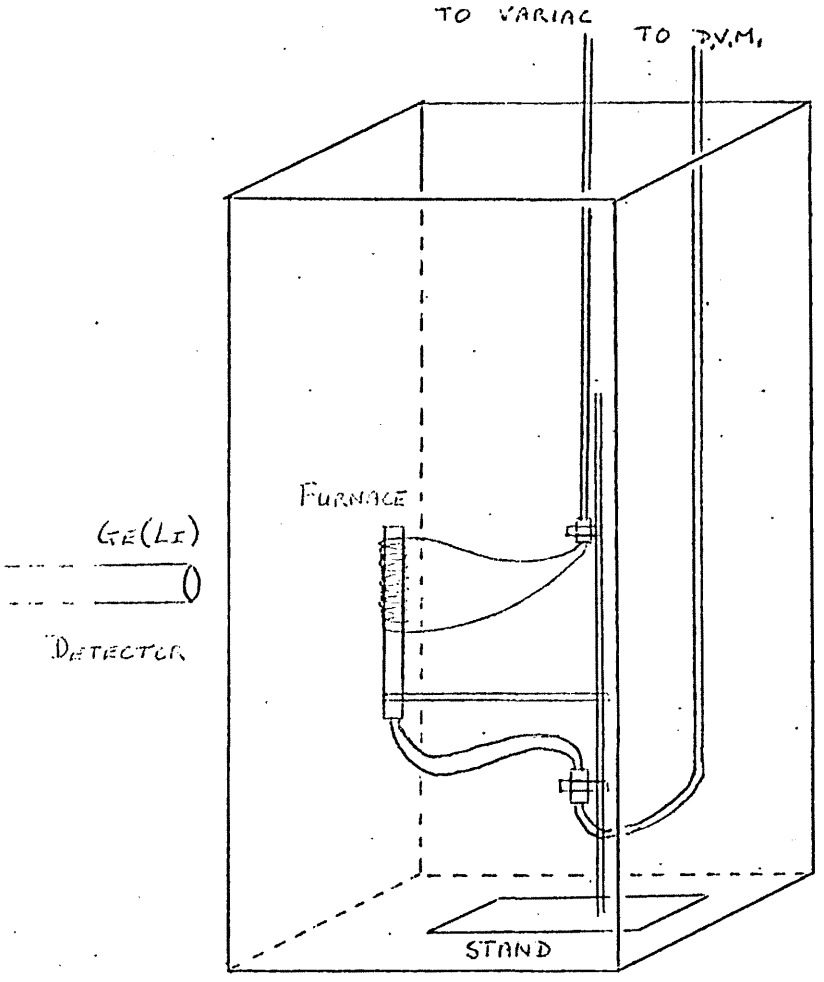

FIG 5.2 TEMPERATURE ENCLOSURE.

the calorimeter dictated a lower temperature when the annealing period was extended. The annealing period was intended to remove all point defects in the source and calorimeter except vacancies.

After the annealing the annihilation gamma ray spectra were obtained with a Ge(Li) detector with an active volume of 40 cc. which had an integral low temperature pre-amplifier. Signals (bipolar) from the pre-amplifier were amplified by an Ortec 485 amplifier and then fed to a Tracor 512 channel multi-channel analyser, Fig. 5.3. Digital biassing on the analyser allowed the 512 channels to be offset to the top quarter of an apparent 2048 channels spread across the range 0 to 10 V. input. The annihilation peak was thus expanded across some forty channels. To lower the analyser dead time the lower level discriminator was set to 1.4 volts, the zero level at 0.14 volts and the high level discriminator to 10.0 volts.

Data was collected for one hour at various temperatures over the range 0 to 1050°C going in both directions for the copper (approx. 20°C lower than the respective melting point for other metal calorimeters) calorimeter ensuring that the peak channel count was always in the range (40 to 50) x 10^3. This was achieved by stabilising the dead time at just less than 10% by moving the detector progressively nearer the calorimeter as the source strength dropped (^{64}Cu half life is 12.8 hours).

The multi-channel analyser spectra were analysed on the London University C.D.C. 7600 computer using the Sampo program devised by Routti (1969). The F.W.H.M. of

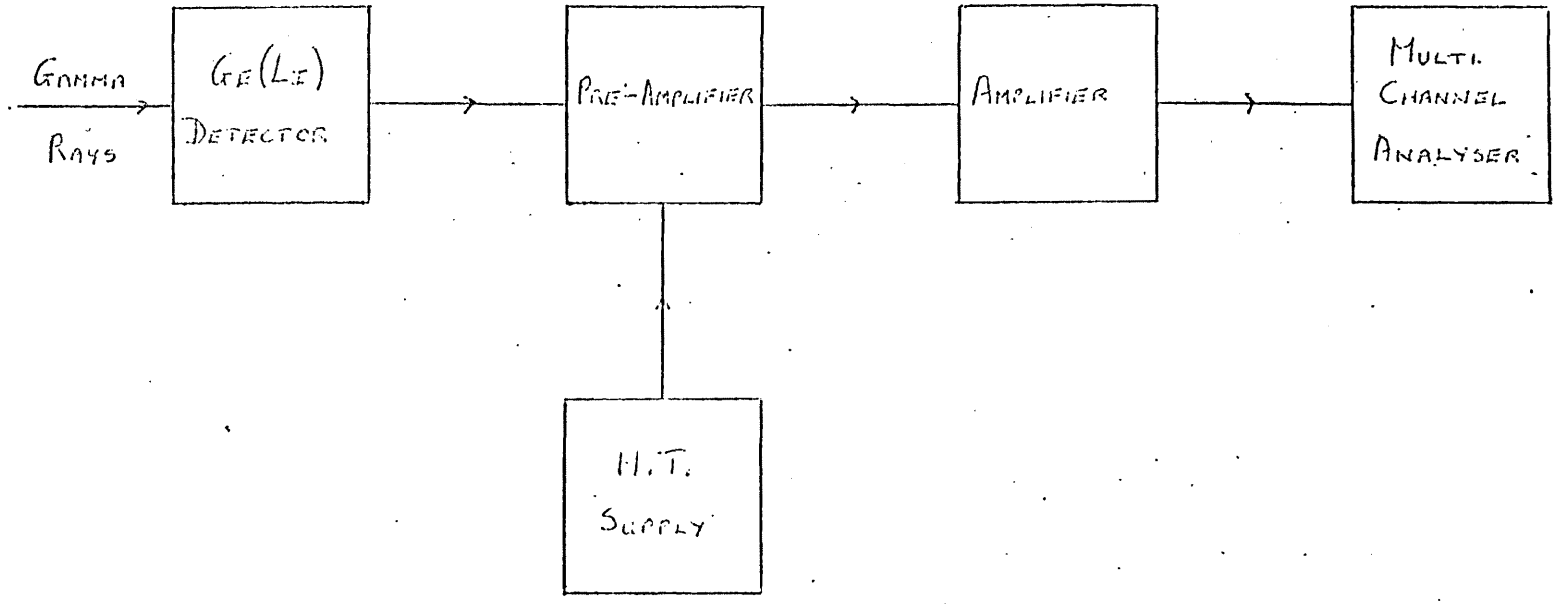

Fig 5.3 Ge(Li) Detector System for Vacancy Experiment.

the peak was given by the program as well as the error in the value typically 0.2%. Tests were conducted to investigate the effect of the dead time on the analyser and these showed that for dead times $\leq$ 10% any effect was within the error in the peak width given by SAMPO. The results are shown in Figs. 5.4, 5.5 and 5.6, the metals used were copper, aluminium and zinc, the bars show typical errors in the points. These curves were fitted by the computer to give the best values of E_F^V for the three metals which were:

Copper $E_F^V = (1.128 \pm .012)$eV (Melting Point = 1083°C, lattice f.c.c.)

Zinc $E_F^V = (0.464 \pm .002)$eV (Melting Point = 420°C, lattice h.c.p.)

Aluminium $E_F^V = (0.578 \pm .010)$eV (Melting Point = 660°C, lattice b.c.c.)

It should be noted that the temperature range over which aluminium and zinc effects were obtained ended below the critical temperature for copper. Changes in the peak width due to the very small number of positrons annihilating in the copper source can therefore be discounted. These results were obtained by fitting with the program Vacancy I. However this program gave slightly varying answers depending on the initial guess values fed in and this effect could not be completely removed. It was decided, therefore, that the method of fitting used by this program was not sufficiently sensitive and we could not put sufficient confidence in the results to accept them as final answers. A new program Vacancy II (described in the appendix) was used to reanalyse the data

FIG 5.4 PEAK WIDTH AS A FUNCTION OF TEMPERATURE — COPPER

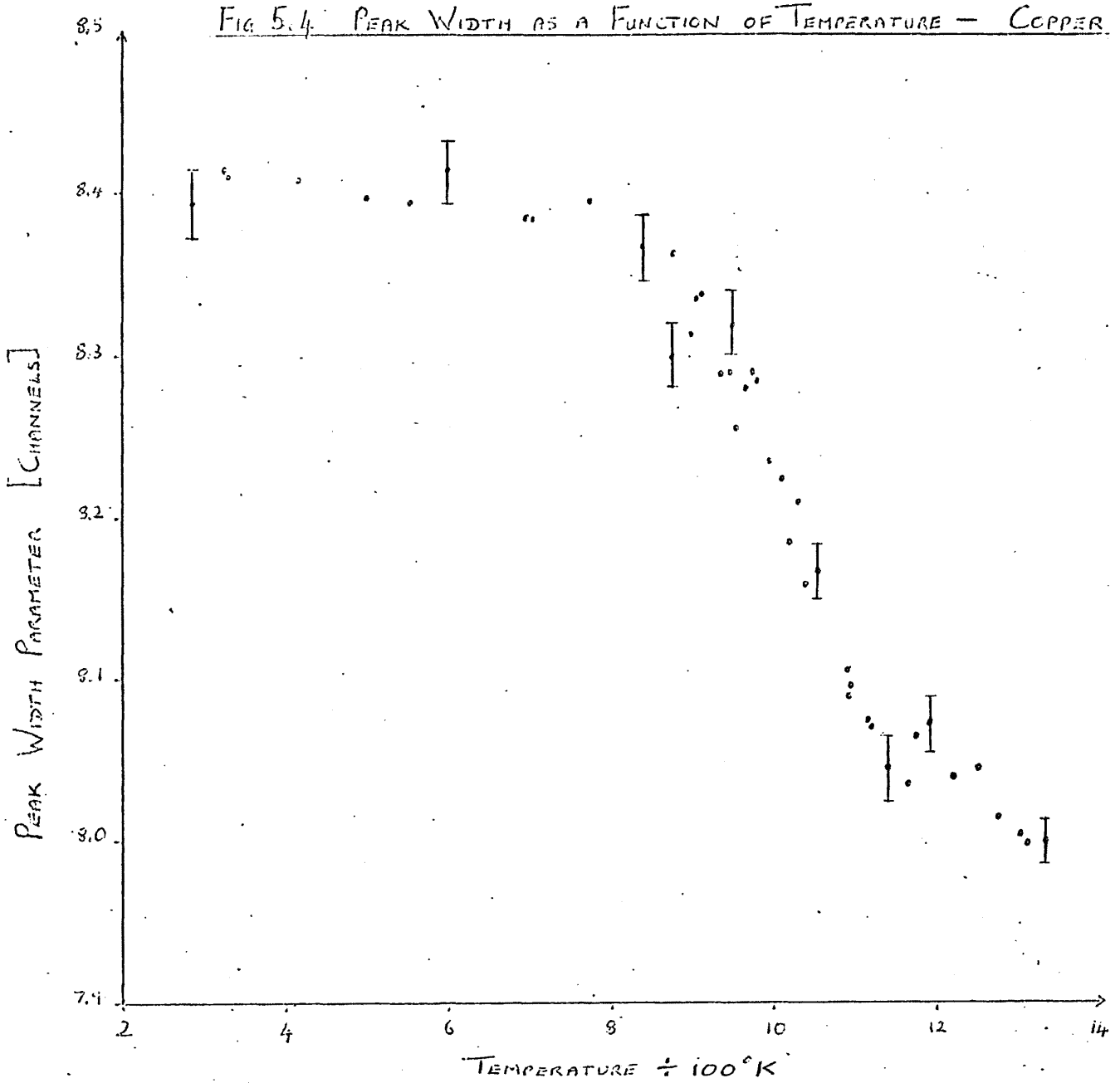

FIG 5.5 PEAK WIDTH AS A FUNCTION OF TEMPERATURE — ALUMINUM

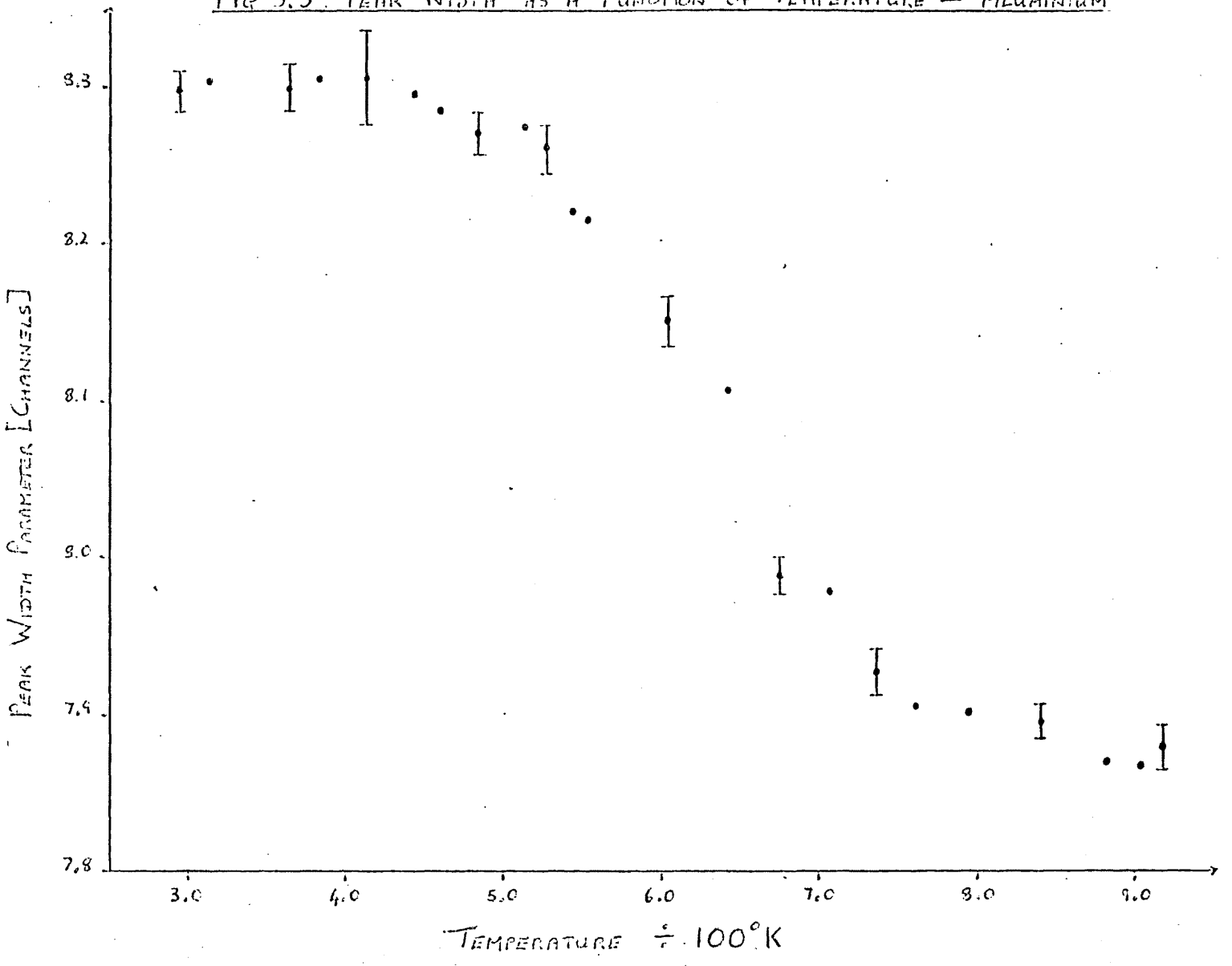

FIG. 5.6 PEAK WIDTH AS A FUNCTION OF TEMPERATURE — ZINC

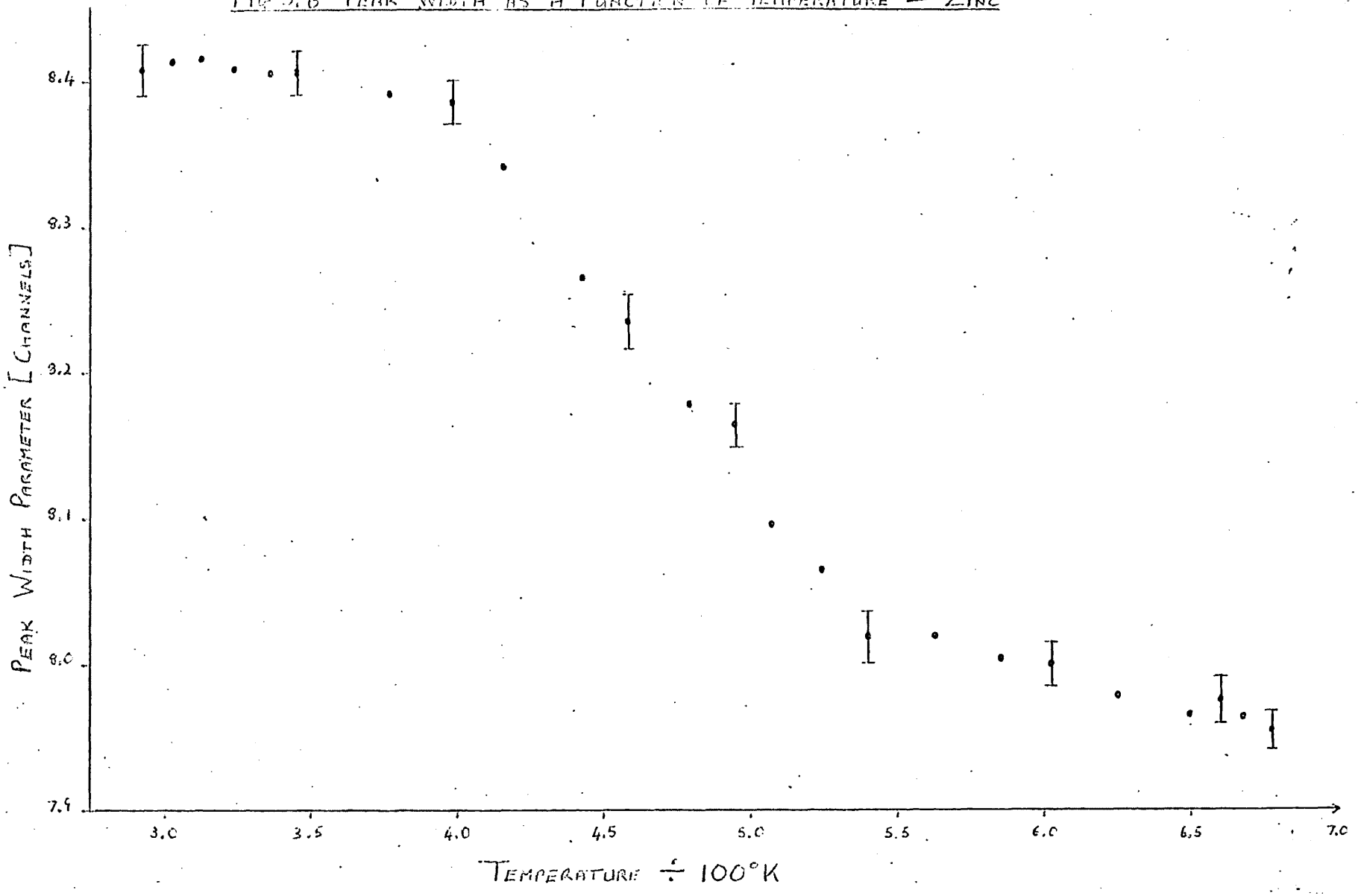

using a maximum likelihood technique and this new program proved to be much more powerful so that far more confidence could be placed in the results given below. The errors quoted were obtained from the Arrhenius plots using the parameters given by Vacancy II in a third program Vacancy III. This technique was necessary in order to give the errors direct in eV.

Copper	$E_F^V = (1.017 \pm .022)$ eV
Zinc	$E_F^V = (0.510 \pm .033)$ eV
Aluminium	$E_F^V = (0.612 \pm .035)$ eV

These are the final results and the programs used are described in the appendix. The Arrhenius plots obtained are shown in Figs. 5.10, 5.11, 5.12. It should be noted that the Arrhenius Plot only contains those points on the slope above the critical temperature between FF and FV. These points are subject to much less error because of the large differences produced in them as the temperature changes. Also, since points above FF or below FV cause unreal logarithms some of the points on the plateau regions could not be plotted and using only the 'real' log points would distort the form of the graph.

5.6 DISCUSSION OF RESULTS

The statistical spread of points in the Copper experiment is much greater than in the Aluminium or Zinc experiments. This is probably due to the temperature of the Copper sample varying during the run and inaccurate temperature measurement. The Copper results were obtained without the use of the Aluminium foil temperature enclosure

FIG 5.10 ARRHENIUS PLOT FOR COPPER DATA.

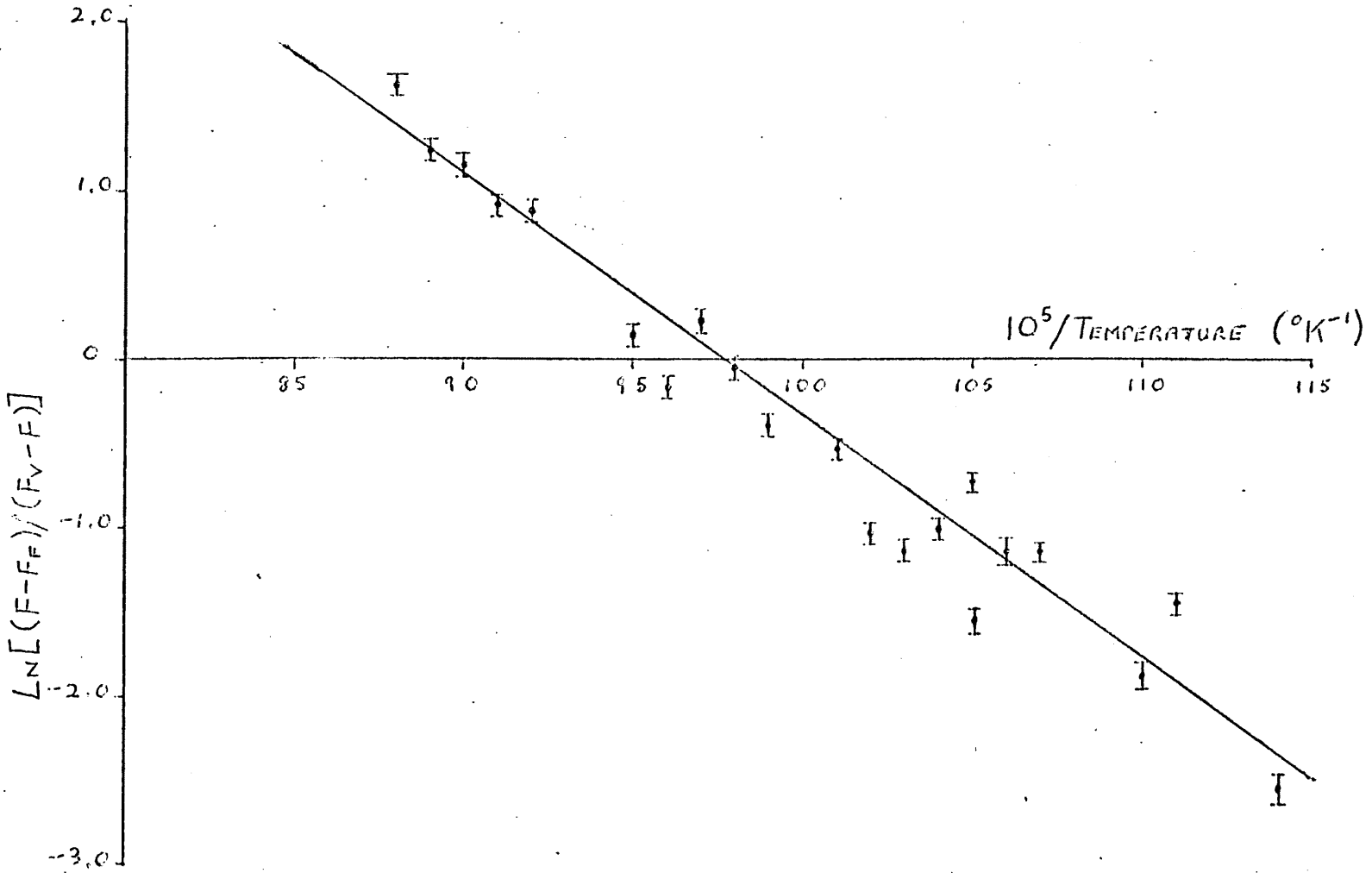

FIG 5.11 ARRHENIUS PLOT FOR ZINC DATA.

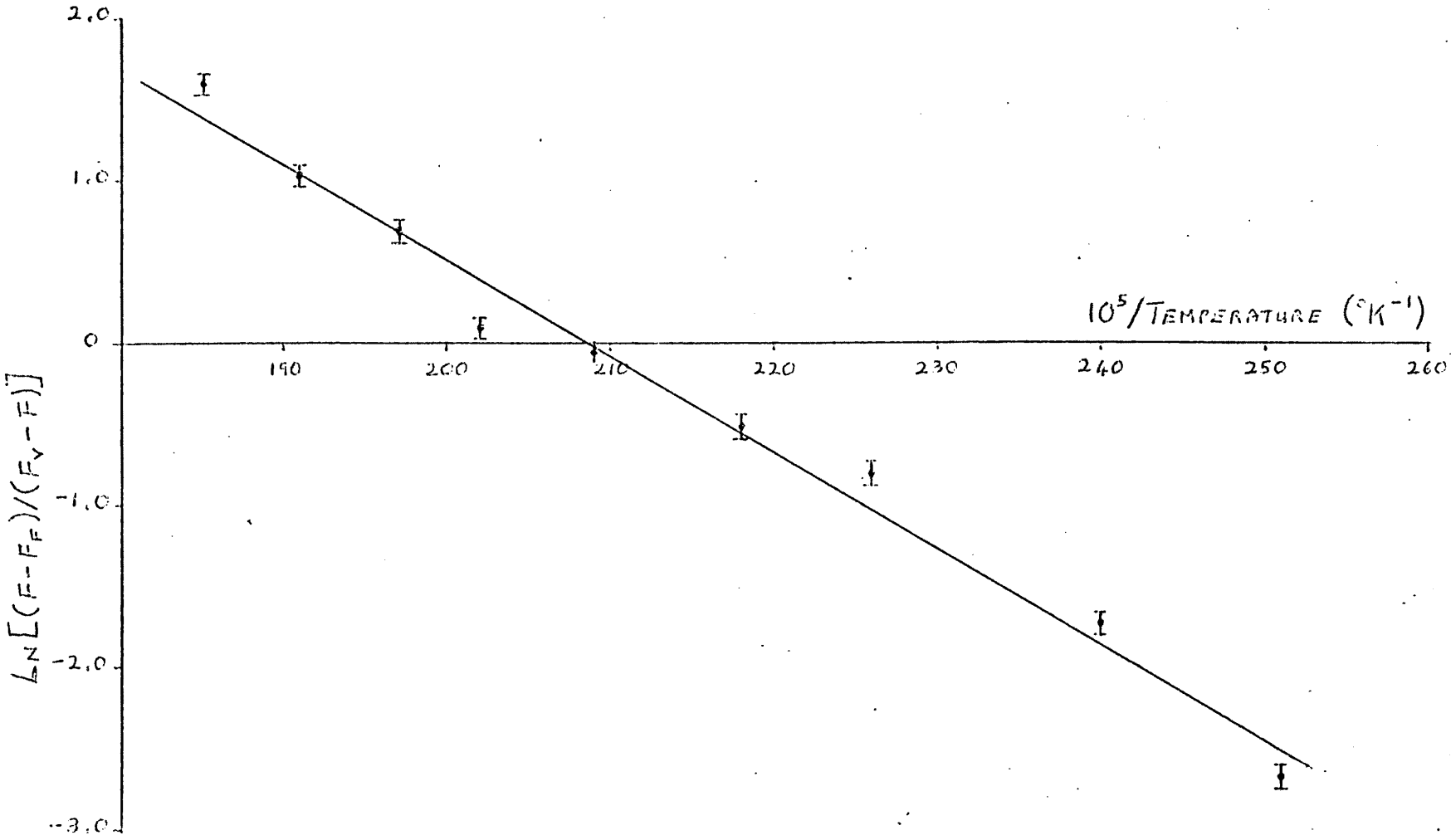

FIG 5.12 ARRHENIUS PLOT FOR ALUMINIUM DATA.

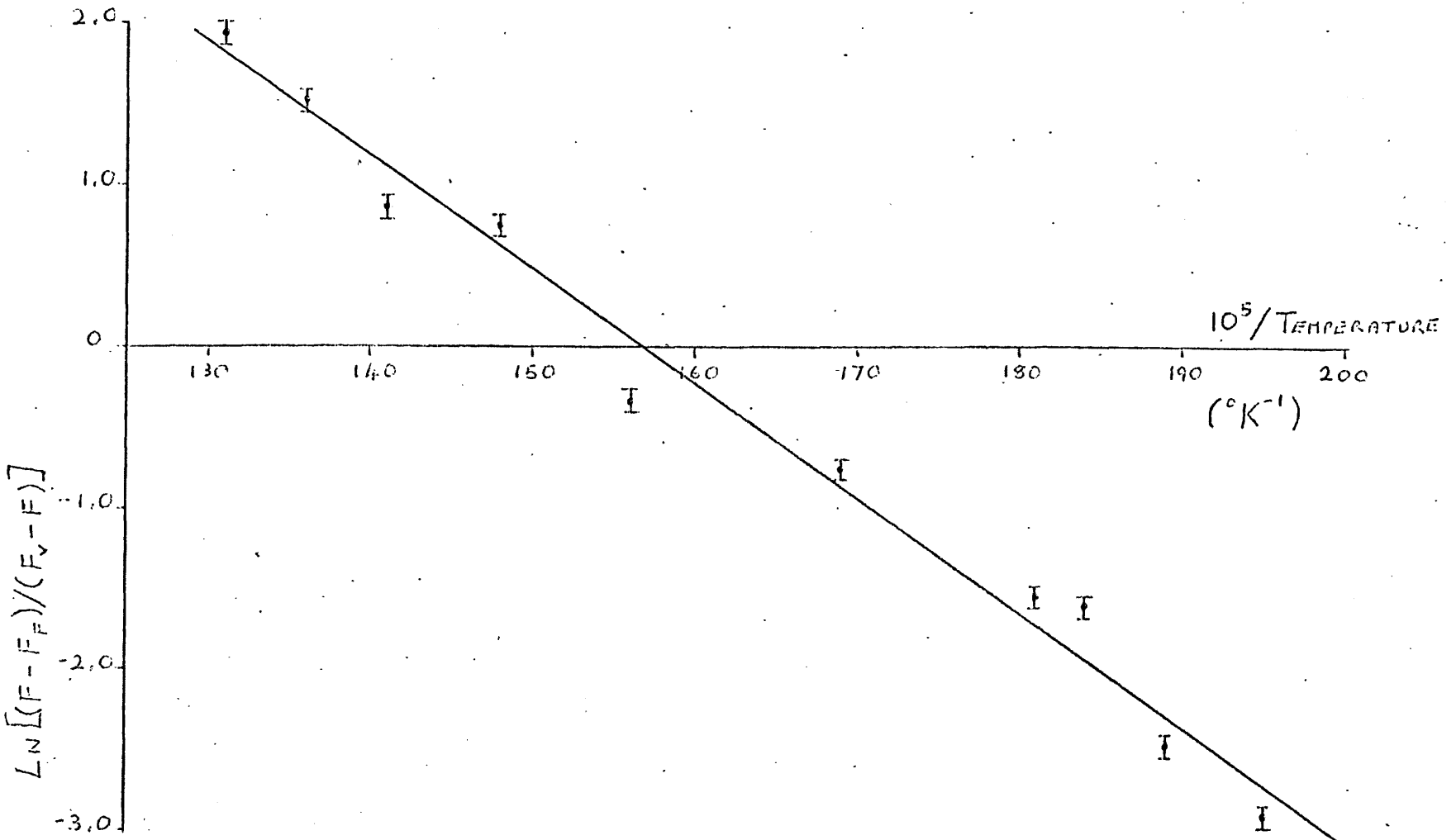

although the furnace was shielded by a brick wall to prevent draughts. Also, the Copper sample temperature was measured with a thermocouple connected to a milliameter which could be read to ± .25 of a division which on a less sensitive range could produce an error of ± 10°C. In the later experiments a digital voltmeter was used and this was accurate to ± .1 mV giving an error of ± 2°C.

The errors in the peak widths are shown in the graphs. Figs. 5.7, 5.8, 5.9 show the widths corrected for the resolution of the system. The count in the peak channel was always greater than 30,000 so that the statistical counting errors were minimal. It should be noted that the analysis of the results was based on the assumptions that none of the four parameters FF, FV, A or E_v was temperature dependent. In discussing the results we have borne in mind that saturation trapping is likely to occur at vacancy concentrations of 10^{-5} whereas deviation from the background FF, i.e. vacancy concentration begins to affect results, starts at a concentration of about 10^{-7}. If this is constant then the critical temperature T_c at which deviation begins must be proportional to the vacancy formation energy.

Copper - the vacancy formation (enthalpy) energy has been measured by an angular correlation technique and was found to be (0.98 ± 0.07) eV by McGervey and Triftshaüser (1973). This compares with our value of (1.017 ± 0.22) eV. They assumed whilst fitting their data that positron trapping occurred at a constant rate independent of the temperature. Nanao et al. (1973), who performed the same angular correlation experiment, used a temperature dependent trapping

FIG 5.7 COPPER DATA CORRECTED FOR RESOLUTION.

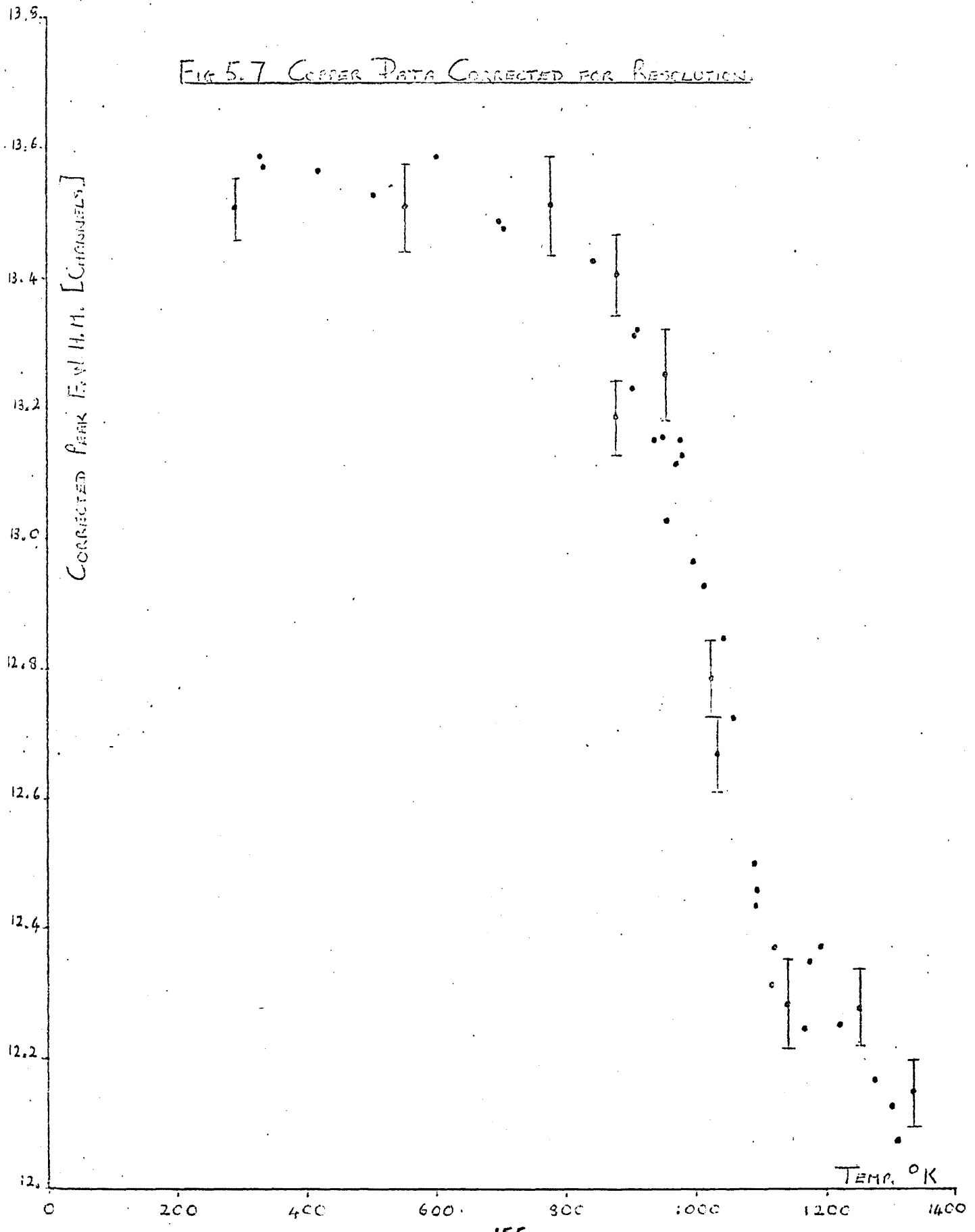

FIG 5.8 ALUMINIUM DATA CORRECTED FOR RESOLUTION.

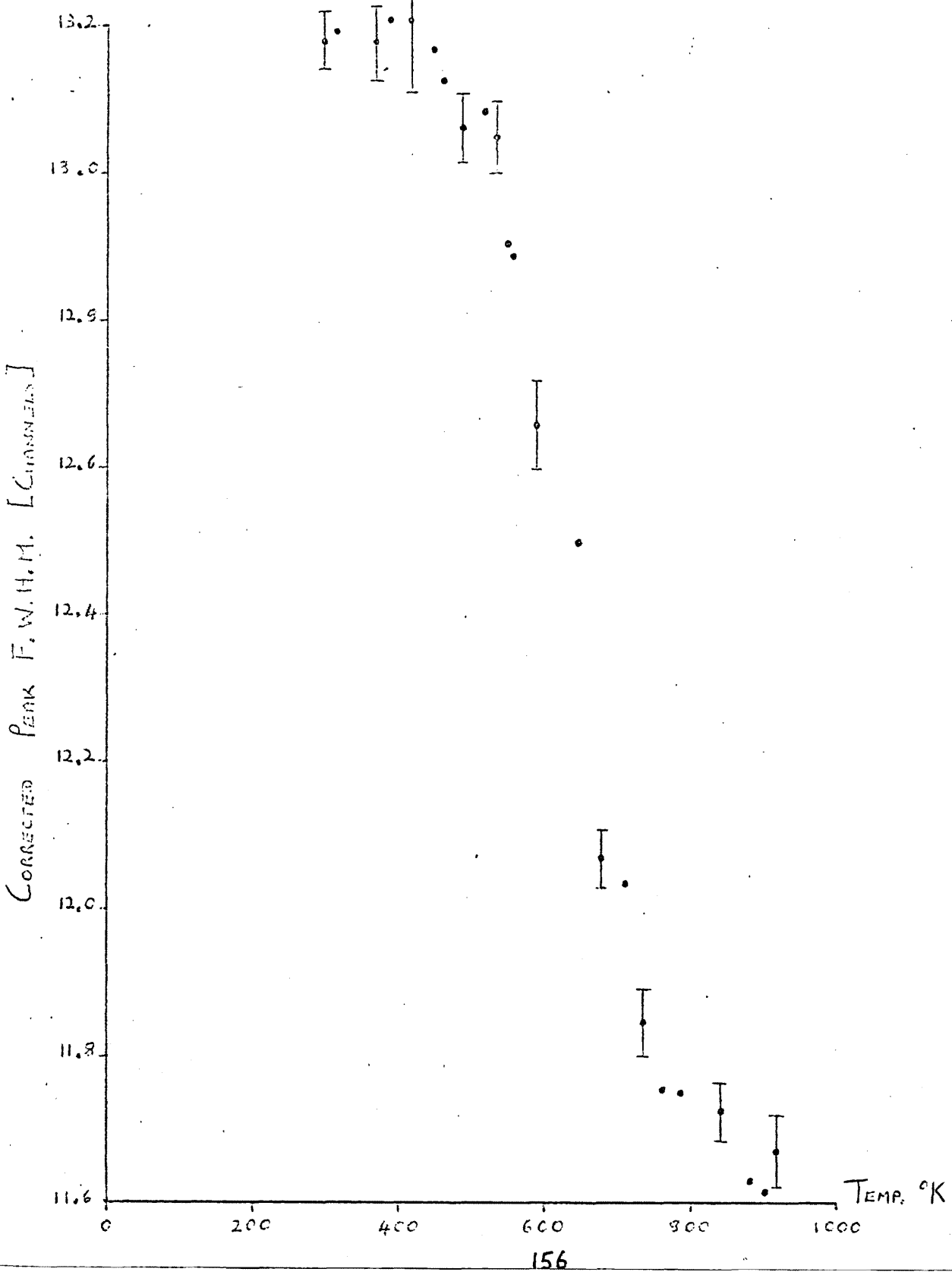

FIG 5.9 ZINC DATA CORRECTED FOR RESOLUTION.

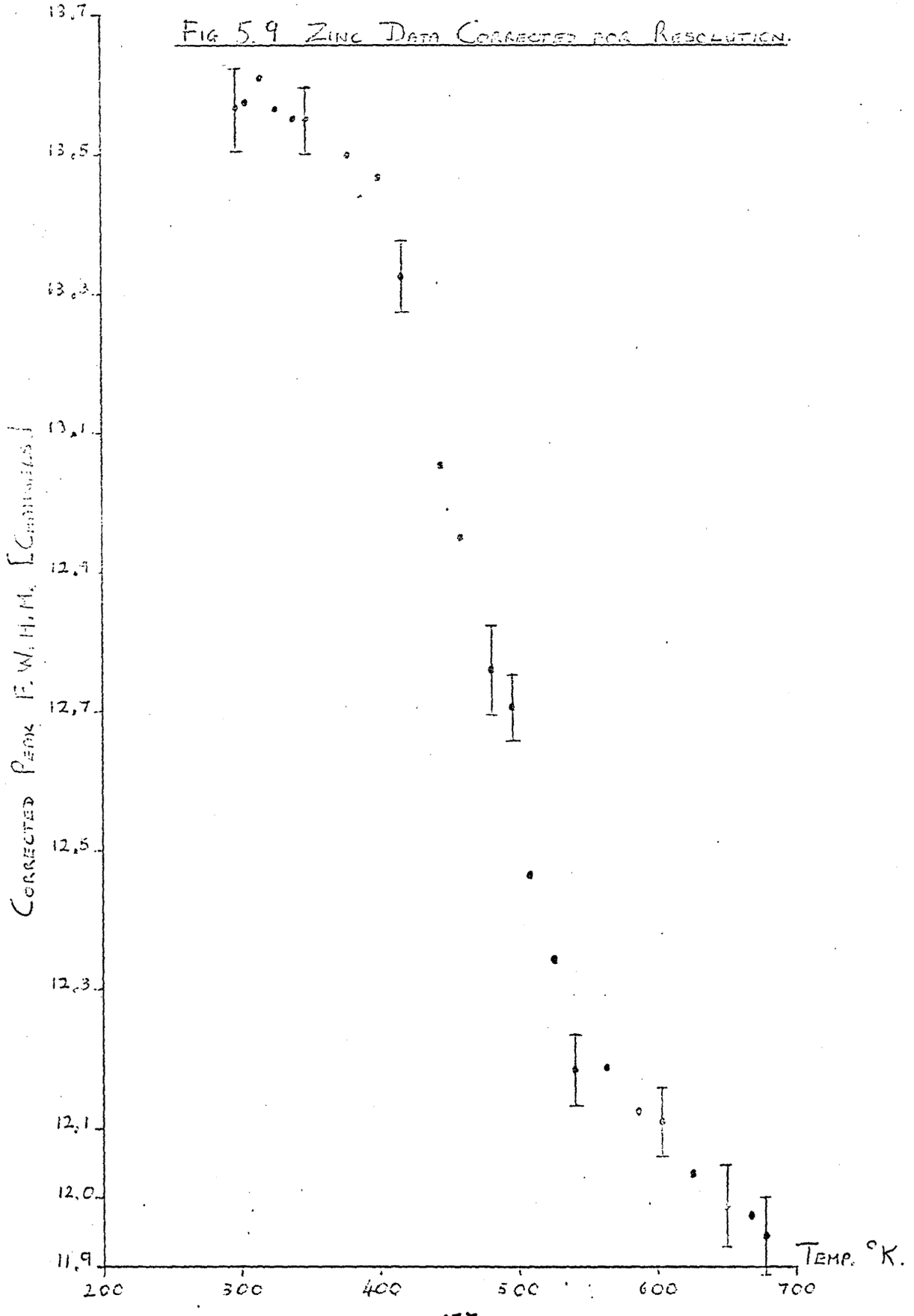

rate in analysing their results so that they obtained a value of (1.17 ± 0.07) eV. This is similar to the result obtained by Simmons and Balluffi (1963) who used a lattice expansion method and obtained a value of (1.17 ± 0.11) eV. Airoldi et al. (1959) had obtained a value of 1.0 eV and Kraftmakher and Strelkov (1969) using a specific heat method obtained E_F^V = 1.05 eV. Seeger and Mehrer (1969) also obtained this value but used a self diffusion method.

Aluminium - Simmons and Balluffi (1960) using the thermal expansion method obtained a value for the vacancy formation energy of 0.76 eV, whereas Bianchi et al. (1966) found the value to be 0.71 eV. Both these values have been criticised by Seeger (1970) as being too big because of faulty data fitting. He re-analysed this data and obtained E_F^V = 0.66 eV which is in close agreement with McKee et al. (1972) who used the angular correlation technique to obtain E_F^V = (0.66 ± 0.04) eV. On the other hand, Doyama (1972) took positron detrapping into account and using McKee's data obtained a value of 0.76 eV which does not compare well with our value of (0.612 ± 0.35) eV. Kraftmakher and Strelkov used a specific heat method and obtained 1.17 eV which they regarded as too high. Seeger and Mehrer (1970) used a self diffusion method and found E_F^V = 0.65 eV.

Zinc - Our value for the vacancy formation energy of Zinc is (0.51 ± 0.33) eV. which compares with 0.55 quoted by Karbayashi et al. (1972). McKee et al. (1972) used the same angular correlation method to get a value of (0.54 ± 0.02) eV. although Doyama (1973) corrected this to 0.56 eV. taking detrapping into account. McKee et al. (1972)

found a value of (0.52 ± 0.025) eV. by using lifetime measurements.

There seems to be considerable doubt about the correct way of interpreting positron data and any corrections obtained for detrapping, etc. would apply to our data as well (e.g. Doyama, 1972). The analysis is complicated by lack of knowledge about the possible temperature dependence of the three parameters FF, FV and A always assuming that E_F^V is itself independent of temperature.

McGervey and Triftshaüser (1973) noticed a temperature dependence in their angular correlation data for copper below 600°K, i.e. in the region where little trapping is supposed to occur because the concentration of vacancies is very low. Our data and that of Nanao et al. (1973) are inconclusive in this respect since any such dependence is within the experimental errors although this does imply that the effect is not as large as seen by McGervey and Triftshaüser. They suggest that this dependence is due to a contraction of the Fermi surface as the temperature decreases which would have only a small effect and/or a decrease in the rate of annihilation with core electrons. Both of these are ascribed to the expansion of the lattice as the temperature increases and will, of course, affect the plateau region at high temperatures (F_V) although to a lesser extent because the core electron annihilation contribution is already reduced by trapping at vacancies. The error in the value of E_F^V produced by the temperature dependence of F_F is very small and within the statistical error in the values quoted. Jackman et al.

(1974) opine that the effect seen by McGervey and Triftshaüser is probably due to surface effects.

Perhaps more important is the temperature dependence of the parameter, A, through its relationship with the trapping rate μ. We have already shown that thermal detrapping may be important (page 134) which implies that the value of E_V at high temperatures may be considerably underestimated (Doyama, 1972). This in turn will cause the vacancy concentration to be underestimated and hence the formation energy. Doyama has calculated corrections to the monovacancy formation energies taking this into account, e.g. E_F^V for zinc is raised by 0.2 eV. Seeger (1973) opines that copper vacancies may be fairly inefficient traps at high temperatures although divacancy trapping may become important. This could explain why values for E_F^V obtained by positron methods are consistently less than those obtained by other methods unless detrapping is taken into account, e.g. Nanao et al., 1973.

Another temperature dependence introduced into the parameter A is the possible relationship between the trapping rate μ and temperature. Seeger (1973) postulates a $T^{1/2}$ relationship at temperatures above the boiling point of liquid nitrogen. This is caused by the effective capture radius of the vacancy increasing with temperature and errors of 0.01 eV, 0.02 eV and 0.03 eV respectively are quoted for metals with critical temperatures of 300°K, 600°K and 900°K, e.g. E_F^V for aluminium is increased by 0.02 eV to 0.66 eV. However, McKee et al. (1973) constructed an experiment to find the temperature

dependence of the positron trapping rate in gold and concluded that in fact μ is independent of temperature and this is probably true for all metals.

All the results given by various workers for the different metals seem to encompass each other within their experimental errors and might give the same result if analysed in the same way. There are considerable difficulties in analysing the experimental data at present especially if detrapping, lattice expansion and surface effects which vary with positron sources need to be considered to give consistent acceptable results. Better experimental data would also help considerably in sorting out what parts of the curve really are temperature dependent. Jackman et al. (1974) have recently reported doppler broadening studies in which they use a parameter S defined as the ratio of intensities in the central region and in a symmetrically placed outer region to describe the width of the annihilation curve. This parameter is supposedly very sensitive to change in the peak width. However, they have not reported any temperature data, only measurements concerned with deformation produced traps obtained by cold working the sample and the subsequent rate of 'recovery' annealing of these traps at various temperatures as a function of the metals' melting point.

I feel that our method is superior to any of the positron methods both for the reasons given earlier when I considered the various methods of obtaining the vacancy formation energy and because of its possible application in a more mobile form. Positrons are sensitive to other defects besides vacancies, e.g. dislocations (McKenzie et al., 1970),

and the technique may become a simple non-destructive test apparatus for investigating purity, hardness, strain and fatigue in metals.

CHAPTER 6

VACANCY CONCENTRATION AND NEUTRON IRRADIATION

6.1 INTRODUCTION

If the annihilation mechanism of positrons is affected by impurities or point defects, however caused, then it will also be affected by radiation damage to the crystal. The angular correlation curves obtained from pure samples and additively coloured samples shows that F centres with their 'optical' electrons will affect the annihilation mechanism (Berezin, 1970). This, of course, is not radiation damage but it is an analogous effect in that the crystal structure is distorted and the positron may form a bound state at vacancies present at an F centre.

An attempt was made (Hadley and Hsu, 1970) to correlate the intensity of the longer positron lifetime τ_2 in acetyl methione with the concentration of a charged radical produced by irradiation. Although the value of τ_2 was not significantly affected by the radiation dosage or temperature, its intensity was dependent on both. Electron paramagnetic spectra showed that irradiation produced a negatively charged radical which disintegrated into two stable radicals if it was heated. Thus the longer lifetime due to a pick-off process from triplet positronium was reduced in intensity by the charged radical because either the unpaired electron exchanged spins with the triplet positronium which became singlet with the shorter lifetime, or the charged radical enhanced the possibility of direct positron electron annihilation.

A similar experiment on Teflon again showed that the longer lifetime component was reduced in intensity although to a greater extent in air than in vacuum. This could be related to an irradiation produced free radical which was stable in air but not in a vacuum.

To elucidate what the longer lifetime was really due to, a sample of 10M sodium hydroxide solution was taken down to 85°K producing a transparent glass in which excess electrons produced by gamma irradiation would be effectively frozen in position. These excess electrons did not affect the longer lifetime component which was extraordinary since this lifetime was supposedly due to orthopositronium which would undergo a strong interaction with excess electrons. Eldrup et al. (1971) suggested that the positrons must be trapped in a hole in the ice structure by Na^+OH^- ions before annihilating. Since the excess electrons were frozen in position the excess electron density at a hole would be negligible. However, angular correlation studies in pure ice had shown that positronium was delocalized so in the NaOH glass the positrons must have formed positronium after they had been trapped.

Further evidence against the idea that the longer lifetime component was due to positronium was obtained using near perfect alkali halide crystals in which positronium formation is forbidden (Tumoza et al., 1971). Experiments suggested that the second lifetime was due to the positron becoming attached to a crystal defect where the electron density was much lower. Irradiation by both gamma and X-rays increased the intensity of the second

component (in the same way as doping the crystal with Aluminium) until a limiting value was reached which could be explained by assuming an interaction between a positive ion vacancy and the positron. The electron density at the vacancy would be lower and hence the longer lifetime. This conclusion from irradiation produced effects is, of course, the same as that arrived at by Hodges (1970) using temperature measurements in metals.

From first order kinetics the number of positrons populating the two states can be obtained. Suppose:

a) thermalised positrons either annihilate at a rate λ_o or are captured at a rate K which is proportional to the defect density;

b) trapped positrons either annihilate at a rate λ_1 or escape at a rate γ ;

c) N = number of free positrons and N_1 = number of trapped positrons.

Then: $$\frac{dN}{dt} = -(\lambda_o + K)N + \gamma N_1$$

and $$\frac{dN_1}{dt} = -(\lambda_1 + \gamma)N_1 + KN$$

These two must give the two observed lifetimes or annihilation rates λ_A and λ_B. If $\lambda_A = \lambda_o + K$ and $\lambda_B = \lambda_1$ when γ tends to zero then this would not explain the results. So alternatively, K and γ must be much less than λ_1 or λ_o when $\lambda_A = \lambda_o + K$ and $\lambda_B = \lambda_1 + \gamma$. These could explain the results as both λ_A and λ_B are now dependent on the defect concentration, λ_B because γ may depend on

the defects interacting. If capture and escape rates are similar then there will be a saturation lifetime when all the positrons are captured or when as many positrons are captured as possible by the number of effective traps.

Using an angular correlation technique to measure the lifetimes in pure semiconductor crystals, Sen (1971) found similar results and concluded that the two components in the lifetime, which were both sensitive to radiation damage or lattice defects, were due to trapping and not a bound state, i.e. positronium. A similar technique was used to study the effect of radiation damage in CuNi single crystals on positron annihilation (Tanigawa et al., 1971). A ^{64}Cu source was produced in situ by neutron irradiation doses of up to 10^{17} n.cm^{-2}. After each irradiation the angular correlation curve showed that the hump and shoulders due to the $\langle 110 \rangle$ necks in the Fermi surface decreased in prominence as the dosage increased. This was due to the presence of vacancies which would trap the positrons in an electron density primarily due to S electrons, since higher energy neck electrons would be repelled. Similar results in solid and liquid copper have been demonstrated by Itoh et al. (1972).

6.2 Neutron Irradiation and Damage

There are three basic defects in solids which can be caused by neutron irradiation:

1) Vacant lattice sites may be created by collisions between the neutrons and lattice atoms. The energy

transferred in these collisions is usually so large that the displaced atom will recoil and create further lattice vacancies by subsequent collisions, i.e. a cascade process.

2) For every vacancy created there must be a displaced atom in an interstitial position provided, of course, that it does not fall into another vacancy.

3) Impurity atoms are created by neutron irradiation by transmutation and in our experiment one particular impurity ^{64}Cu is actually used to produce the positrons needed for the experiment.

There are three other important processes which can occur:

4) If a moving atom collides with a stationary atom so that the stationary atom is knocked on leaving a vacancy then the original moving atom may be left with so little kinetic energy that it will fall into the vacancy itself. In fact, the number of such replacement collisions may exceed the number of displacement collisions.

5) A fast moving neutron or atom that has been hit hard enough to cause it to vibrate with large amplitude will transfer energy to nearby atoms. The surrounding area will become locally heated and will expand and then will rapidly lose energy and be quenched. There may be melting and turbulent flow in such a displacement spike.

6) The neutrons may cause ionisation by knocking electrons of atoms as they go past although this effect will be much more effective for a charged particle.

A fast neutron colliding with a nucleus imparts momentum and the nucleus will recoil taking its electron cloud with it (except possibly an electron whose orbital

velocity is less than the recoil velocity of the nucleus). If elastic collisions are the most probable interactions and the energy transferred can be between 0 and a maximum T_m then the distribution of recoil energies is related to the distribution of angular deflections of the neutron. Similarly, if the neutrons are scattered isotropically then all the recoil energies between 0 and T_m are equally probable and the mean energy transfer is $T_m/2$. Neutrons from fission have a broad spectrum from zero to 15 MeV with an average of about 2 MeV though the spectrum seen by a sample will depend on the amount of moderator between it and the feed elements (Watt, 1953). In fact, experiments have shown that neutrons are not scattered isotropically but preferentially in a forward direction so the average energy transferred would be less than $T_m/2$ (Watt and Barschall, 1954; Watt and Beyster, 1955).

The production rate of defects is defined as the increment of the atomic concentration of defects produced by one unit of integrated neutron flux density. To get a sensible measurement of this rate the measurements must be done at temperatures low enough to prevent thermally activated migration of the defects once formed.

A vacancy will only be formed if the energy transferred is greater than the threshold energy for atom displacement T_d. This is related to the interatomic potential and is difficult to obtain without assuming that there are no thermal vibrations and that the collision is essentially between two bodies. Furthermore, because of the lattice structure T_d will depend on the knock on direction with respect to the crystal axes and there will be a separate

threshold energy for every direction. So if a neutron imparts energy greater than the particular T_d for the knock on direction the atom will recoil and if sufficiently energetic collide with and knock on further atoms. In neutron irradiation most of the defects are produced by the secondary atoms in this way. Since a lot of interstitials and vacancies recombine spontaneously due to the high local defect density the threshold energy is effectively increased. This is demonstrated by comparing a neutron which transfers say 10^4 eV and has an effective threshold energy of 65 eV to an electron which transfers only 56 eV (no cascade) and has an effective threshold energy of 46 eV (Wollenberger, 1969).

The number of primary knock-ons produced per unit volume in a bombardment, n_p, is given by:

$$n_p = \Phi\, t\, n_o\, \sigma_d$$

where flux Φ = number of bombarding particles traversing unit area/unit time

t = duration of bombardment

n_o = number of atoms per unit volume

σ_d = the cross section per atom for displacement collisions.

If all recoil energies are equally probable then the differential cross section for a transfer of energy T to T + dT is given by:

$$d\sigma = (\sigma_T / T_m)\, dT$$

where σ_T = total neutron cross section for elastic

collisions typically between 1 and 10 barns. Suppose that the neutrons have a mean energy of 2 MeV then the mean energy of primary knock-ons in Rutherford scattering is given by:

$$T \approx 4/A \text{ MeV}$$

where A = atomic mass of target.

Suppose now that the average primary knock-on produces $\bar{\nu}$ displaced atoms itself then the total number of vacancies per unit volume is:

$$N_d = n_p \bar{\nu}$$

This is a drastic simplification based on the assumption that moving particles interact by screened Coulomb forces with individual lattice atoms (Harrison and Seitz, 1955).

In order for the defects produced to remain the temperature must be kept very low ($10^{\circ}K$) for at higher temperatures the vacancies and interstitials tend to recombine. This is especially easy for neutron produced defects because they tend to be in a small area, due to the cascade process, which has a very high defect concentration. Interstitials migrate freely below the boiling point of liquid nitrogen but annealing appears to be slow below $223^{\circ}K$ but quite fast at $283^{\circ}K$ (for copper) and the vacancy production rate at $283^{\circ}K$ is about one fifth of that at $223^{\circ}K$. There does not seem to be any correspondence between an irradiation produced defect, activation energy 0.1 eV, and thermally produced defects with a formation energy of 1.0 eV. It is only at $600^{\circ}K$ that vacancies become fairly mobile, when, as has been said, the greater part of the vacancy-interstitial annealing has already

taken place due to interstitial migration. However, there will still be some residual defects.

Annealing of these point defects involves their diffusion in the lattice until they encounter an immobilising trap or an absorbing sink. Thus vacancies and interstitials can annihilate each other or they can be absorbed at grain boundaries, dislocations, etc. They may be trapped in the local field of a substitutional impurity or an interstitial may replace a substitutional impurity atom or a vacancy may be filled by a substitutional impurity atom. Also there is a very real possibility that vacancies will congregate to form divacancies or higher conglomerates. A simple view of annealing at room temperature would be that it was essentially a diffusion process. Therefore, to see whether vacancies or interstitials are the principal agents (given that they are not already produced by irradiation) we only need to compare their self diffusion energies which are the sum of the formation energy and the migration energy:

$$E_D = E_F + E_M$$

The migration energies are (for copper) about 0.13 eV for interstitials and 0.9 eV for vacancies. However, the formation energy of an interstitial is 5.5 eV compared to only 1.0 eV for a vacancy. Hence diffusion of vacancies would appear to be the main mechanism for annealing (Huntingdon, 1953) at room temperature.

The process of vacancy diffusion is complicated by the tendency of vacancies to either cluster together or to be attracted to impurity sites either singly or in

clusters. This would cause an effective migration energy higher than that quoted depending on the impurity concentration. Copper, in fact, shows four annealing stages but since two of them are completed under room temperature they can be discounted. The third stage which occurs over the temperature range 240-320°K has been ascribed to the movement of vacancies and positron measurements indicate that vacancies are active over this stage. However the concentration of vacancies does not increase substantially until about 800°K which is in the last stage of annealing which would explain an increase in vacancy annealing at that temperature. Suggestions that the room temperature annealing may be due to interstitial movement can be discounted because of the very high diffusion energy of interstitials. A feasible explanation of annealing at room temperature would appear to be due to the migration of vacancy clusters or divacancies which would have a low diffusion energy than monovacancies (Bartlett and Dienes, 1953).

6.3 EXPERIMENTAL METHOD

A small ball with 1 mm. diameter was made from pure copper (1 in 10^6 impurity), annealed at 900°C for 2 hours, and then etched for five minutes in concentrated nitric acid to clean and prepare the surface. The ball was then irradiated in the University Reactor in a flux of 1.3×10^{12} n/cm^2/sec. for timed periods so that its total exposure time was known. At the end of each

irradiation period the sample was left for 48 hours at room temperature so that the first three stages of annealing would be completed. The annihilation gamma ray spectra (due to the ^{64}Cu source produced in situ by the irradiation) was then measured with a high resolution Ge(Li) detector and the peak obtained was analysed on the University Computer using the SAMPO program. The sample was then returned to the reactor to continue the irradiation procedure. The apparatus used is described in Chapter 5. The exposure times were 5, 15, 30 minutes then every hour up to a total of 14. The results shown in Fig. 6.1 have been corrected for the inherent detector system resolution.

6.4 CONCLUSIONS

From the graph 6.1 the F.W.H.M. of the gamma ray energy peak narrows gradually with neutron dose until a minimum is reached. From the positron annihilation theory previously used it would appear that increasing radiation damage produces point defects which can trap positrons and which have an anomalously low core electron density. One of the point defects produced by neutron bombardment has been given as vacancies and these may be the traps. If stages 1 to 3 of the annealing had been completed before the spectrum was taken and the narrowing of the peak is caused by increased annihilation at vacancies we can postulate:

a) the concentration of vacancies initially increases with neutron dose;

b) either the concentration of vacancies tends towards

FIG. 6.1 EFFECT OF NEUTRON IRRADIATION ON POSITRON ANNIHILATION.

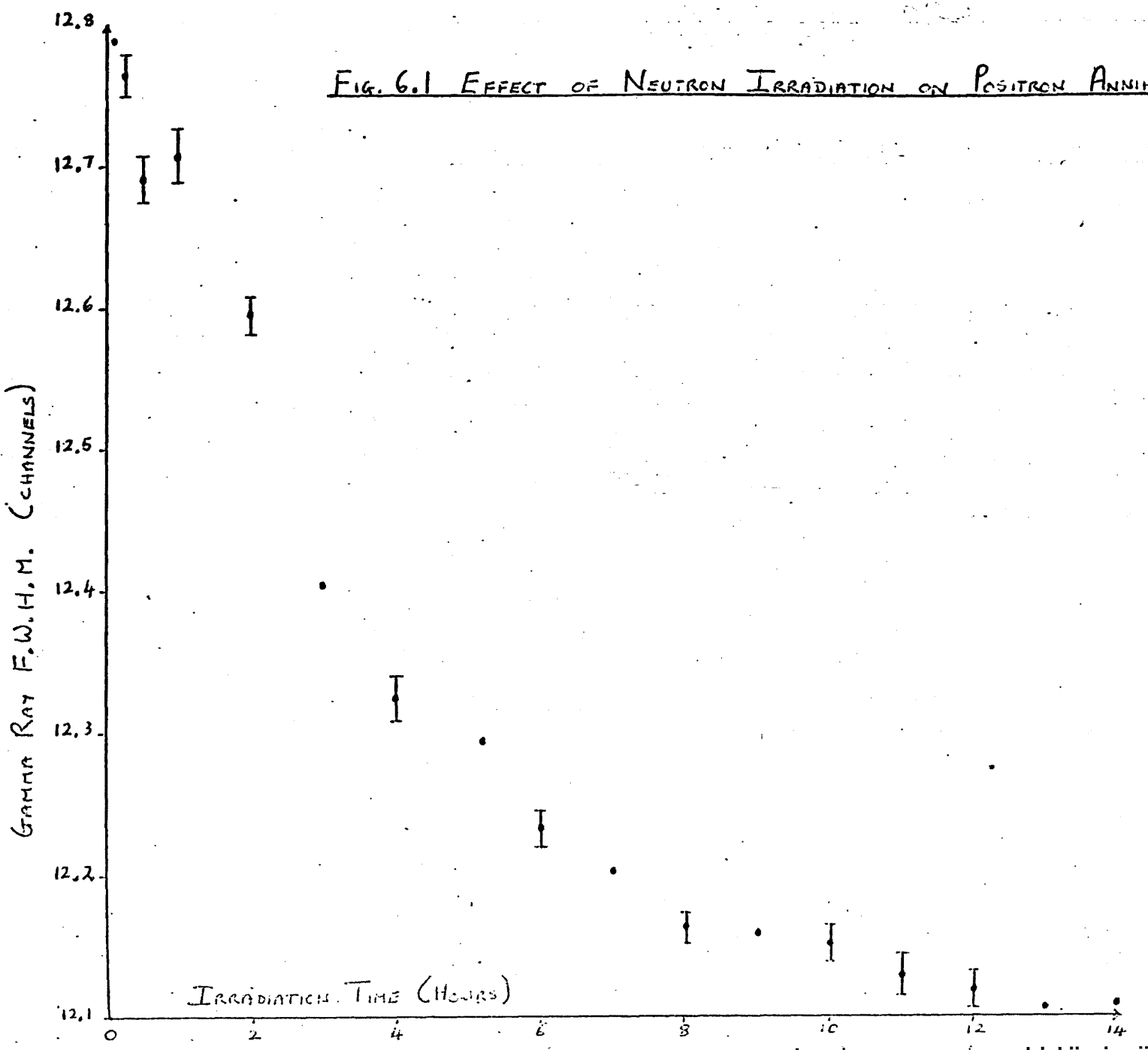

a maximum or becomes so large that all the positrons tend to annihilate in vacancies, i.e. saturation occurs. From our temperature experiments saturation annihilation in vacancies produces a 11% narrowing of the F.W.H.M. and can occur fairly easily at a concentration of about 10^{-5} because positrons are very sensitive to vacancy traps.

In this case the maximum amount of narrowing is 5.5% which would indicate that saturation trapping of positrons has not occurred. If the greater part of the defects produced by irradiation are annealed after 48 hours at room temperature then the narrowing of the line width cannot be explained by normal vacancies trapping the positrons. However, if vacancies and divacancies were being trapped at impurity sites etc. (Cattaneo and Germagnoli) then the results could be explained by:

either a) the narrowing of the linewidth is caused by positrons being trapped in vacancies which are themselves trapped (Seeger, 1972). The probability of a vacancy being trapped increases with the number of defects produced, i.e. with the neutron dose. The plateau part of the linewidth curve is due to saturation vacancy trapping when all the impurity atom sites have a trapped vacancy or if an equilibrium is involved, the maximum number of vacancies which can be trapped has been reached.

or b) the positrons are again trapped by vacancies which are themselves trapped at other lattice defects such as dislocations, thermal spikes, grain boundaries and either the number of such defects fails to increase or the maximum allowed number of positrons has been reached.

or c) the positrons are trapped in vacancy clusters, e.g.

divacancies which may be fairly stable at room temperature whether associated with a lattice defect, e.g. impurity or not. The plateau of the curve could be due to the maximum concentration of such clusters being reached for room temperature.

Using the formula to calculate the number of primary knock-ons produced in the reactor at a flux density of 1.3×10^{12} n/cm^2/sec, we obtain a value of $n_p \approx 2 \times 10^{10}$/cc/sec. The number of secondary knock-ons produced by one primary is about 380 in copper so that the total number of vacancies and interstitials produced is 7.6×10^{12}/cm^3/sec. If there are approximately 10^{22} atoms/cm^3 then the saturation positron trapping vacancy concentration given as 10^{-5} would require 24 hours of irradiation at a temperature at which none of the vacancies produced were lost. Positrons are sensitive to vacancy concentrations of about 10^{-8} which would require an irradiation time of only 20 seconds at such low temperatures. Our minimum irradiation time was five minutes which would produce a vacancy concentration noticeable by positrons except that most of the vacancies are annealed. Therefore the mechanism of positrons annihilating from vacancies which are themselves trapped is a reasonable explanation of our results.

The picture of the process is therefore that the irradiation will produce many defects, the majority of which will be vacancies and interstitials. 48 hours later the first three stages of annealing will have been completed and these stages are ascribed to interstitial migration, etc. But these interstitials were the ones

produced by the irradiation and the concentration of such interstitials is now very low and will not be increased substantially by the increase in temperature because of the high diffusion energy. If any vacancies are left, i.e. not annihilated with an interstitial, then they are probably trapped so that it is difficult for interstitials to get at them. The measurements indicate that the number of trapped vacancies increases with the neutron dose, i.e. probably, the number of traps increases with dosage, until a saturation number of such traps is reached. The fourth stage of annealing may therefore encompass the detrapping of the trapped vacancies as well as or instead of production of more vacancies as the temperature increases.

APPENDIX

ANALYSIS OF DATA PROGRAMS [CHAPTER 5]

A.1 INTRODUCTION

The experiment from Chapter 5 produced data concerning the positron annihilation gamma ray energy peak width as a function of temperature (Figs. 5.4, 5.5, 5.6). The theory used suggests that the curves obtained are given by the equation:

$$\frac{F - FF}{FV - F} = A \exp [- E_V / kT] \qquad (1)$$

where F = Peak width at temperature T^oK

FF = Peak width when all the positrons are free

FV = Peak width when all the positrons are trapped

A = constant

E_V = Vacancy formation energy

k = Boltzmann's constant

From (1):

$$\ln \left[\frac{F-FF}{FV-F} \right] = \ln A - E_V / kT \qquad (2)$$

The program is to find the best value of E_V to fit the experimental data.

A.2 PROGRAM VACANCY I

This program allows the peak width parameter generated by SAMPO to be read in directly. The corrected

full width half maximum is calculated (and associated error) taking the inherent detector system resolution into account. A library function on the University computer F.M.F.P. (based on a method by Fletcher and Powell) is then called and this attempts to fit equation (1) to the data thereby generating the best values of FF, FV, A and E_V. These values are then used by a CERN library routine E200 (Escoubès and de Unamuno-Escoubès, 1964) which uses them to plot a straight line as in equation (2). From this line and the experimental data points the routine generates the errors in the value of E_V and A.

Program Format

a) Reads in N, R, L, M where N = total number of experimental points
R = detector resolution
L = code number so E200 fits a straight line
M = minimum number of points fitted by E200.

b) Reads in T_i, F_i, DF_i where T_i = data point temperature in ^oK
F = SAMPO CW parameter for data point (peak width)
DF_i = SAMPO CW parameter error

c) Value of Boltzmann Constant k is given.

d) Calculates the true F.W.H.M. for each data point using SAMPO CW parameter and detector resolution R.

$$\text{True Width } TF_i = \sqrt{F_i^2 - R^2}$$

e) Calculates the true error in the true width given:

$$TF_i = \sqrt{F_i^2 - R^2}$$

$$\therefore \quad \frac{\delta TF_i}{\delta F_i} = \frac{1}{2}(F_i^2 - R^2)^{-1/2} \times 2F_i = \frac{F_i}{TF_i}$$

$$\therefore \quad \delta TF_i = F_i \cdot \delta F_i / TF_i$$

g) Initial guesses for FF, FV, A and E_V are given.

h) The routine F.M.F.P. is called and this fits the corrected data with equation (1). Chisquare is defined as:

$$\chi^2 = \Sigma_i \frac{[\text{calculated } F_i - \text{experimental } F_i]^2}{DTF_i^2}$$

So χ^2 is an indication of how near the calculated curve the experimental points lie, i.e. goodness of fit. For each of the four parameters a graph of χ^2 versus the parameter value is of the form of an inverted parabola. Starting with the initial guess value of the parameter the gradient of the curve at that point is calculated and this indicates in which direction the value of the parameter should be adjusted. By successive calculations the minimum value of χ^2 is obtained which corresponds to the best value of the parameter. This value for each of the parameters and the final minimum value of χ^2 are returned to the main program together with a code number which indicates that a minimum has been found.

i) Calculation of the parabola gradients is actually done by a subroutine called FUNCT. For each parameter the

parabola gradient can be obtained by differentiating χ^2 with respect to that parameter and substituting the parameter values under test in the resulting equation. The gradient equations must be worked out and given in the subroutine.

Let $$\chi^2 = \left[\frac{F_{calc} - F_{exp}}{\Delta F\ exp}\right]^2$$

where $$F_{calc} = \frac{FF + FV \cdot Ae^{-E_v/kT}}{1+Ae^{-E_v/kT}}$$

$$\chi^2 = \left[\frac{FF + FV \cdot Ae^{-E_v/kT}}{\Delta F_{exp}\ (1+Ae^{-E_v/kT})} - \frac{F_{exp}}{\Delta F_{exp}}\right]^2$$

$$= \left[\frac{FF}{\Delta F\ (1+Ae^{-E_v/kT})} + \frac{FV \cdot Ae^{-E_v/kT}}{\Delta F\ (1+Ae^{-E_v/kT})} - \frac{F}{\Delta F}\right]^2 \triangleq Z^2$$

Let $e^{-E_v/kT} \triangleq EE$

Now $\frac{\delta \chi^2}{\delta FF} = 2Z \times \frac{\delta Z}{\delta FF}$ and $\frac{\delta Z}{\delta FF} = \frac{1}{\Delta F(1+A.EE)}$

$$= \frac{2Z}{\Delta F(1+A.EE)} \qquad (3)$$

Now $\frac{\delta \chi^2}{\delta FV} = 2Z \times \frac{\delta Z}{\delta FV}$ and $\frac{\delta Z}{\delta FV} = \frac{A.EE}{\Delta F(1+A.EE)}$

$$= \frac{2Z.A.EE}{\Delta F(1+A.EE)} \qquad (4)$$

Now $\frac{\delta \chi^2}{\delta A} = 2Z \times \frac{\delta Z}{\delta A}$

$$\text{and } \frac{\delta Z}{\delta A} = \frac{-FF(1+A.EE)^{-2}.EE}{\Delta F} + \frac{FV}{\Delta F}\left[(1+A.EE)^{-1}.EE - A.EE(1+A.EE)^{-2}.EE\right]$$

$$= \frac{-FF.EE}{\Delta F(1+A.EE)^2} + \frac{FV}{\Delta F}\left[\frac{EE}{(1+A.EE)} - \frac{A.EE^2}{(1+A.EE)^2}\right]$$

$$\therefore \frac{\delta \chi^2}{\delta A} = 2Z\left[\frac{-FF.EE}{\Delta F(1+A.EE)^2} + \frac{FV}{\Delta F}\left[\frac{EE}{(1+A.EE)} - \frac{A.EE^2}{(1+A.EE)^2}\right]\right] \quad (5)$$

$$\text{Now } \frac{\delta \chi^2}{\delta E_V} = 2Z \times \frac{\delta Z}{\delta E_V}$$

$$\text{and } \frac{\delta Z}{\delta E_V} = \frac{+FF(1+A.EE)^{-2}.A.EE}{\Delta F.KT} + \frac{FV}{\Delta F}\left[-(1+A.EE)^{-1}.\frac{A.EE}{KT}\right.$$

$$\left. +A.EE(1+A.EE)^{-2}.\frac{A.EE}{KT}\right]$$

$$= \frac{FF.A.EE}{\Delta F.KT(1+A.EE)^2} + \frac{FV}{\Delta F}\left[\frac{-A.EE}{KT(1+A.EE)} + \frac{A^2.EE^2}{KT(1+A.EE)^2}\right]$$

$$\therefore \frac{\delta \chi^2}{\delta E_V} = 2Z\left[\frac{FF.A.EE}{\Delta F.KT(1+A.EE)^2} + \frac{FV}{\Delta F.KT}\left[\frac{-A.EE}{(1+A.EE)} + \frac{A^2.EE^2}{(1+A.EE)^2}\right]\right] \quad (6)$$

j) On returning to the main program with the best values of the parameters the differences between the calculated and experimental points are obtained (δF_i).

k) If the F.M.F.P. routine did not reach a minimum value of χ^2 then the program stops. Otherwise the calculated data is used by the E200 routine which fits a straight line of the form $y = mx+c$ to equation (2) and calculates m and c and their associated errors given that the error in each calculated data point has been worked out in j). In this part $F = F_{calc}$ and:

$$y_i = \ln\left[\frac{F_i - FF}{FV - F_i}\right] \triangleq \ln(fn\ F_i), \qquad x_i = -1/T;$$

$$c = \ln A \qquad\qquad m = E_V / k$$

$$\therefore \quad \frac{\delta y_i}{\delta F_i} = \frac{1}{fn(F_i)} \times \frac{\delta\ (fn\ F_i)}{\delta\ F_i} = \frac{1}{fn(F_i)}\left[\frac{(FV-F)+(F-FF)}{(FV-F)^2}\right]$$

$$= \frac{FV-F}{F-FF}\left[\frac{(FV-F)+(F-FF)}{(FV-F)^2}\right]$$

$$\therefore \quad \delta y_i = \frac{(FV-F)+(F-FF)}{(F-FF)(FV-F)} \times \delta F_i$$

1) The values of m and c are obtained from:

$$m = \frac{\begin{vmatrix} \Sigma_i w_i & \Sigma_i w_i y_i \\ \Sigma_i w_i x_i & \Sigma_i w_i x_i y_i \end{vmatrix}}{D_2} \qquad c = \frac{\begin{vmatrix} \Sigma_i w_i y_i & \Sigma_i w_i x_i \\ \Sigma_i w_i x_i y_i & \Sigma_i w_i x_i^2 \end{vmatrix}}{D^2}$$

where $D_2 = \begin{vmatrix} \Sigma_i w_i & \Sigma_i w_i x_i \\ \Sigma_i w_i x_i & \Sigma_i w_i x_i^2 \end{vmatrix}$ and $w_i = 1/(\Delta y_i)^2$ the 'weight' of the i th point.

There is no internal error due to the statistical spread of the points since they have been calculated to be on the line.

m) The external error due to the errors in the points are calculated from:

$$\Delta m = \left[\frac{\Sigma_i w_i}{D_2}\right]^{1/2} \qquad \text{and} \qquad \Delta c = \left[\frac{\Sigma_i w_i x_i^2}{D_2}\right]^{1/2}$$

n) The following information is printed out:

1) Data point temperature, corrected width and error, calculated width and error;

2) initial guesses of the four parameters FF, FV, A and E_V;

3) best values of the four parameters FF, FV, A and E_V, minimum value of χ^2 and F.M.F.P. error code;

4) calculated values of data point X_i, Y_i, δY_i used by E200;

5) calculated best values of A and E_V and their associated errors.

This program was found to be not very effective because of the search technique used in conjunction with the data available. If the inverted χ^2 versus parameter value parabola has a saddle point then the program may indicate that this is the minimum value of χ^2. It is especially vulnerable if two data points are close together. So, although results were obtained which seemed fairly reasonable it was decided that a better result could be obtained by using another method of fitting the data.

A.3 PROGRAM VACANCY II

The SAMPO CW parameter are again fed straight in and the program will calculate the corrected F.W.H.M. of the peak taking the detector system resolution into account. To obtain the best fit to the data points, given that the errors in the points are all approximately the same, then the data points will lie on either side of the best fit line such that the distances between the

points and the curve have a gaussian distribution. The probability of the fitted curve being the best one is given by the area under the associated gaussian distribution and the best fit curve will have the highest probability. The program used is MALIK (F. Grard, 1962).

Assume that the probability function is represented by:

$$f = f\ (a_1 a_2 \ldots a_n\ ,\ X\ )$$

where $a_1 - a_n$ = parameters to be found

X = measured quantities, in this case the error distance between a data point and the calculated curve.

The likelihood function is given by:

$$L = \prod_{i=1}^{N} \left[f\ (a_1 a_2 \ldots a_n,\ X_i) \Big/ \int_x f dX \right]$$

where N = total number of points

$f(a_1 a_2 \ldots a_n, X_i)$ = probability of a data point resulting in the value X_i

$\int_x f dX$ = the integral of the probability function extending over the whole range of measurements made.

The procedure used to find the best fit is to determine the maximum of the likelihood function (and the error matrix) by a method of steps by maximising the function F = ln(L). The initial values (guesses) of the 'a' parameters and an appropriate step size are given and the first parameter is increased or decreased by steps of the stated size to find

a larger value of F. When successfully found the new value of the first parameter is used and the operation is repeated for the next parameter and so on. The cycle is repeated as long as F increases and when no improvement can be made with the step sizes given, the steps are all reduced by a common factor and the next iteration is started. This continues until a satisfactory solution is found for each of the parameters.

The likelihood function approaches a multi-gaussian distribution and at the end of each iteration the largest value of F is compared with that from the previous iteration. When the difference is 0.001 or less the two corresponding solutions differ by less than 1/20 of a standarddeviation. Hence a solution very close to the maximum may be obtained.

The error matrix is computed by inversion of the matrix built with all the second derivatives of F at its maximum calculated by differences. The width of the distribution is determined as being the + and - quantities one has to add to each of the fitted parameters so as to lower the likelihood function by $e^{-1/2}$ of its maximum value. If L is multigaussian with no correlation between the parameters then these quantities are the standard errors. The steps used to compute the second derivative are taken equal to a certain fraction β of the standard errors. For a perfect multi-gaussian distribution the results would be independent of the size of the step.

Since the errors are computed from F by changing two parameters at a time a better value of the maximum may

be generated than the value obtained originally. If this happens then the values of the parameters are put back into the start and the whole iteration procedure is restarted to find a new maximum.

Program Format

a) Reads in the number of parameters, their initial values and the corresponding assigned step.

b) Reads in factors α and β used in the program.

c) Calls subroutine Input which itself reads in the data points and produces the corrected values which take the detector resolution into account.

d) Calls subroutine FUNCT to calculate the value of the maximum likelihood function using the values of the parameters taken to it. The subroutine calculates the curve corresponding to the parameter values and the corresponding errors between the data points and this curve. Because there are not many data points the subroutine generates an overlapping histogram of the errors and integrates the curve to obtain the probability of the calculated curve being the best fit. Thus the likelihood function can be obtained and the value of this is returned to the main program.

e) When the likelihood function only changes by a small amount the values of the parameters are printed out as being the most satisfactory and the errors are computed.

A.4 PROGRAM VACANCY III

Program Vacancy II which is based on the maximum likelihood technique is far more efficient in fitting the

experimental data than Vacancy I. It was especially good at producing the parameter values for FF and FV but it had some difficulty with E_V and A because of the statistical spread of points near the critical temperature. To eliminate errors due to the inherent sensitivity of the program the parameter values for FF and FV produced by Malik were fed into the E200 library program which used them to fit the corrected experimental data with equation (2):

$$\ln \left[\frac{F-FF}{FV-F} \right] = \ln A - E_V / kT$$

The program fits the equation to the data between the two plateau regions (FF and FV) and produces the best values of E_V and A and their associated errors. In this program the F values used are the corrected experimental values and the errors are similarly the corrected experimental errors. The remainder of the program is identical to the E200 section of Program Vacancy I.

REFERENCES

AIROLDI, BACHELLA, GERMAGNOLI	Phys. Rev. Lett.	2(1959)145
ALEXANDER, POATE	Rad. Eff.	12(1972)211
ANDERSEN	Phys. Rev.	43(1933)491
ANDERSON, AUGUSTYNIAK, UGGERHOJ	Phys. Rev. B.	(1971)705
ANDERSON, LAGSGARD	Atomic Collisions in Solids IV Gordon and Breach	1972
APPLETON, ERGINSOY, GIBSON	Phys. Rev.	161(1967)330
APPLETON, MOAK, NOGGLE, BARRETT	Phys. Rev. Lett.	28(1972)1307
ARMSTRONG, GIBSON, GOLAND, GOLOVCHENKO, LEVESQUE, MEEK, WEGNER	Rad. Eff.	12(1972)143
BARTENEV, VARISOV, GOL'DANSKI, MOHRUSHKIN, TSYGANOV	Sov. Phys. - Solid State	12(1970)2806
BARTLETT, DIENES	Phys. Rev.	89(1953)848
BATRA, SEHGAL	Nuc. Phys. A.	156(1970)314
BEHRISH, SCHERZER, SCHULZE	Rad. Eff.	13(1972)43
BELL, GRAHAM	Phys. Rev.	90(1953)644
BELYAKOV	Jetp. Lett.	13(1971)179
BEREZIN	Sov. Phys. - Solid State	12(1970)2684
BERGERSON, STOTT	Sol. State. Commun.	7(1969)1203

BERKO, HEREFORD	Rev. Mod. Phys.	28(1956)299
BIANCHI, MALLEJAC, JANOT, CHAMPIER	Compt. Rend. Acad. Sci.	263(1966)1404
BOGH, DAVIES, NIELSON	Phys. Lett.	12(1964)129
BRANDT	Positron Annihilation Academic Press	1967
BRANDT, FAHS	Phys. Rev. B.	2(1970)1425
CAMPBELL, SCHULTE, MACKENZIE	Phys. Lett. A.	38(1972)377
CARSTANYEN, SIXMANN	Atomic Collisions in Solids IV Gordon and Breach	1972
CATTANEO, GERMAGNOLI	Phys. Rev.	124(1961)414
CHANG, COCK, PRIMAKOFF	Phys. Rev.	90(1953)544
CONNORS, CRISP, WEST	J. Phys. F.	1(1971)355
CONNORS, CRISP, WEST	Phys. Lett. A.	33(1970)180
CONNORS, WEST	Phys. Lett. A.	30(1969)24
COOK	Phys. Rev.	178(1969)895
DAVIES, JENNINGS	J. Phys. B.	3(1970)804
DEARNALY, MITCHELL, NELSON, FARMERY, THOMPSON	Phil. Mag.	18(1968)985
DE BENEDETTI, COWON, KONNEKER, PRIMAKOFF	Phys. Rev.	77(1950)205
DE BENEDETTI, RICHINGS	Phys. Rev.	85(1952)377
DEKHTYAR	Sov. Phys. - Solid State	12(1970)488
DEKHTYAR, CIZEK	Phys. Lett. A.	34(1971)345

DELLA MEA, DRIGO, LOROSSO, MAZZOLDI	Rad. Eff.	13(1972)115
DIDENKO, VOROB'EV, TSEKHANOVSKII	Jetp. Lett.	12(1970)209
DIXON, TRAINOR	Phys. Rev.	97(1955)733
DOYAMA	J. Phys. Soc. Japan	33(1972)1495
DOYAMA, HASIGUTI	Crys. Latt. Deff.	4(1973)139
EISEN, UGGERHOJ	Atomic Collisions in Solids IV Gordon and Breach	1972
ELDRUP, MORGENSEN, KEWAN	Chem. Phys. Lett.	10(1971)379
FARACI, PENNISI, TURRISI, SCHWENGLER, SLITZER	Lett. Nuovo Cim.	5(1972)75
GARWIN	Phys. Rev.	91(1953)1571
GLEASON, TAYLOR, TABERN	Nucleonics	8(1951)12
HADLEY, HSU	Chem. Phys. Lett.	7(1970)465
HAMILTON, QUINTON	Phys. Lett.	22(1966)312
HARRISON, SEITZ	Phys. Rev.	98(1955)1530
HAUTOJARVI, TAMMINEN, JAUHD	Phys. Rev. Lett.	24(1970)459
HODGES	Phys. Rev. Lett.	25(1970)284
HOTZ, MATHIESON, HURLEY	Phys. Rev.	170(1968)351
HSU, HADLEY	Phys. Lett. A.	34(1971)317
HUNTINGDON	Phys. Rev.	91(1953)1092

HUNTINGDON, SEITZ	Phys. Rev.	61(1942)315
HUSAIN, PUTMAN	Proc. Phys. Soc.	70(1957)304
ITOH, KUROKA, KAI, TAKEUCHI	J. Phys. Soc. Japan	33(1972)567
JACKMAN, SCHULTE, CAMPBELL, LICTENBERGER, MACKENZIE, WORMALD	J. Phys. F.	4(1974)LI
KIM, STEWART, CARBOTTE	Phys. Rev. Lett.	18(1967)385
KLEMPERER	Proc. Camb. Phil. Soc.	30(1934)347
KOMAKI, FUJIMOTO, ISHII, NAKAYAMA	Phys. Lett. A.	37(1971)271
KRAFTMAKHER, STRELKOV	Vacancies and Interstitials in Metals, North Holland,	1969
KUMAKHOV	Phys. Lett. A.	32(1970)538
KURIBAYASHI, TANIGAWA, NANAO, DOYAMA	Sol. State Commun.	12(1973)1179
LEHMANN, LIEBFRIED	Journ. Appl. Phys.	34(1963)2821
LINDHARD	Mat. Fys. Medd. Dan. Vid. Selsk.	34(1965)NR.14.
McGERVEY, TRIFTSHAUSER	Phys. Lett. A.	44(1973)53
McGERVEY, WALTERS	Phys. Rev. B.	2(1970)2421
McKEE	Phys. Lett. A.	30(1972)115
McKEE, JAMIESON, STEWART	Phys. Rev. Lett.	31(1973)634

McKEE, JOST,MACKENZIE	Can. Journ. Phys.	50(1972)415
McKEE, TRIFTSHAUSER, STEWART	Phys. Rev. Lett.	28(1972)358
MACKENZIE, CRAIG, McKEE	Phys. Lett. A.	36(1971)227
MACKENZIE, EADY, GINGERICH	Phys. Lett. A.	33(1970)279
MACKENZIE, LEBLANC, McKEE	Phys. Rev. Lett.	27(1971)580
MALLARD, HSU	Phys. Lett. A.	38(1972)164
MARTYNENKO	Sov. Phys. - Solid State	13(1971)876
MICAH, YOUNG	Phys. Lett. A.	33(1970)391
MORGAN, VAN VLIET	Atomic Collisions in Solids IV, Gordon and Breach	1972
MOROKHOVSKII,KOVALENKO, GRISHAEV, FISON, KASILOV, SHRAMENKO, KRINITSYN	JETP. Lett.	16(1972)112
MORY, QUÉRÉ	Rad. Eff.	13(1972)57
NANAO, KURIBAYASHI, TANIGAWA, MORI, DOYAMA	J. Phys. F.	3(1973)L5
NELSON, THOMPSON	Phil. Mag.	8(1963)1677
NIP, KELLY	Phys. Rev. B.	3(1971)2884
NIP, WILLIAMS	Rad. Eff.	12(1972)175
ORE, POWELL	Phys. Rev.	75(1949)1696
PATHAK, YUSSOUFF	Phys. Rev. B.	2(1971)4723
PATRICK, RUPAAL	Phys. Lett. A.	35(1971)235

PATRO, SEN	J. Phys. A.	4(1971)856
PEDERSON, ANDERSON, AUGUSTYNIAK	Atomic Collisions in Solids IV, Gordon and Breach	1972
POIZAT, REMILLIEUX	Rad. Eff.	13(1972)51
RAMA REDDY, CARRIGAN	Nuovo Cim.	66B(1970)105
RICH	Phys. Rev.	81(1951)140
ROBINSON, OEN	Phys. Rev.	132(1963)2385
ROHRLICH, CARLSON	Phys. Rev.	93(1954)38
RUPAAL, PATRICK	Phys. Lett. A.	38(1972)387
SEEGER	J. Phys. F.	3(1973)249
SEEGER	Phys. Lett. A.	41(1972)267
SEEGER, MEHRER	Vacancies and Interstitials in Metals, North Holland, 1969	
SELIGER	Phys. Rev.	100(1955)1029
SEN	J. Phys. A.	4(1971) 744
SIEGBAHN	α , β , γ Ray Spectroscopy, North Holland	1968
SIMMONS, BALLUFFI	Phys. Rev.	129(1963)1533
SINGH, SINGRU	Chem. Phys. Lett.	10(1971)329
STARK	Phys. Z.	13(1912)973
STEWART, SHAND	Phys. Rev. Lett.	16(1966)261
TAKAGI, KURIBAYASHI, NANAO, TANIGAWA, DOYAMA	Sol. State Commun.	9(1971)2155
TAKHAR	Brit. Journ. Appl. Phys.	18(1967)246
TAKHAR	Phys. Lett. A.	23(1966)219
TAKHAR	Phys. Rev.	157(1967)257
TANIGAWA, NANAO, KURIBAYASHI, DOYAMA	Phys. Lett. A.	35(1971)159

THONTADARYA, UMAKANTHA	Phys. Rev. B.	4(1971)1632
TUMOSA, NICHOLAS, ASHE	J. Phys. Chem.	75(1971)2030
UGGERHOJ	Phys. Lett.	22(1966)382
WALKER, BERMAN, DER, KAVANAGH, KHAN	Phys. Rev. Lett.	25(1970)5
WATT	Phys. Rev.	87(1953)1037
WATT, BARSCHALL	Phys. Rev.	93(1954)1062
WATT, BEYSTER	Phys. Rev.	98(1955)677
WEST	Sol. State Commun.	9(1971)1417
WOLLENBERGER	Vacancies and Interstitials in Metals, North Holland, 1969	

ACKNOWLEDGEMENTS

I wish to express my appreciation to my supervisor, Dr P.Rice-Evans, for the guidance and help extended by him during the course of this research.

I also wish to thank Professor H.O.W. Richardson, Professor E.R. Dobbs, Mr R.N. Thomas, Dr R. Thomas, Dr P. Pal, Mr W.A.G. Baldock, Mr A.K. Betts, Mr T. Le Mottee and Mr J. Sales for their help and interest and Mr F.A. Grimes and Mr A.H. King for technical assistance.

I wish to thank the Science Research Council for the Studentship Award and for the support of the research. I would also like to thank Metals Research Ltd for their support and the staff of the University Reactor for providing the sources.